SATELLITE DERIVED RAINFALL OVER TROPICAL AFRICA. ITS PATTERN, VARIABILITY AND CALIBRATION

Lukiya Tazalika

Department of Geography and Environmental Studies,
University of Zululand

Thesis submitted to the Faculty of Science
For the degree of Master of Science

APRIL, 2004

Abstract

The major spatial and temporal structure of rainfall and zonal wind at seasonal and intra-seasonal time-scales over tropical Africa are identified by principal component analysis. Pentad CMAP rainfall and NCEP 700hPa zonal wind for the period 1980-2000 were used. Wavelet analysis is used to filter the data sets for cycles between 20-70 days for the intra-seasonal oscillations.

The first mode of seasonal rainfall that explains 36% of the total variance is dominated by the annual cycle associated with the ITCZ and is loaded over equatorial Africa. The dominant mode for the zonal wind is loaded over eastern Africa with an extended axis in the Indian Ocean (25.8%). A strong relationship exists between the zonal wind and rainfall modes at the seasonal time scale.

The dominant mode for the intra-seasonal rainfall is loaded over northern Congo (29%). The second and third modes are over northeast Angola and East Africa respectively. The intra-seasonal oscillations are phase locked to the seasonal cycle and reveal cycles of 30-50 days typical of Madden Julian oscillation.

The 700hPa zonal wind intra-seasonal oscillation reveals a dominant mode over the equatorial east Atlantic Ocean. The second and third modes are over the west Indian Ocean and southeast Atlantic. A strong relationship between zonal wind over the equatorial Atlantic and rainfall over both northern Congo and east Africa is observed. Cross correlation reveals that the zonal wind leads rainfall by a few pentads.

Hovmoller plots for OLR and velocity potential reveal that the intra-seasonal oscillations over tropical Africa are dominated by eastward propagation. However, standing and westward propagation are also observed. Propagation is weak over east African coast due to strong meridional flow of the Indian Monsoon.

Results from the satellite rainfall calibration and validation are examined. While satellite radiance values generally underestimate rainfall over Uganda, they naturally provide better spatial distribution than the gauges. Following calibration algorithm development, validation tests indicate that satellite rainfall explains 81% of rainfall received in the year 2000. These results should be interpreted with caution since rain gauges give point measurements while satellites provide pixel values.

To my parents Buluhan Zilabamuzale and Mastula Nakakawa.

ACKNOWLEDGEMENTS

I wish to thank the Uganda Government and Professor Mark R. Jury for funding this study. I am grateful to my supervisor Professor M.R Jury, Head, Centre for Environmental Studies, University of Zululand for his guidance, critical discussions, suggestions and comments for the period of my study.

I am extremely indebted to the staff members at the Uganda Meteorological Department and the Centre for Environmental Studies, University of Zululand for their contribution towards the success of this study. The study leave, which the Uganda Government granted me, is highly appreciated.

I wish to thank my husband Abu-Baker Mwima, my children, Ibrahim, Ismail and Yusuf for their constant encouragement and accepting living in separation for the whole period of this study.

Lastly, I wish to acknowledge the contribution made by the National Centres for Environmental Prediction (NCEP) of the National Oceanic and Atmosphere Administration, Climate Prediction Centre, TAMSAT and Uganda Meteorological Department for providing data used in this thesis.

TABLE OF CONTENTS

CHAPTER ONE: INTRODUCTION AND LITERATURE REVIEW

CHAPTER TWO: DATA AND METHODOLOGY

CHAPTER THREE: SEASONAL RAINFALL AND CIRCULATION OVER TROPICAL AFRICA

CHAPTER FOUR: INTRASEASONAL OSCILLATIONS OVER TROPICAL AFRICA

CHAPTER FIVE: EVOLUTION AND PROPAGATION OF AFRICAN INTRASEASONAL OSCILLATIONS.

CHAPTER SIX: SATELLITE RAINFALL ESTIMATION

CHAPTER SEVEN: AN OVERVIEW OF DATA PROBLEMS IN AFRICA

CHAPTER EIGHT: CONCLUSIONS AND RECOMMENDATIONS

LIST OF FIGURES

FIGURE

LIST OF TABLES

Chapter One

Introduction and Literature Review

1.1.1 General

Developing states such as Uganda, Tanzania, Congo and others in Africa occupy less than 55% of the geographical area of the world but carry over 60% of the world's population, suffer from a shortage of resources and low productivity (Donaldson and Tsui, 1990). The pressure on land due to deforestation, overgrazing, mining and agriculture make climate variability a threat to the region. Droughts, floods, unreliable rainfall, and desertification have been experienced in many African countries. However, the future can be improved with better management of resources underpinned by scientific research with a view to restoring long-term sustainability.

Space technology can contribute significantly to the planning of production. Satellite remote sensing is a vital tool for assessment and management of natural resources, as well as monitoring the environment for long term effects caused by anthropogenic activities that could result in irreversible global changes. The advent of geo-stationary satellites over the equator at 5-6 positions around the globe has significantly improved the accuracy in forecasting severe weather such as thunderstorms and associated heavy rain. Satellites provide the primary means of obtaining a global perspective and comparing different parts of the globe. They play a great role in providing data for climate monitoring. A long global climate record is not practicable without a major satellite component (Trenberth et al., 2002).

In recent years, polar-orbiting satellites have increasingly expanded global monitoring of the earth's surface conditions. Satellite data derived from the NOAA Advanced Very High Resolution Radiometer (AVHRR) are characterized by spatially fine but temporally coarse resolution, yielding a valuable basis for observation of the annual cycle of land-surface conditions over very large areas.

Mathematical expressions have been developed that combine the visible and near-infrared reflectance to provide a normalized difference vegetation index (NDVI) of plant vigor. The NDVI from the NOAA satellites has proved to be a useful measure in depicting the continental-scale distribution and phonological seasonal changes of vegetation (Tucker et al., 1985). For tropical Africa, the NDVI integrated over the growing season is highly correlated with the ground-observed total dry biomass production of natural vegetation (Tucker et al., 1983).

The Outgoing Long wave Radiation (OLR) observed since 1974 has been invaluable in the study of meteorological phenomena, both over land and ocean. OLR is a measure of energy leaving the top of the earth's atmosphere in the form of thermal radiation. The OLR data also bridge a wide gap in conventional meteorological data over large remote land and oceanic areas. Because of relatively high and stable surface temperature over the tropics, OLR variations are related to changes in the distribution of cloudiness and precipitation (Arkin et al., 1989).

In the tropics, cloud top temperatures largely modulate OLR. Regions of intense convection in the tropics appear as regions of low OLR, whereas cloud free regions appear as regions of high OLR. These properties of OLR data make them extremely useful in monitoring and understanding tropical climate variability reflecting both dry and wet extremes quite well. Low (high) values of OLR indicate greater (less) cloudiness and hence increased (decreased) depth of cumulus convection. It should be noted that high clouds can produce identical OLR signature as convective clouds, while substantially different productions of rainfall occur between the two types of clouds (Lyons, 1990).

The measurement of rainfall in the tropics is difficult due to its great spatial variability and the fact that a large proportion of tropical rainfall occurs over inaccessible areas such as tropical Oceans, forests and mountain ranges. Accordingly, there has been much interest in satellite-based estimations of

tropical rainfall and their use in the development of tropical rainfall climatologies at a variety of temporal and spatial scales.

Satellite remote sensing offers a number of advantages over conventional methods for generating information on natural resources. Satellites provide a means of extracting data for any point regardless of country boundaries, and inhospitable conditions. Furthermore, by using a single source of data, the errors of sampling and calibration are maintained at a uniform level for every point. The concept of obtaining multi-spectral data has become a reality with operational satellite remote sensing. The ability of satellites to provide synoptic observations over large areas in a timely and objective manner, and to provide reliable and flexible means for speedy communications, undoubtedly makes them indispensable tools in the public weather services (Porc'u et al., 1999).

Weather and climate have pervasive influences on human activities. Consequently, weather information, forecasts and warnings along with climatological and hydrological data analyses have a very broad range of applications. Their products and services can significantly improve public safety and be of enormous socio-economic benefit if properly understood and acted upon. Improved knowledge on climate-weather interactions can be used in the planning of agricultural, health, water resource management, industrial, transport, town planning, communication, and tourism activities.

On-going developments in science and technology in the utilization of satellite data continue to enhance short to medium range forecasting as well as seasonal to annual time-scale climatological predictions. With the advent of internet data exchange, an individual does not need a satellite receiver to monitor the earth. However there are many situations in which a broader overview at high resolution is needed. The low cost and availability of remotely sensed data make satellite retrieved data set an ideal tool and the necessary compliment to ground based measurements.

1.1.2. Motivation

Rainfall is the climatic factor of maximum significance for tropical African countries, with extreme drought and flood often associated with food, energy and water shortages, loss of life, and property, and many other social economic disruptions (Indeje *et al.*, 2000). The economies of tropical African countries largely depend on agriculture, which is highly vulnerable to the amount and distribution of rainfall. The efforts to achieve food security in most parts of the African continent have been long hampered by civil volatility, pressure of international trade, rapid population growth, floods and droughts. Although natural events cannot be controlled, there are prospects for rainfall prediction in tropical Africa (Dyer, 1981).

Accurate intra-seasonal, seasonal to inter-annual climate monitoring and forecasting could therefore contribute to improved planning and management of climate sensitive activities, involving agricultural and water resource, hydroelectric power supply, tourism, fire and spread of diseases such as malaria. Climate information is also helpful in the design of urban infrastructure such as construction of roads, storm water routing and others that are linked to climate variability.

Rainfall variability has a major impact on national economies. Large gaps exist in our understanding of many features of tropical African climate, including the role of continental convection, the seasonal and intra-seasonal cycles, and tropospheric jet streams. This has been due to the limitations of data availability in many parts of tropical Africa where conventional observations are scarce.

This research will depend on satellite-retrieved data sets to study spatial and temporal rainfall variability at seasonal and intra-seasonal time scales. Calibration and validation of satellite rainfall data over a part of the study region will provide a basis for assessing their accuracy and reliability. It is hoped that the

study will improve our understanding of intra-seasonal rainfall variability and reduce the related risks.

1.1.3 Objectives of the study

Rainfall variability is a major stakeholder in the economies of tropical African countries. Agriculture depends mainly on rainfall in most parts of the region. Understanding the temporal and spatial variability of rainfall at different time scales can provide useful guidance to policy makers for sustainable management of resources. Therefore the main objectives of this study are to;

- Identify major seasonal and intra-seasonal patterns of satellite rainfall variability over tropical Africa.
- Investigate the influence of zonal wind in relation to intra-seasonal convection over the study region.
- Investigate the evolution and propagation characteristics of the intra-seasonal oscillations over tropical Africa.
- Calibration and validation of satellite rainfall estimates over Uganda to assess their accuracy and reliability.
- Based on the above, recommend observational strategies to enhance the rainfall observing network over tropical Africa with particular attention to gaps in the Angola-Congo-Sudan axis.

1.1.4 Study area

The study area stretches from 15°S to 15°N in tropical Africa (figure 1.1). It covers tropical Africa and the neighbouring east Atlantic and west Indian Oceans.

1.1.5 Some aspects of climate of tropical Africa

The weather and climate of tropical Africa is influenced by a number of factors. They include the tropical rain forest of central Africa; the existence of many large inland lakes, rift valleys, snow capped mountains on the equator, extensive low-lying swampy land and tall mountains like Kilimanjaro. The Congo basin is a significant region of seasonally modulated deep moist convection. Locally heavy rainfall events are a common occurrence that feed agriculture in the region's periphery (McGregor and Niewolt, 1998). The Inter tropical convergence zone (ITCZ), the adjacent Indian and Atlantic Oceans, the monsoon, sea surface temperatures, and the African jet streams play an important role in the modulation of tropical African climate (Matitu, 2002).

Over equatorial Africa, the main process causing rainfall is convection, however seasonal variations are mainly as a result of large air mass movements (McGregor and Niewolt, 1998). Hadley cell overturning plays a prominent role in the development of convection. Upward motion is greatest over the Congo basin and shifts according to the solar angle (Yeshanew, 2003). Over the Congo basin, convergence between air masses from west and east cause maximum rainfall during June/September, when the main zone of convergence is over this region (Griffiths, 1972).

East Africa has relatively low rainfall with a complicated distribution pattern showing a general increase from north to south. The main reason for the aridity is the monsoon system, which prevails over east Africa during a large part of the year (Asnani, 1993). The main source of rainfall over east Africa is the ITCZ that follows the latitudinal position of the sun with a time lag of about 4-6 weeks. Over most of east Africa there are two rainy seasons; the long rains around March to May and the short rains around September to November. However the mountainous nature of much of east Africa causes many departures from this general pattern and over some areas trimodal or unimodal rainfall prevails.

Rainfall variability in east Africa is generally high and the arrivals of the rainy seasons differ from year to year (Mutai et al., 1998).

1.1.6 Uganda and its climate

Uganda is located in east Africa and lies between latitude 1° 30′ S, 4° N and longitude 29° 30′ E, 35° E. It occupies an area of about $2.4x10^5$ km^2 of which 15.3% is open water, 3% permanent wetlands, and 9.4% seasonal wetlands. It is also characterized by flat topped hills in the central and western parts of the country (UNEMA, 2000).

It's climate is influenced by various factors which include, ITCZ, Lake Victoria, the Arabian ridge, sea surface temperatures, the Mascarine high, St. Helena high, Congo air mass, and topography among others. The distribution of rainfall through the year is bimodal over most areas with the first season from March to May and a second season from September to November, which are associated with the movement of the ITCZ. However, there are variations in this general pattern due to a number of factors mentioned above. For example there is a noticeable difference between the western and eastern half of the country in the amount of rainfall received in the two peaks. The western half usually receives more rainfall from August to November and the eastern half from the beginning of March (Morgan, 1982).

Uganda's economy depends mainly on rain fed agriculture, which employs 80% of the work force. The failure of rain therefore can lead to serious socio-economic hardship famine and economic decline. Satellite rainfall estimates are of great importance in mitigating the effects of rainfall excesses and deficits in many parts of the world. Estimates for periods of a week or 10 days can be used to identify areas of low rainfall which may lead to crop shortfalls, while estimates at a daily or shorter times are essential for driving rainfall run-off models used for flood forecasting and river management (Grimes, 1999). Rain gauges have been the

main source of rainfall data in Uganda, unfortunately their distribution are sparse for monitoring such a key variable parameter and therefore calibration of satellite rainfall estimates is most appropriate in this regard.

1.1.7 Role of Topography and vegetation on Circulation

The topography of tropical Africa (figure 1.2) contains a complex array of mountains, lakes and rift valleys, which combine with the size and shape of the continent to create a unique climatic setting. Orography plays an important role and rainfall generally increases with altitude, river basins such as the Congo's influence on circulation and modification of climates both local and remote. Another feature is the role of the east African highlands that recurve the boreal summer circulation (Findlater, 1971). Other mountains that play a major role include the Ethiopian highlands and the eastern escarpment. These areas generate high rainfall, hence diabatic forcing of regional climate (Semazzi et al., 1993).

Vegetation, along with other characteristics of the land surface, plays a key role in modulating the earth's water cycle. Vegetation is a dynamic state variable of the climate system, not just an indicator of climate state. Vegetation cover affects precipitation. During cloud-free daytime conditions, the partitioning of absorbed radiative energy into sensible and latent heat, affect heat fluxes near the ground surface. On bare dry land, this results in a strong heating of the surface, a strong sensible heat flux in the atmospheric surface layer and a large soil heat flux. Moisture fluxes are limited. In wet/vegetated land the incoming radiation is mostly converted to evaporation. In that case, the sensible heat flux and the soil heat flux is much smaller than the latent heat flux. Such differences lead to significantly different atmospheric boundary layers above bare and vegetated land. Weak ascent may produce rainfall for example over the Congo basin.

1.1.8 Problems of Surface Rainfall Measurements

Rainfall is a notorious difficult parameter to evaluate satisfactorily because of its high spatial and temporal variability. Rainfall can vary in both space and time over distances less than 100 km in a matter of minutes by orders of magnitude of intensity (Bellerby and Barret, 1993). At the other extreme, because gradients of intensity can also be quite shallow, it is often difficult for any surface based spatial analysis (whether gauge network, radar or visual observation) to determine rain /no rain boundaries with confidence.

Historically, rain gauges have been the main source of rainfall data. For global weather forecasting purposes rainfall is measured by rain gauges, whose data are circulated via the Global Telecommunication System (GTS) of the World Meteorological Organization (WMO). For climate purposes supplementary rain gauge networks are operated in most countries of the world, though typically by more than one environmental monitoring agency causing problems when attempts are made to collect data for best possible rainfall analysis.

More recently, radar has played an increasingly important role in technologically developed countries, particularly with regard to the provision of data used locally or regionally for very short term forecasting activities (real time) and related research. (Grimes et al.1999). However in many parts of the world such as Africa, the rain gauge network (figure 1.3) is too sparse to produce reliable estimates, and a radar is not feasible either on grounds of cost, technological infrastructure or topography.

This problem has been partially solved by the use of rainfall estimation algorithms based on satellite imagery (figure 1.4). The estimation of rainfall rate over land and sea by satellite remote sensing has become an increasingly important tool in climate and weather studies. The bird's-eye view of the satellite can therefore contribute greatly towards rainfall monitoring over the entire globe.

1.2.1 Rainfall variability over tropical Africa

The monsoon circulation extending across large parts of the Atlantic and Indian Oceans has a great impact on tropical African rainfall particularly on the seasonal time scale. Low level winds corresponding to the seasonal maxima of the monsoon circulation indicate that from November to March, the NE monsoon sweeps across the west Indian Ocean delivering moisture to south and east Africa. In the May-September period the Indian SW monsoon diverts moisture away from eastern Africa, yet the Atlantic SW monsoon brings moisture across the Guinea coast of West Africa to feed synoptic disturbances (Asnani, 1993).

The El Niño-Southern Oscillation (ENSO) phase via east-west SST differences and a corresponding Walker circulation (Goddard and Graham, 1999) modulate the cross-equatorial NE flow in austral summer. During warm phase, the NE monsoon initially strengthens in the east, then recurves over the western basin, thereby regulating the flow of moisture to eastern and southern Africa (Ogallo, 1988). Both monsoon systems are dependent on meridional thermal gradients and are modulated by large-scale features such as the ENSO, which largely act on the zonal plane.

The global ENSO warm events most often influence rainfall east and south of the Congo basin during the austral spring and summer, respectively, as part of a seasonally dependent response (Meehl, 1988). A strengthening of upper westerly flow throughout the region during warm events, results in a concomitant decline (increase) in moisture confluence over southern (eastern) Africa (Hastenrath et al., 1995).

Strong relationships between East Africa seasonal rainfall and an east-west dipole pattern across the Indian Ocean which is controlled by the Southern Oscillation (SO) has been observed, particularly for the coastal region during the October-December period (Hastenrath, 1995). Warm (cold) water anomalies in

the western Indian Ocean during low (high) phase of the SO, enhance (suppress) convection. Rainfall anomalies over the coastal regions of east Africa in the March-May long rainy season are positively correlated with SST anomalies over the Arabian Sea and the tropical Indian Ocean.

Over the equatorial Atlantic, deep convection is confined to a narrow region that spans the entire ocean. This region of inter-tropical convergence overlies maximum SST, generally north of the equator and is associated with moisture flux convergence and latent heat release in the lower troposphere. South of the equator southeasterly trades are strong and steady. In the Gulf of Guinea winds are more meridional and rotate clockwise towards Africa. This turning of the wind modulates the spatial distribution of tropical African rainfall (Asnani, 1993).

Matari (2003) observed that over the Congo, axes of upward motion from the continental source extend southeastward during the austral summer to the Indian ITCZ and westward to the Atlantic ITCZ in boreal summer. Over the Atlantic the vertical structure reveals lower westerly / upper easterly flow. However over the equatorial Indian Ocean in the December to February season, the westerly flow is deep and the upper easterlies are weak. Along the West African coast in the June to August season, the westerlies are shallow and upper easterlies develop as two jets.

The ITCZ in the Atlantic experiences a large seasonal migration, reaching 14°N over western Africa in August. It is furthest south in March near the equator. The seasonal changes in the wind in the western Atlantic induce an equatorial wave guide response which enables changes in slope of the thermocline. Kelvin waves have been observed at seasonal frequencies to propagate eastward to the Angola dome and Gulf of Guinea (McGregor and Nieuwolt, 1998).

Some regions of tropical Africa have their own distinctive rain bearing systems. For example, during boreal Autumn, disturbances can form in near-surface

westerlies across equatorial Africa, bringing heavy rain to equatorial and eastern Africa. In Southern Africa, a cloud band emanating from the Congo linked with a higher latitude trough, is one of the circulation patterns most favorable for rain across the sub-region (Jury and Pathack 1993). This leads to a zone of convergence and cloudiness that will extend from the tropics to midlatitudes oriented northwest to southeast.

Most rainfall in tropical Africa results from organized convection. While critical to the climate processes in tropical Africa, the physics and dynamics of the different types of systems has received very little attention. Within tropical Africa, knowledge on the descriptive nature of the systems exists, but has not been widely published. Therefore this study will also consider rainfall variability at intra-seasonal time-scale to bridge the gap of our understanding of tropical convection. Attempts have been made to study the intra-seasonal oscillations over tropical Africa by Kabanda (1995); Mpeta (1997); Mutai and Ward (2001); Mpeta and Jury (2001) and Tennant and Hewitson (2002). A review of research that has been done on tropical intra-seasonal oscillations follows in the next section.

1.2.2 Intra-seasonal Oscillation research

The intra-seasonal oscillation is a major component of low-frequency variations of tropical general circulation and has drawn much attention in the last decade. These are oscillations in the atmosphere with periods longer than synoptic scale but shorter than the seasonal time scale and were first observed by Madden and Julian (1971). They described the oscillations as a large-scale eastward propagating zonal circulation cell along the equator. They noticed coherence between surface pressure, zonal winds and temperature at various levels with a period from 40 to 50 days.

Recent work on intra-seasonal convective structure and evolution over tropical East Africa by Mpeta and Jury (2001) using pentad Outgoing Long wave Radiation (1979 to 1994) found most significant spectral energy concentration in periods of 16 to 33 days. Hovmoller diagrams revealed eastward (62%), westward (11%) and quasi-stationary (27%) convective features. They also found that deep convection events are associated with an initial influx of northeasterly Indian monsoon flow followed by increased westerlies from the Guinea/Congo region.

An investigation of the East African rainfall and tropical circulation/convection on intra-seasonal to inter-annual time scales was carried out by Mutai and Ward (2000). 5-10 days before the rainfall event, low level westerlies start to develop in the equatorial Atlantic. These penetrate across equatorial Africa and into eastern Africa. Five days after the rainfall event, upper level divergence shifts into the Indian Ocean and resembles the Madden Julian Oscillation.

Using 200 hPa velocity potential data Michele (1999) showed evidence of the oscillation outside of the Indian /Pacific Oceans. Areas of activity were found in Africa and south/central America. Vincent et al. (1991) examined the intra-seasonal (40-50) day oscillation in convection over the tropical southern Hemisphere (0°-15°S) using velocity potential at 200hpa and OLR. They found spectral peaks at 33 and 50-67 days in the data. Intra-seasonal oscillations propagated eastward. They also found that a dynamic wave could be followed continuously around the world, but the convection (OLR) associated with the intra-seasonal oscillation was weak and difficult to track.

Rui and Wang (1990) investigated the development and dynamical structure of intra-seasonal low frequency convection anomalies in the equatorial region. They found an initiation stage over equatorial Africa whilst rapid intensification is in the Indian Ocean. The lower level convergence leads convection and mid-tropospheric upward motion by about 30° longitude in the development phase.

Equatorial upper (lower) level easterly (westerly) anomalies and associated twin anomalous anticyclonic (cyclonic) circulation anomalies couple with equatorial convection anomalies.

Composite intra-seasonal oscillation life cycle studies suggest that the equatorial Indian Ocean is the most favorable geographical location for the development of low frequency convection anomalies (Chen and Tzeng, 1990). Besides the warm ocean surface conditions, the interaction between Walker circulation and transient intra-seasonal disturbances and the interaction between monsoon circulation and equatorial intra-seasonal mode may be important factors in determining favored locations for convective development.

While investigating the intra-seasonal propagation characteristics, Zhang and Hendon (1996) demonstrated that no dominant standing oscillation could be identified in tropical convection. Instead intra-seasonal variability of convection is dominated by an eastward propagation mode. The propagation component accounts for almost all of the convective variance that is coherent with the eastward propagating disturbance in the zonal wind.

Jury et al. (1991) noted a westward movement of large convective elements in the 10°-20°S latitude band of the southwest Indian Ocean during the southern summer in the southwest Indian Ocean. The study revealed climatological features, including zonal propagation speeds for maritime systems in the range 2-4 m s^{-1}. Transient convective waves over the tropical southwestern Indian ocean are slower and diverse. A wet summer over southeast Africa corresponds with an increased frequency of westward moving convective systems, whereas in a dry summer the convective systems tend to be quasi-stationary. Upper level extra-tropical westerlies are stronger then.

Owing to the sparse distribution of conventional observations over much of tropical Africa, the aforementioned investigations and objectives are achievable

using regular satellite measurements suitably averaged and interpolate. Satellite data cover a sufficient period of time (late –1970's onwards) to enable an objective analysis. Its gridded formats and near continuous record makes it more preferable to the scanty conventional data sets. A calibration and validation process will be carried out for rainfall over Uganda to ascertain the accuracy of satellite-retrieved data sets. Satellite rainfall estimation algorithms used by other researchers for producing rainfall estimates over tropical Africa will also be discussed.

1.2.3 Satellite Rainfall estimation.

Precipitation plays a crucial role in the earth's global climate system, especially in the tropics where the resulting release of latent heat is the main source of energy for driving large-scale atmospheric motions. Knowledge of the amount of regional rainfall is essential to the welfare of society. Rainfall also drives the hydrological cycle, and to improve weather and climate predictions, an accurate global coverage of rainfall records is necessary (Tait et al., 1999). The rain gauge network is sparse especially in tropical Africa hence satellite technology can play a major role in rainfall monitoring over the region.

Satellite rainfall methods seek to identify areas of probable precipitation through the recognition of the most likely rain/no rain boundaries, evaluation of associated rain rates and the estimation of the accumulated rainfall for a given area (Tait et al., 1999). In order to achieve appropriate results, analyses are often made of satellite data along with surface (rain gauge and /or radar data) for algorithm calibration. Often the results will later be compared with independent sets of surface data for algorithm validation (Dugdale, 1994). Several algorithms have been developed basing on Visible/Infrared (VIS/IR) and Microwave (MW) images in the hope of producing reliable rainfall estimates.

The basic physical principal in the VIS region of the spectrum is that cloud brightness is an indicator of cloud thickness, and this in turn is an indicator of rainfall. Unfortunately, not all bright clouds precipitate. On the other hand, the thermal IR physical principal is that cloud top temperature is a function of cloud top height, and that higher and colder cloud tops evidence thicker clouds which are more likely to rain. However, not all cold clouds precipitate, nor does rain always fall only from cold clouds (Barret, 1970).

Attempts to combine the different yet complimentary evidences of VIS and IR data were then made with considerable success (Austin, 1979), though practical problems arise with such methods because the VIS data are available for only part of the 24 hour day. The advantage of such an approach is that by using VIS and IR data together it is possible to screen out clouds which are cold but not highly reflective (for example thin cirrus), and those which are reflective but warm (for example stratocumulus).

The problems of diurnal coverage in the VIS region of the spectrum has ensured that most of the more widely used satellite rainfall algorithms are based on IR data only, in conjunction with one or more types of surface data. Increasingly more sophisticated approaches have been developed to supplement the basic pixel temperature information. For example, analyses of cold cloud growth rates, cold cloud duration, and cloud top textural information help discriminate between cirrus (which rains gently or not at all) and convective tower clouds (which rain very heavily) (Adler and Negri, 1988).

Microwave (MW) channel provides a more direct approach to rainfall estimation. MW radiation measures either the scattering of high frequency radiation by hydrometors or the emission of low-frequency radiation by raindrops. The technique is based on the fact that MW radiation at frequencies below 30GHZ are absorbed/emitted by liquid raindrops while higher frequencies are scattered by ice crystals and raindrops (Spencer et al., 1997). MW radiation from the

surface depends on the angle of view, the surface emissivity and the frequency of the radiation being detected. Oceans have greater reflectivity and thus lower emissivity than land surfaces. Moreover the emissivity of marine surfaces is near constant while changes in emmisivity of land surfaces is highly variable. Therefore MW rainfall estimation is more readily carried out over ocean surfaces without problems; however, estimation is adversely affected over land surfaces (Morland et al., 1997). The low temporal resolution (1-2 images per day) and spatial resolution (at least 10 km) of MW sensors makes the application of this technique difficult for continuous monitoring of variable rainfall (Barret and Beaumont, 1994).

The Special Sensor MW Image (SSM/I) instruments have stimulated interest in satellite rainfall monitoring in the passive MW since 1987. They usually look at emission /absorption, scattering properties of rain or the combination of both. The arrival of the SSM/I sensor increased the scope for rainfall detection, and many of the new algorithms using SSM/I data have used radars to provide calibrations/validation data (Barret and Beaumont, 1994).

Although rainfall monitoring was expected to be significantly improved by the SSM/I, the spatial resolution of passive MW sensors has been relatively low compared with those of most VIS and IR sensors. Its spatial resolution is about 15 km. The MW sensors have flown only on low- earth orbiters and their swath widths have supported less than two imaging overpasses per day below about 55° latitude. Therefore, the past and present uses of the passive MW data for rainfall measurements have been mainly climatological rather than meteorological. However, there is increasing interest in the use of VIS, IR and passive MW data, where the latter are useful for initializing models and calibrating geostationary based VIS and IR rainfall algorithms (Adler, 1990).

TRMM (Tropical Rainfall Measuring Mission), a joint U.S/Japan satellite project is also dedicated to observing and understanding the tropical rainfall and how it

affects the global climate. The satellite was specifically designed to provide more accurate rainfall estimates and vertical latent heating profiles. The primary instruments for measuring precipitation are the Precipitation Radar (PR), the TRMM Microwave Imager (TMI), Visible and Infrared Scanner (VIRS) (Rouault, 2001). One of its most important features is the ability to provide vertical profiles of reflectivity. TMI provides quantitative rainfall by measuring the minute amounts of MW energy emitted by the earth and the atmosphere. TMI quantifies the water vapor, the cloud cover, and rainfall intensity in the atmosphere.

The basis of measuring rainfall with MW is in Planck's radiation law, which describes how much energy a body radiates given its temperature (Nesbitt and Zipser, 2000). Raindrops appear to have a temperature that equals their real temperature. They appear warm to a passive MW radiometer and therefore offer a contrast against cold water surfaces (the more raindrops, the warmer the whole scene appears).

On land there is little contrast to observe the warm rain drops, however, the high frequency microwaves (85.5GHz) measured by TMI are strongly scattered by ice present in many raining clouds. This reduces the MW signal at the satellite and offers a contrast against the warm land background. The VIRS has the ability to delineate rainfall from brightness or temperatures of the clouds, however it cannot discriminate between the high cold cirrus and the rain giving convective clouds. It also tends to underestimate rainfall from warm clouds. Therefore improved rainfall estimates are obtained by comparing the VIRS observations on the TRMM with the rainfall estimates of TMI and precipitation radar (Rouault, 2001).

More recently, the launch of the Meteosat Second Generation (MSG) in August 2002 by the European Space Agency (ESA) is seen as a big step in the history of satellite meteorology. MSG carries a new radiometer, the Spinning Enhanced Visible and Infrared Imager (SEVIRI) and in addition to these, is the

Geostationary Earth Radiation Budget (GERB) instrument. The GERB will provide valuable data on reflected solar radiation and thermal radiation emitted by the earth and atmosphere. It's high temporal (fifteen-minute cycle of imaging) and spatial (1km) resolution will significantly improve the accuracy in forecasting severe weather such as thunderstorms, heavy rain, snow or fog.

1.3 Summary and Outline

The main aim of this chapter was to provide a motivation and historical background for this research. The main objectives have been given and previous related work has been discussed to provide a basis for this research. The outline of the thesis is as follows:

Chapter two describes the data, sources and the methods used in this study. Chapter three provides the mean circulation of the study area; the time and space variability of seasonal rainfall is also discussed. Evidence for intra-seasonal oscillations in satellite-derived rainfall, OLR and zonal wind over tropical Africa and its adjacent Oceans is presented in chapter four, while chapter five deals with the evolution and propagation characteristics of the Intra-seasonal oscillations. Satellite rainfall estimation and validation are covered in chapter six, whereas chapter seven elaborates on the data availability over tropical Africa and outlines some of the observational strategies to enhance the observing network over the region. The conclusions and recommendations are presented in chapter seven.

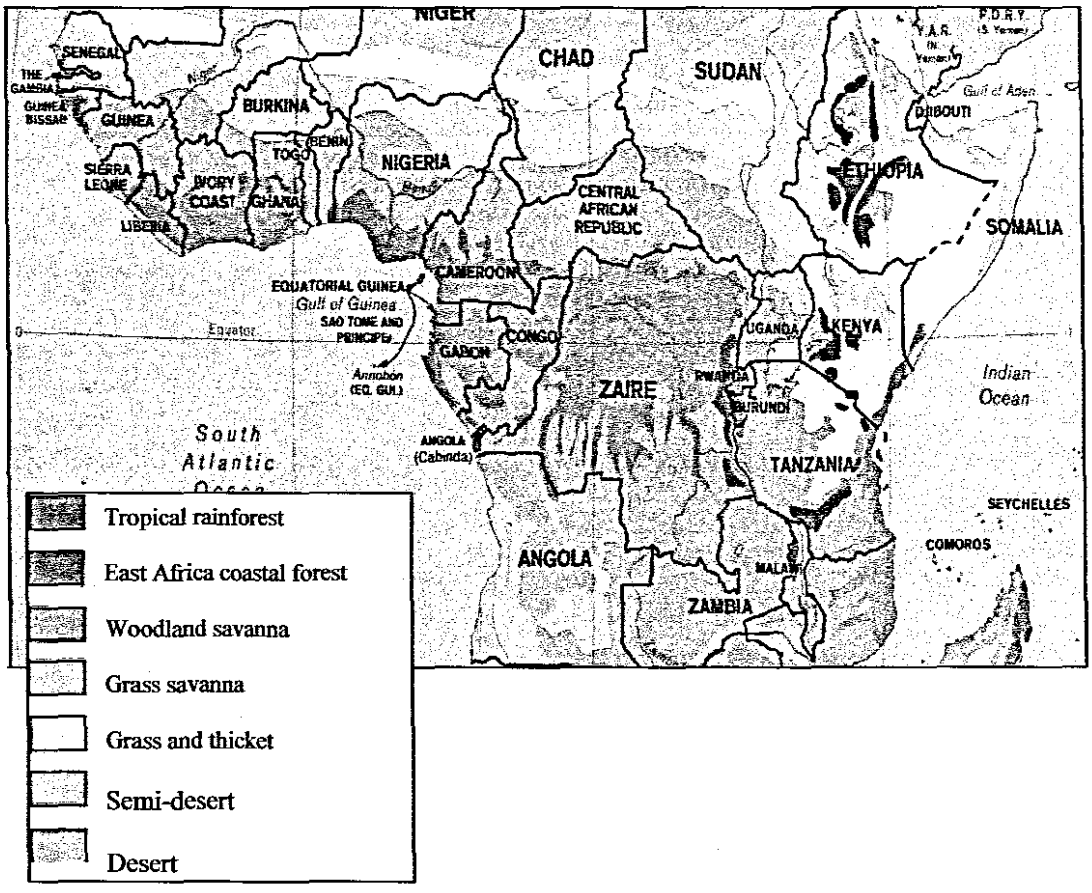

Figure 1.1 shows the study area and the nature of vegetation over this region. The Congo basin is characterized by the evergreen tropical rainforest (taken from Azimuthal Equal-Area Projection).

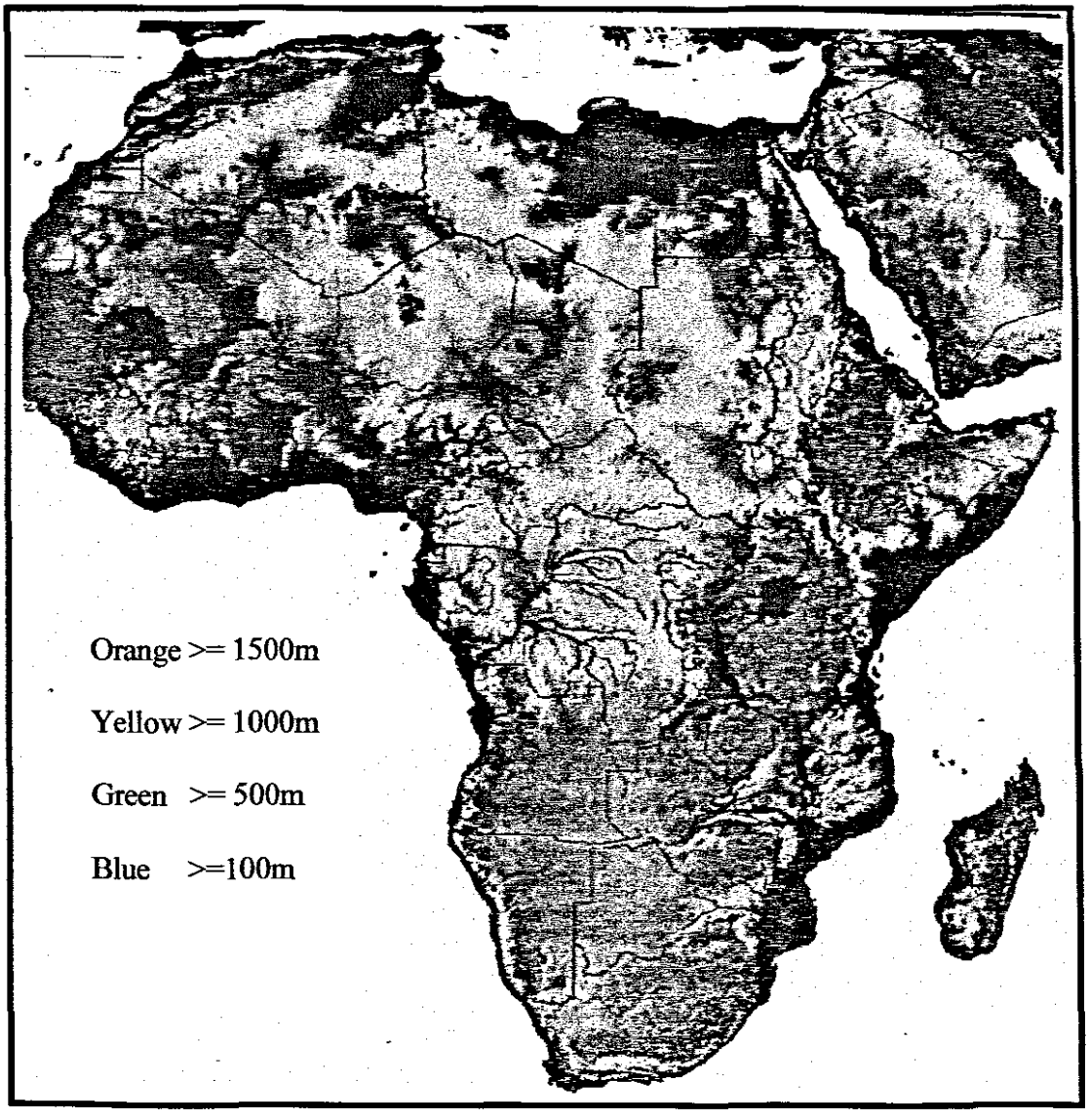

Figure. 1.2 is a relief map of Africa showing rivers. Topographic heights are given by colors.

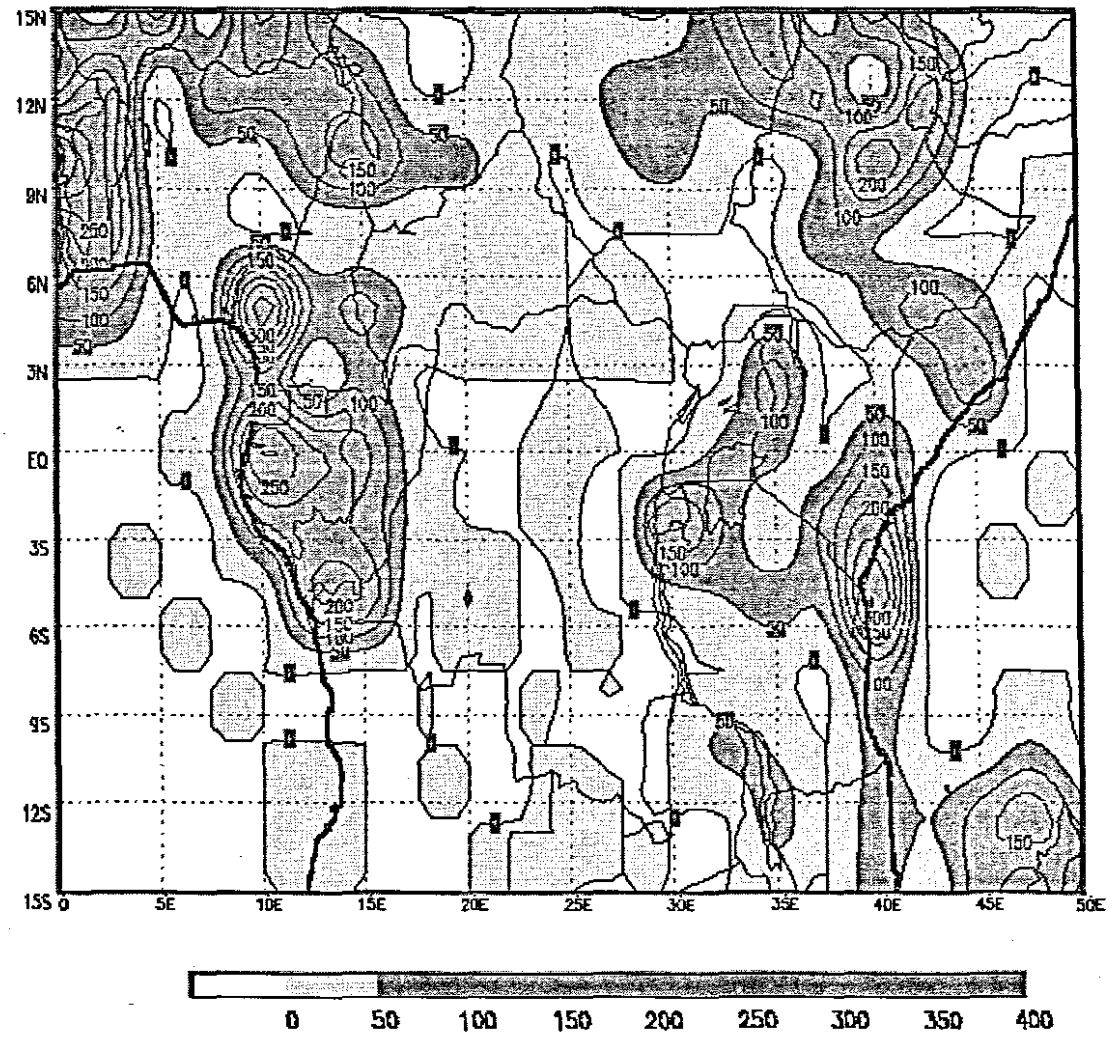

Figure 1.3 shows the rain gauge density per 2.5° x 2.5° grid box for the year 1998 over equatorial Africa. The above figure portrays a scarce distribution of gauges over Angola, Congo and Sudan axis. Rain gauges range from 0 to 50 over a 2.5°x 2.5°grid box. Such a network is insufficient in monitoring rainfall that vary greatly in both space and time (source of map: http://wesley.wwb.noaa.gov)

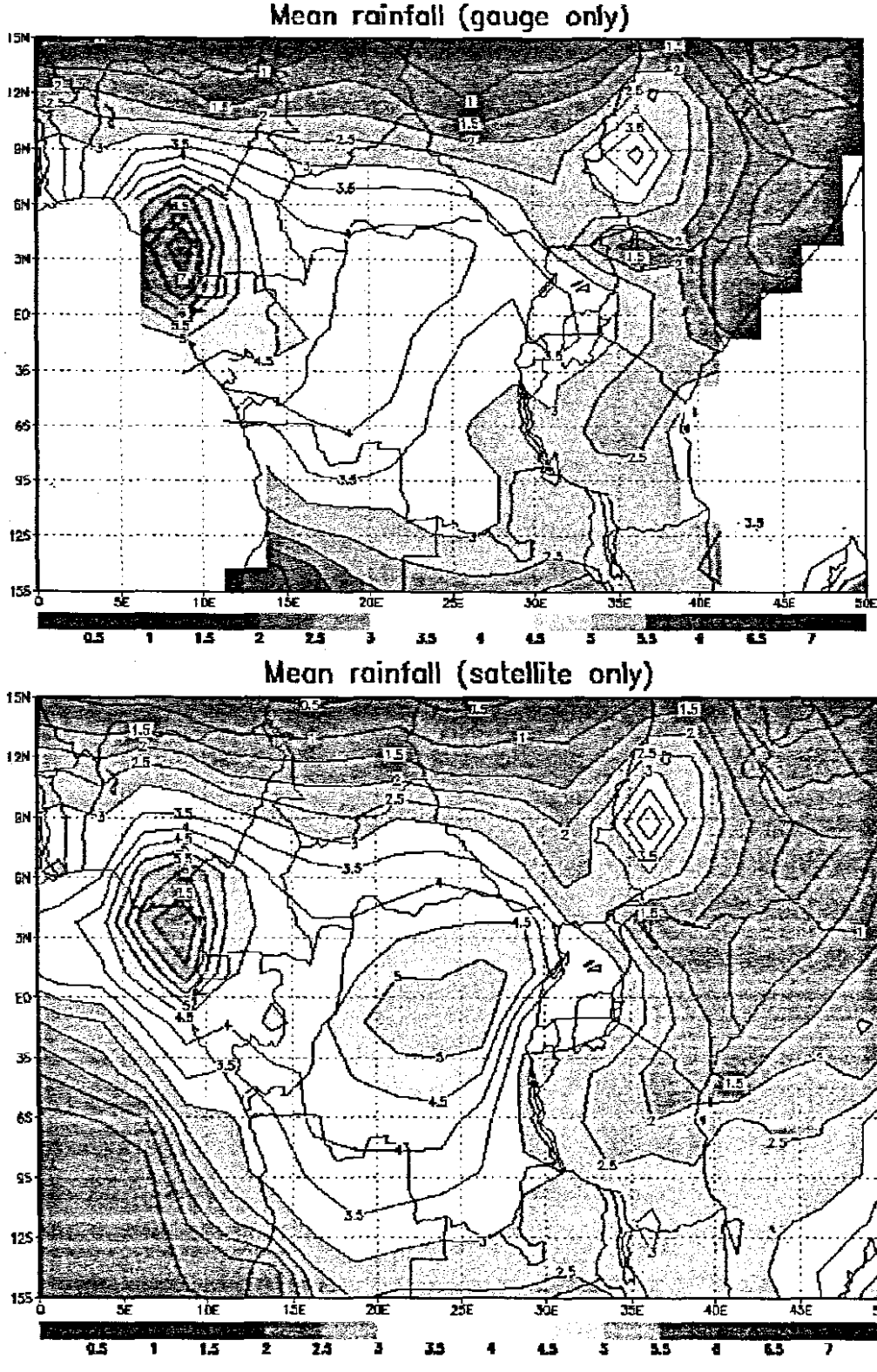

Figure 1.4 Comparison of gauge and satellite rainfall measurements over the study region. The satellites estimate much higher rainfall over the eastern Congo, where observing infrastructure is limited.

Chapter Two

Data and Methodology

2.1 Data

Data that has been used in this study was obtained from the following sources: the Climate Prediction Center (CPC), the National Center for Environmental Prediction (NCEP), the Uganda Meteorological Department and the Tropical Application of Meteorological Satellites (TAMSAT). Detailed discussion of the data sets follow in the next section.

2.1.1 Climate prediction center (CPC) Merged Analysis of Precipitation (CMAP)

Pentad rainfall data was obtained from the Climate Prediction Center (CPC). The CPC Merged Analysis of Precipitation (CMAP) is a technique which produces pentad and monthly analyses of global precipitation in which observations from rain gauges are merged with precipitation estimates from several satellite-based algorithms (infrared and microwave) (Xie and Arkin, 1997). The analyses are on a 2.5° x 2.5° latitude/longitude grid and extend back to 1979. It is important to note that the input data sources to make these analyses are not constant throughout the period of record. For example, SSM/I (passive microwave - scattering and emission) data became available in July of 1987; prior to that the only microwave-derived estimates available are from the Microwave sounding Unit (MSU) algorithm which is emission-based thus precipitation estimates are available only over oceanic areas. Furthermore, high temporal resolution IR data from geo-stationary satellites (every 3-hr) became available during 1986; prior to that, estimates from the OPI technique (Xie and Arkin, 1997) are used based on OLR from polar orbiting satellites.

Briefly, the merging technique is a two-step process. The random error is reduced by linearly combining the satellite estimates using the maximum

likelihood method. Over global land areas the random error is defined for each time period and grid location by comparing the data source with the rain gauge analysis over the surrounding area. Over oceans, the random error is defined by comparing the data sources with the rain gauge observations over certain islands. Bias is reduced when the data sources are blended using the blending technique of Reynolds (1988). The satellite data define the "shape" of the precipitation field and the rain gauge data constrain the amplitude.

2.1.2 NCEP/NCAR data

The National Centre for Environmental Prediction (NCEP) and the National Centre for Atmospheric Research (NCAR) re-analysis project that began in 1991 produces daily atmospheric and surface fields considered to be an optimal estimate of the evolving state of the atmosphere (Kalnay et al., 1996). It has been argued that some fields such as upper air mass velocity and temperature fields are generally well defined by satellite, ship and land based observations. Given the statistical interpolation, representation of physics, and first guess assimilation techniques, numerical models provide an estimate of the state of the atmosphere better than would be obtained using observations alone.

The project was initiated to produce global analysis of atmospheric fields in support of needs of the atmospheric research and climate monitoring communities. The project uses a state-of-the-art global data assimilation system and a database as complete as possible. Different countries and organizations have contributed observational data not available in real time.

Parameter	Level	Units
Zonal Wind	700hPa and 200hPa	$m\ s^{-1}$
Vertical Motion (Omega)	500hPa	$Pascal\ s^{-1}$
Velocity Potential	200hPa	$m^2\ s^{-1}$
Specific Humidity	500hPa	$g\ kg^{-1}$
Outgoing Longwave Radiation	Surface emission	$W\ m^{-2}$

Table 2.1 gives the summary of the NCEP data used in this study

2.1.3 Outgoing long wave radiation (OLR)

The term "outgoing long wave radiation" refers to the sum total of all the long wave electromagnetic energy, or infrared radiation at wavelengths ranging from 5 to 100 micrometers, that escapes from the top of the earth's atmosphere back into space. The sensitivity of OLR at the top of the atmosphere to small changes in convective cloudiness provides a good estimate of relative changes in the distribution of heat sources and sinks in the tropical atmosphere, and associated vertical motion and precipitation (Gill, 1980). OLR data is observed from the AVHRR instrument aboard the NOAA polar orbiting spacecraft. These data are available as twice-daily observations from NOAA satellites in the form of pentad means, pentad anomalies and monthly means on a 2.5° x 2.5° latitude/longitude grid. Daily OLR data from January 1979 to present are available at the Climate Diagnostic Center web site.

OLR data has been used as a proxy for cumulus convection/cloud variability over convectively active regions of the tropics by Prasad et al (2000), Jury (1997) and many others. Low (high) values of OLR indicate greater (less) cloudiness and hence increased (decreased) depth of cumulus convection. Caution should be exercised when interpreting OLR as convection/rainfall, since thick, high clouds can produce an identical OLR signature to convective clouds, while substantially different rainfall can occur between the two types of clouds (Lyons, 1990)

2.1.4 Cold Cloud Duration data

Dekadal Cold Cloud Duration (CCD) data for Uganda at thresholds -30, -40, -50, -60 (°C) for the period 1993-2000 were obtained from the Tropical Application of Meteorological Satellite (TAMSAT) group, University of Reading, UK. CCD is defined as the length of time during which the temperature at a given location (pixel) is below a given temperature threshold.

Thermal infrared (TIR) data are acquired in real time using Autosat software and the CCD images are produced using the TAMSAT rainfall estimation software (TRES) normally running under the Meteosat Operations Manager (MOM) (Milford et al., 1994). The TIR images are transmitted by METEOSAT every 30 minutes. It is from these that CCD images are derived. METEOSAT raw TIR images are in the form of radiometer counts that are related to the radiance of the observed surface by the following equation: $L=\alpha(C-C_o)$... (1)
Where L is radiance and C is the radiometer count. α and C_o are calibration coefficients which depend on the radiometer. To allow for calibration drift, the values of α and C_o are adjusted with the calibration system on the satellite and transmitted with the imagery. EUMETSAT provides fitted equations relating radiance to brightness temperatures of the form: $L= \exp. (A+(B/T))$... (2)
The values of A and B depend on the radiometer used. T is brightness temperature. (1) and (2) are combined to obtain an equation relating temperatures to digital counts or digital counts to temperature for any date and METEOSAT satellite. To apply these equations, it is important to know which METEOSAT satellite the data come from (for the correct A and B coefficients) and the date (to know the value of the calibration coefficients α, C_o).

For generation of dekadal CCD images, a temperature threshold (T_t) is selected which is converted to a radiometer count via the calibration relationship. Each TIR image is then used to derive a secondary image in which a pixel has the value 1 if the count in the corresponding pixel in the TIR image is less than T_t,

and zero if TIR counts is greater than T_t. The secondary image is a boolean image or a mask image whose pixel values take only the values 1 and 0. The thresholding is repeated for 24-hourly TIR images to obtain 24-boolean images. The 24 boolean images are added up to give the daily CCD image in half hour units or slots. Each pixel value is the number of hours that the pixel's temperature was below the threshold temperature. For CCD purposes, a day is defined as beginning with the image transmitted at 06:34UT to ensure rough comparability with rain gauge measurements which are generally read at 06:00Z. The MOM software automatically saves the daily total images i.e. cold cloud in half-hour units (CCU).

Missing or corrupt TIR data

Due to reception or transmission problems, occasional lines on a TIR image may be missing or corrupt. In the MOM, these lines are interpolated simply by copying the good lines from either side of the gap. The maximum number of missing or corrupt lines, which is allowed before the image is discarded is 20.

Missing or corrupt secondary images are allowed for by weighting the previous and subsequent images according to the formula: M=(1+int (T/2))P+(1-int(T/2))S. Where M, P, and S refer to missing, previous and subsequent images and T is the number of missing images.

To produce dekadal CCD images, the daily CCU images in slots are totaled over the appropriate number of days and divided by 2 to give the cold cloud duration in hours for that dekad. In general, completed cold cloud duration images for a particular time period are archived as pixel values in hours. If any CCU images are missing, the dekadal CCD is flagged.

2.1.5 Gauge Rainfall data.

Gauge dekadal rainfall data for the period 1993-2000 for fifty stations was obtained from the Department of Meteorology, Uganda. Table 2.2 gives the summary of the station locations used for calibration purposes.

	Name	Longitude (degrees)	Latitude (degrees)
1	Arua	30.917	3.05
2	Moyo	31.717	3.65
3	Kitgum	32.883	3.3
4	Kotido	34.1	3.017
5	Wadelai	31.4	2.733
6	Gulu	32.283	2.783
7	Morulem	33.767	2.617
8	Pachwa	31.28	1.13
9	Masindi	31.717	1.683
10	Bulindi	31.47	1.48
11	Aduku	32.72	1.98
12	Kakoge	32.47	1.07
13	Apac	32.533	1.983
14	Serere	33.45	1.517
15	Soroti	33.617	1.717
16	Arapai	33.633	1.783
17	Kiige	33.033	1.183
18	Namalu	34.62	1.82
19	Buginyanya	34.367	1.283
20	Kijura	30.433	0.817
21	Kilembe	30	0.2
22	Rwimi	30.217	0.55
23	Kasese	30.1	0.183

24	Rwebitaba	30.433	0.65
25	Kyenjojo	30.65	0.6
26	Mubende	31.367	0.583
27	Makerere	32.633	0.25
28	Nakifuma	32.783	0.567
29	Entebbe Airport	32.45	0.05
30	Namulonge	32.617	0.533
31	Kampala SW	32.617	0.317
32	Kituza	32.767	0.267
33	Mityana	32.83	0.2
34	Kigo Prison	32.6	0.28
35	Entebbe	32.467	0.05
36	Ikulwe	33.48	0.43
37	Jinja	33.183	0.45
38	Tororo Met	34.167	0.683
39	Liri (Sukulu)	34.167	0.617
40	Tororo DFI	34.2	0.67
41	Mbarara	30.683	-0.6
42	Rwomuhoro	30.47	-0.13
43	Rubale	30.317	-0.567
44	Bushenyi	30.167	-0.567
45	Kikunda	30.55	-0.817
46	Ruhengeri	30.8	0.4
47	Kamenyamigo	31.67	-0.3
48	Kabale	29.983	-1.25
49	Kisoro	29.683	-1.283
50	Kiriima	29.933	-1.117

Table 2.2 Stations used in the calibration process. Station locations are shown in figure 6.1.

2.2 Methodology

2.2.1 Principal component Analysis

Principal Component Analysis (PCA) is a method which decomposes/reduces the number of variables from the original data set into linear combinations called Principal Components (PC's). It offers researchers opportunities to compress big data sets and concentrate only on significant components while describing important patterns of the data variability. PC's or modes are produced via PCA, each consisting of eigen values that quantifies the variance, a set of loadings (eigen vectors) that describe the spatial distribution and a set of time scores that define the temporal structure. This type of analysis extracts the non-transient or stationary patterns. The first PC is a linear function accounting for the highest variance, i.e. the dominant pattern. The second PC is the linear function with the next highest subject to being uncorrelated with the first PC. Subsequent PCs are all linear functions ranked in order of decreasing variance which are not correlated with each other or with the first and second PCs. When carrying out PCA the correlation matrix technique was chosen to avoid the analysis being dominated by high variance. This approach enables a focus on relative rather than absolute variance.

Rotation

PCA assumes that the subsequent clusters are orthogonal (independent) while many physical variables are not. Meteorological parameters like rainfall are influenced by synoptic and regional factors, giving some degree of similarity (non-orthogonality) between rainfall patterns of neighboring locations. Such similarities are rejected in PCA solutions. Thus, some of the derived patterns may be physically unrealistic. Unrotated PCA modes have some properties that make physical interpretation more difficult. The major characteristics are domain-shape dependence, sub-domain instability, sampling problems and inaccurate

portrayal of the physical relationships embedded within the input matrix. To avoid such problems, varimax rotation was performed. Varimax rotation is applied to eliminate lower order principal components and enhance the coherence of spatial loading patterns for the dominant modes. This makes the associated patterns more interpretable.

Determination of number of significant PCA modes

The scree plot method was used to determine the number of significant PCA modes. A graph is plotted with eigenvalues associated with PCA modes against the PC mode number in descending order. Small eigenvalues are linked with gradual slope while the large eigen values with steep slope (Bjornsson and Venegas, 1997). The region with gradual slope is neglected, as "clusters" in this range are associated with noise. The explained variance is sometimes plotted against the component number. If PCA variance approaches some constant value then the components are measuring random errors. The number of significant components is determined at a point where the graph starts to flatten.

2.2.2 Wavelet Transform (WT)

Wavelets are mathematical functions that divide time series data (such as PC scores) into different frequency components, and then study each component at a resolution matched to its scale. It is an analysis tool well suited to the study of multi-scale, non-stationary processes occurring over finite spatial and temporal domains, (Lau and Weng, 1995). Wavelet Transform (WT) has found wide application in different fields of science for example the earth's climate. A number of scientists have made use of this analysis tool (Mayers et al., 1993; Gollmer et al., 1995; Weng and Lau, 1994 and Mpeta, 2002).

Researchers have used Fourier Transformation (FT) in detecting periodic signals in stationary data sets. However, FT can not provide information on changes in

frequency with time. A wavelet transform gives such information and a slow or fast oscillation that may have taken place at certain times may be detected. WT normally allows wavelets to be scaled to match most of the high and low frequency signals so as to achieve the optimal resolution with the least number of base functions. This means WT has the ability to resolve a time series within the frequency domain. WT has advantages over traditional Fourier methods in analyzing physical situations where the signal contains discontinuities and sharp spikes.

2.2.3 Hovmoller Analysis

Longitude-time (hovmoller) plots are useful in identifying zonal moving meteorological systems. Anomalies of some meteorological parameters, from which we can infer convection, are used in the analysis in order to identify propagation of intra-seasonal convection anomalies.

2.2.4 Composite Analysis

Many researchers in the field of meteorology and climatology have used the composite analysis technique. Composites are useful at indicating common features, trends, and patterns in various variables. This method reduces the number of maps and figures associated with individual cases. Composite analysis enables one to average extreme events with similar characteristics and impacts. However, it is a subjective approach and results should not be generalized.

2.2.5 Correlation analysis

The measure of association between two variables is computed using correlation analysis. The coefficient of correlation (r) is defined by the following formulae:

$$r = \frac{S_{xy}}{S_x S_y}$$

Where S_x, S_y and S_{xy} are standard deviations of *x*, *y* and product of *xy* respectively. Correlation analysis is used in this study to investigate the relationship between rainfall and the Congo River flow. The association of rainfall and zonal wind modes is also examined

2.2.6 Tropical Application of Meteorological Satellite (TAMSAT) method of rainfall estimation

The TAMSAT method of rainfall estimation is used for development of calibration equations for Uganda where estimated rainfall is expressed as a function of the cold cloud duration. The TAMSAT group developed a technique from the GPI algorithm for rainfall estimation over Africa. Unlike other methods, the TAMSAT technique is calibrated against historical gauge data rather than contemporaneous gauge data. The technique assumes the following:

- Rainfall comes mainly from convective storm clouds.
- These clouds only rain when their tops have reached a certain minimum height (the height threshold).
- The cloud top height can be identified by its temperature on the Thermal Infrared (TIR) images. This temperature is referred to as the threshold temperature (T_t).
- A threshold temperature T_t corresponds to the height.
- At a given location the quantity of rainfall can be calculated from the length of time the cloud top has been above the height threshold (or colder than the corresponding temperature threshold T_t). This length of time is the cold cloud duration (CCD). Thus $R=a_0 + a_1 D$ ...Equation (3)

Where R is the estimated rainfall, D is the cold cloud duration, a_0 and a_1 are respectively the offset and slope (or coefficient). a_0, a_1 and T_t depend on local climatic conditions and hence vary both in space and time.

Since the relation between rainfall and CCD is stochastic, a substantial amount of averaging is needed to give meaningful calibration parameters a_0 and a_1 (Grimes et al., 1993). To account for the spatial variability, the area under study is normally divided into a number of calibration zones small enough to be climatically homogeneous but large enough to contain sufficient rain gauges for calibration purposes. For operational purposes a "sufficient" number of gauges is arbitrarily defined as 100 gauge-dekads of data. Thus for a given month which has three dekads, 25 gauges recording for the whole month would give 75 gauge dekads which are insufficient; 35 gauges would give 105 gauge-dekads which would be regarded as sufficient (Grimes, 1999).

For each zone the temperature threshold and calibration parameters are defined by comparison with available historical gauge data. In recognition of the temporal variability to be expected with the progression of the rainy season, a separate calibration is normally used for each calendar month in each zone.

The calibration method investigated here involves the following steps: estimation of rainfall occurrence, determination of the optimum threshold temperature (T_t), determination of optimum calibration parameter a_0 and a_1 for each calibration zone and calculation of rainfall estimates and their evaluation.

CCD data at different thresholds are compared with the historical gauge data to determine the optimum temperature threshold for each zone. The optimum threshold is the one that shows the highest level of agreement with the gauge data as to whether or not rainfall has occurred within pixels containing gauges.

	CCD=0	CCD>0
Gauge=0	n_{00}	n_{01}
Gauge>0	n_{10}	n_{11}

Table 2.3 Contingency table for estimation of rainfall occurrence.

n_{00} - if rainfall did not occur and no rainfall was estimated.

n_{11} - if rainfall occurred and was estimated to occur.

n_{01} - if rainfall did not occur but was estimated to occur.

n_{10} - if rainfall occurred but was not estimated to occur.

Thus n_{00} and n_{11} represent agreement, while n_{01} and n_{10} represent disagreement between the gauge and the satellite. For optimum temperature threshold: $n_{00}+n_{11}>>n_{01}+n_{10}$ and $n_{01}\cong n_{10}$. Basing on the above results, bias (B) is calculated using the following formula: $B=(n_{10}+n_{11})/(n_{01}+n_{11})$. This gives the ratio of estimated rain days to actual rain days. B varies between 0 and ∞ (1 unbiased). If B=1 it is fine, B<1 under estimation and B>1 is over estimation. Results of bias are plotted on maps for determination of optimum threshold temperatures and delineation of regions (cluster of gauges) with homogeneous rainfall.

In the determination of calibration parameters a_0 and a_1, rainfall estimates should be accurate at the low end of the scale. The calibration relationship may be biased by one or two unusually high rainfall events resulting in skewness of the distribution of rainfall over a time scale of dekads. The use of median (rather than mean) rain gauge values minimizes this problem. Furthermore, only pixels with non-zero CCD values are used for calculation of the calibration parameters. This is because a_0 and a_1 will only be applied to calculate rainfall estimates for non-zero CCD pixels. Finally the gauge and CCD values for the pixels containing gauges are binned and the median gauge value for each bin is regressed against the mean mid class CCD value.

2.2.7 Kriging

There is a difficulty in comparing data from gauges with those from satellites in that they provide two different kinds of information. Satellite estimates are essentially averages over the area of the satellite pixel, whereas gauges provide measurements made at a point. For meaningful comparison between the two

data sets, one must either derive point values from the satellite pixels or compute pixel averages from the rain gauge data. Here we chose the latter approach. This can be conveniently carried out using block kriging (Journel and Huijbregts, 1978).

The kriging procedure was used to calculate the 'best' mean rainfall estimates for the rain gauges and the standard error estimate on each pixel value which is equivalent to the root mean square error based on a large number of realizations of the estimated rainfall field. Standard error estimate depends on distance from gauges taking into account spatial structure of rainfall. However this method requires sufficient density of rain gauges to give meaningful results. The best estimate of rainfall (P_t) at point (t) is a weighted average given by the formula below.

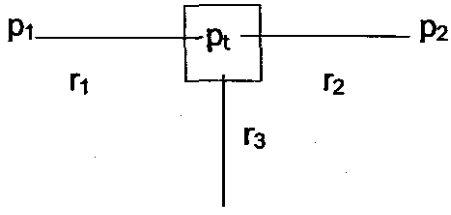

$$P_t = \sum_{i=1}^{n} \lambda_i P_i$$

Where n is the number of gauges and λ_i are the weights. λ depends on correlation between rainfall measurements at distance r_i. Kringing is advantageous in that best estimates can be calculated so that comparison with satellite values can be done correctly.

2.3 Summary

In this chapter data types and methods of data analysis have been covered. The data sources, the spatial and temporal characteristics of the remote sensed and conventional data used in this study have been examined. The preferred data sets and methodologies have been justified. The whole procedure is summarized in Table 2.4 and 2.5.

Data	Techniques of analysis	Objective
NCEP-Ocean atmospheric variables,	Composite	Mean JJAS and MAM circulation
	Hovmoller	Onset and decay of climatological systems
	Correlation analysis	Impacts of rainfall variability on Congo River flow
CMAP, Zonal wind and river flow data	PCA	Temporal and spatial distribution of rainfall and zonal wind at seasonal time scale
Results in Chapter Three	Cross correlation	Influence of zonal wind on rainfall modes over equatorial Africa
CMAP rainfall and zonal wind filtered for cycles between 20-70 days.	PCA	Intra-seasonal spatial and temporal characteristics
	Correlation analysis	Association of zonal wind and rainfall modes on intra-seasonal time scale.
Results in Chapter Four.		
OLR, and Velocity potential, anomalies	Composite and Hovmoller analysis	To examine the evolution and propagation characteristics of intra-seasonal oscillations
Results in chapter Five		

Table 2.4 Summary of low-resolution data and methods of analysis.

Data	Techniques of data analysis	Objectives.
Cold cloud and rain gauge data **Results in chapter Six**	Contingency table	Estimation of rainfall occurrence
	Calculation of bias	To determine the optimum threshold temperature and delineation of regions with homogeneous rainfall.
	Regression analysis	Determination of calibration parameters a_0 and a_1
	Kriging and correlation analysis	Validation of satellite rainfall estimates

Table 2.5 Summary of high-resolution data and methods of analysis.

Chapter Three

Seasonal rainfall and circulation over tropical Africa

3.0 Introduction

The purpose of this chapter is to gain some understanding of the seasonal structure of rainfall and circulation over tropical Africa. The seasonal mean structures over tropical Africa for March to May (MAM) and June to September (JJAS) for some parameters are discussed. The impact of seasonal rainfall variability over the Congo River is examined. Hovmoller analysis averaged from 2.5°S to 12.5°N is done to investigate the circulation systems over the Congo. Some of the researchers who have described the mean pattern of the climatological parameters over tropical Africa include; Mulenga (1998); Matitu (2002); Mpeta (2002); Matari (2003) and Yeshanew (2003) among others. The main features are the ITCZ, the monsoon pattern, Jet streams and the subtropical high-pressure systems. Maximum upward motion is over the Congo basin and has strong interaction with the surrounding climate system (Matari, 2003).

Results of principal component analysis of rainfall and zonal wind are presented and discussed in section three to understand the spatial and temporal patterns. The spatial and temporal variability of rainfall in tropical Africa has been studied by a number of researchers. These include Ogallo (1988); Nyenzi (1990); Nicholson (1996); Jury (1997) and Mulenga (1998).

3.1 Seasonal mean analysis for MAM and JJAS season

The seasonal analyses of the March-May (MAM) and June-September (JJAS) seasons provide insight on the circulation of the African monsoon and its influence on the rainfall variability over equatorial Africa. The onset season of the African monsoon is MAM whilst JJAS is the peak season (Asnani, 1993). Heavy

rainfall is usually to the south of the equator during the MAM and to the north in the JJAS season.

3.1.1 MAM Precipitation and OLR

The mean rainfall for the MAM season is presented in figure 3.1a. High rainfall values > 4 mm day^{-1} are observed over central and eastern Africa. The band extends further south to about 10°S with a V-shape. During this season, the ITCZ is to the south of the equator and the meriodianal arm is in full control of rainfall over the region. OLR values (figure 3.1b) are consistent with the rainfall pattern with enhanced convection over the Congo basin and southern Sudan, however it is suppressed over the Atlantic and the southern Indian Ocean.

3.1.2 MAM Omega at 500hPa and Specific humidity at 500hPa

Figure 3.2a shows the mean MAM omega pattern at 500hPa. Strong upward motion (negative values) is revealed over east and central Africa and part of Madagascar. Negative values are also seen over the Indian Ocean. Maximum rising motion due to strong convergence is over the Congo basin resulting in cloud development if moisture is available in the atmosphere. Sinking motion dominates the northern and southern parts including the Atlantic Ocean. Development of uplift in a northwest-southeast axis portrayed by the omega values is crucial for good rains during the MAM season over eastern Africa (Matitu, 2002).

Figure 3.2b shows the mean specific humidity for the MAM season. It is used as a measure of moisture availability in the atmosphere. The highest specific humidity values are consistent with rainfall pattern and the omega values. Relatively high values are observed over central Africa. Values > 2.4 g kg^{-1} are revealed over the Congo basin while little moisture is to the south and north of the continent.

3.1.3 JJAS Precipitation and OLR

The mean rainfall for the JJAS season is presented in figure 3.3a. High rainfall values stretch from western Africa through central to Ethiopian highlands. Highest values > 8 mm day^{-1} stretch from the Guinea coast through central Africa to about 38°E north of the equator. In the south, the rainfall band reaches into the Congo. This region is one of the most intense convection regions of the tropics (Yeshanew, 2003). It is the northern half of the Congo basin that receives rainfall during the JJAS season. However, dry conditions prevail over the rest of the African continent. During this season the ITCZ is to the north of the equator and the rainfall belt shifts accordingly.

The corresponding OLR values (figure 3.3b) depict a similar pattern as rainfall. Enhanced tropical convection (values < 220 W m^{-2}) cover western and central Africa while values > 280 W m^{-2} stretch from the Atlantic to south west of the Indian Ocean and parts of Madagascar. Convection is also suppressed (values > 260 W m^{-2}) north of 15°N towards the Sahara desert. Deep convection (OLR < 200 W m^{-2}) is observed between 25°-38°E (Congo basin) in the JJAS season.

3.1.4 JJAS Omega at 500hPa and Specific humidity at 500hPa

Figure 3.4a shows the mean JJAS Omega pattern at 500hPa. Upward motion (negative values) is observed over western Africa through central to some parts of Ethiopia. Negative values extend to about 5°S with a V-shape over central Africa. Upward motion is also revealed over the northern Indian Ocean. Maximum upward motion is seen over the Congo basin with values < -0.04 pascal s^{-1}. Positive values (indicating sinking motion) cover the rest of the region with highest values > 0.04 pPascal s^{-1} in the southern Indian Ocean and some parts on east South Africa. Further, sinking motion is also seen over the Atlantic Ocean. The Omega values imply low (negative) and high (positive) pressures over the respective areas.

Figure 3.4b shows the mean specific humidity for the JJAS season. The highest specific humidity values are consistent with rainfall pattern and the Omega values at 500hPa structure. Relatively high values are seen over central Africa north of the equator while small values are to the south. However highest values > 2.4 g kg^{-1} extend from about 25°E-38°E.

3.1.5 Seasonal rainfall variability over northern Congo and the Congo River flow.

To investigate the impacts of seasonal rainfall variability on the stream flow of the Congo River, CMAP rainfall over northern Congo and stream flow of the Congo River were analyzed. The data sets were filtered for the seasonal cycles and correlation analysis performed at different time lags.

Figure 3.5a reveals highest correlation coefficient of 0.82 at three months' lag followed by 0.78 at four months lag. From five months on wards the correlation coefficients become smaller. Similarly at zero and one month lag, the relationship is weak however it strengthens at two months lag. Rainfall over northern Congo explains about 64% of the Congo River flow at three months lag. This means that the Congo River flow responds to rainfall with a three-month lag.

Figure 3.5b shows that rainfall over the northern Congo is phase lagged with the Congo River flow. Peak rainfall is during the JJAS season while stream flow maxima is in the October-December (OND) season.

3.2 Hovmoller analysis for means in the JJAS season

To study the seasonal circulation pattern over the northern Congo hovmoller analysis was performed. This region (2.5°S-12.5°N) receives most of its rainfall during the JJAS season when the ITCZ is to the north of the equator.

3.2.1 CMAP rainfall and Outgoing Longwave Radiation (OLR)

Areas from 10°E-35°E receive rainfall almost throughout the year with a peak > 10 mm day $^{-1}$ in the July-September season (figure 3.6a). In the March-May onset season synoptic disturbances bring some rain over the region. Rainfall shifts to the east beginning June and then to the west of 25°E towards October (values > 6 mm day^{-1}). Areas from 18°W to 12°W in the equatorial Atlantic Ocean receive high rainfall amounts > 6 mm day^{-1} during June to September season. Over the western Indian Ocean (35°E-60°E) there is a relatively dry zone with rainfall amounts < 2 mm day^{-1}. This covers the east African coast.

Similarly, OLR portrays a similar pattern. Values below 220 W m^{-2} are observed between 10° and 40°E. Smaller values < 200 W m^{-2} from June to September implying high convective activity are over areas from 25°E-40°E (figure 3.6b) while values > 240 W m^{-2} are to the east of 40°E in the Indian Ocean. Convective activity propagates eastward as earlier observed in the rainfall pattern.

3.2.2 Specific Humidity at 500hPa and Vertical Velocity at 700hPa

Areas between 15°-35°E portray values of specific humidity > 2 g kg^{-1} during April to October season (figure 3.7a). Higher values are observed between 22°-35°E from June to September implying high moisture availability in the atmosphere that could lead to the formation of convective clouds. Peak values > 2.4 g kg^{-1} are realized from mid July to mid August between 28°-35°E. However little moisture in the atmosphere is observed to the east of 35°E.

Figure 3.7b shows the mean vertical velocity in m s^{-1}. Positive values (upward motion) have a similar pattern to rainfall in figure 3.6a. Areas between 22°-35°E are characterized by strong rising motion (convergence in the lower layers of the atmosphere) from June to September while sinking motion (divergence) is over

the Indian and Atlantic Oceans. However in April strong rising motion is to the west of 22°E revealing an east ward propagation.

3.2.3 Zonal wind at 850hPa and 200hPa

Westerly flow dominates the seasonal evolution in the lower layers of the atmosphere at 850hPa (figure 3.8a). Westerlies at > 4 m s^{-1} cross from the Atlantic Ocean to the mainland. At about 15°E they traverse at a higher speed > 6 m s^{-1}, slow down in east Africa and then pick up in speed around 45°E in the Indian Ocean. Weasterlies retreat over eastern Africa at 28°E and easterlies set in as part of the SE monsoon component over this region.

At upper level 200hPa easterlies are prevalent. Speed varies with respect to longitude and months of the year. Very strong winds originate from the Indian Ocean (> 20 m s^{-1}), crossing over central Africa to the Atlantic Ocean during the June to September season.

3.2.4 Vertical cross section of wind for JJAS

Figure 3.9a shows the cross section of the zonal wind averaged from 2.5°S to 12.5°N. Easterlies dominate the upper level while westerlies prevail at the lower levels. Strong easterlies (> 20 m s^{-1}) are observed to the east of 15°E extending in the Indian Ocean at about 200hPa. At the lower level, westerlies are observed, strongest in the Indian Ocean (> 5 m s^{-1}).
The cross section of the meridional wind (figure 3.9b) reveals strong flow over the east African coast. Southerlies of up to 8 m s^{-1} are observed between 40°E and 50°E at lower levels. Generally, northerlies dominate the upper levels.

3.3 Results of the Principle Component Analysis for the seasonal cycle.

CMAP rainfall data and 700hPa zonal wind were used in this study. CMAP pentad (5-day) data were extracted for 21 years (1980-2000) from 15°S to 15°N and 0 to 50°E. Daily means of zonal wind for the same period from 15°S to 15°N and 30°W to 80°E were extracted and averaged into pentad means. The two data sets were normalized using the following formulae: $z = (x - \bar{x}) / \sigma$. Where; x is individual pentad mean for a grid box, $\bar{x}$ is mean of pentad means for a grid box and σ is standard deviation of pentad means for a grid box. The data described above will also be used in chapter four but filtered for intra-seasonal oscillations only. The data sets were subjected to Principal Component Analysis and the first three Principal Components (PC's) in each case were retained for interpretation.

CMAP rainfall Modes	Variance Explained (%)
PC1	36
PC2	12.5
PC3	5.8
Zonal wind Modes	Variance Explained (%)
PC1	25.8
PC2	18.7
PC3	10.9

Table 3.1 Seasonal Principal Components.

Table 3.1 displays the PCA modes and the associated percentage variance explained by each mode. The first three principal components explained about 54.3% and 55.4% of the total variance of rainfall and zonal wind respectively. The spatial loading, the associated time scores and the modulus spectrum are

shown in figures 3.10, 3.11, and 3.12 for rainfall and figures 3.13, 3.14 and 3.15 for zonal wind.

Rainfall Modes

PC1 (36%)

Figure 3.10 indicates large positive (negative) values south (north) of the equator. Positive loading regions have wet conditions when time score amplitudes are positive. Those with negative loadings have dry conditions. The first mode contains the main annual cycle. This mode reflects the migration of rainfall associated with the inter-tropical convergence zone as governed by the movement of the sun. Rainfall is to the north during northern summer and to the south during the southern summer. The associated time scores reveal an alternating unimodal distribution of rainfall over the two regions. The northern peak is singular while the southern one is broader. During the northern summer the ITCZ migrates rapidly southwards and less rain is received. However During the southern summer the convergence zone tends to be very broad and moves slowly northward, so that there is extensive heavy rain.

PC2 (12.5%) is the East African mode. Spatial loading, time scores and the modulus spectrum are displayed in figure 3.11. Large positive loading is over east Africa. The time score amplitudes show that the region experiences bimodal wet conditions. This region receives rainfall during March/May and September/November seasons as portrayed by the time scores (figure 3.11b). More rainfall is received in the first season compared to the second one. Very high amplitudes are seen in the years 1981,1982 and 1997, the latter is El-Nino related. However the seasonal cycle of rainfall was more limited in 1999 and 2000 due to La-Nina episodes.

Figure 3.12 shows the spatial loading, time scores and modulus spectrum of PC3 (5.8%). It has main loading over the western Congo and positive loadings to the

east and west. The time scores are less organized and peak in the third quarter of the year. High amplitudes are observed in the years 1981,1985, 1989 and 1999. Although the annual cycle dominates this mode, shorter cycles of 30-50 days are also revealed by the modulus spectrum.

The wavelet transform of rainfall PC1 time scores (3.10c) indicates that the major period of oscillation over the respective loading areas is 73 pentads (annual). PC2 and PC3, however, reveal that there is a second period of 30-50 pentads having high amplitudes.

Zonal wind Modes

Figure 3.13 shows spatial loading, time scores and the modulus spectrum of PC1, which explains 25% of the total variance of 700hPa zonal wind. High positive loadings are found over eastern Africa whilst negative loadings are in the southwestern Indian Ocean. The associated time score reveals an annual cycle in the monsoon circulation over eastern Africa. During November to March, north easterlies sweep across the western Indian Ocean delivering moisture to east Africa. However, in the May to September period south-westerly monsoons divert moisture from east Africa (Asnani, 1993). The modulus spectrum shows that this mode is unimodal with a peak occurring in June. Increased westerly flow is known to increase the tropical rainfall at the seasonal scale (Agumba, 1985). This concept is explored further below.

PC2 (18.7%) has high positive loading over the east Atlantic Ocean extending in a northwest/southeast direction (figure 3.14). This mode captures the Atlantic south-westerly monsoon that brings moisture across the Guinea coast to the Congo basin during the JJAS season. However westerly flow over the east African coast is also observed in this mode. The time score suggests that this PC is bimodal with two peaks in April and September. The annual cycle is revealed as well as shorter ones of 50 pentads and below. Stronger spectral power is

observed in the shorter cycles than in the annual ones. This mode is more noisy than PC1 implying non seasonal wind variability over the loading region.

PC3 displays a loading maximum in the northern Atlantic (0° to 10°N) and an opposing maximum in the southwest Indian Ocean (figure 3.15). PC3 basically represents divergence over equatorial Africa. The time score shows that the westerlies peak in the first half of the year whereas the easterlies peak in the second half. The modulus reveals an annual cycle, and other cycles of 50 pentads and below. The years from 1981 to 1989 reveal high spectral power at the annual cycle. However from 1991 to 2000 relatively greater spectral power is observed in the 30-50 pentad range.

3.4 Cross Correlation of rainfall and zonal wind modes

Cross- correlation analysis was done to investigate the relationship of seasonal zonal wind modes (U1, U2, U3) with rainfall modes (R1, R2, R3). Table 3.2 shows the correlation coefficients at different time lags. Strong negative correlation is revealed between U1 and R1. The highest correlation coefficient of –0.91 is observed at lags –1 to –3. The negative relationship means that easterly flow over the Indian Ocean favors more rainfall over equatorial Africa. This flow picks moisture from the Indian Ocean through the SE monsoon component to central Africa (Matari, 2003). The coefficients are higher at negative lags compared to the positive ones implying that rainfall lags the zonal wind.

Correlation coefficients between U2 and R3 show maximum association at zero-lag (table 3.2). The association weakens with increasing lags. This relationship means that in addition to the in situ convection, rainfall activity over the western Congo corresponds directly to increased westerlies over the Atlantic (zero lag).

Lags (pentads)	U1/R1	U2/R3	U1/R3	U2/R2
-6	-0.87	0.23		-0.32
-5	-0.89	0.26		-0.33
-4	-0.90	0.30		-0.33
-3	-0.91	0.34		-0.31
-2	-0.91	0.40		-0.29
-1	-0.91	0.46		-0.27
0	-0.90	0.49		-0.28
1	-0.87	0.47	-0.16	-0.28
2	-0.84	0.42	-0.22	-0.28
3	-0.80	0.36	-0.27	-0.24
4	-0.76	0.32	-0.32	-0.17
5	-0.72	0.30	-0.36	
6	-0.66	0.28	-0.40	

Table 3.2 shows correlation coefficients for seasonal rainfall and zonal wind modes. Weak associations r < 0.15 are omitted.

The relationship between U2 and R2 reveal relatively strong negative correlation coefficients. The association is strongest at –5 lag (r = -0.33) becoming smaller from –3 to +6 lag. These results are consistent with other authors who observed that rainfall over eastern Africa is influenced by the strong westerly flow over the Atlantic. These westerlies gather moisture as they traverse the Congo forests to eastern Africa. Rainfall responds after 5 pentads (20 days).

Mean pentad structure was computed for rainfall and zonal wind modes with strong relationships to establish seasonal phase-lockness. Some values are inverted for comparison (figure 3.16). The two variables are in phase for most of the relationships. Rainfall over the northern Congo responds to the westerly flow after 15 days (figure 3.16a.). However, over western Congo (R3) the westerlies in the Atlantic have an immediate positive impact on rainfall activity. Over eastern

Africa, rainfall lags the zonal wind in the Atlantic by 4 pentads (20 days) (figure 3.16c).

3.5 Summary

This chapter has focussed on a seasonal analysis of climatological parameters. Congo basin is identified as a region of interest due to the unique circulation over this part of the continent. Correlation analysis revealed strong association between rainfall variability over the northern Congo and the Congo River flow. Hovmoller analysis was done over this region to investigate the development and decay of the monsoon circulation.

PCA was used in the understanding of the spatial and temporal variability of rainfall and zonal wind at seasonal time scale over the region. It is observed that the annual cycle is the dominant mode. Cycles of 30-50 days have also been identified. These results are consistent with the findings of Mpeta (2002). Cross correlation revealed a strong relationship between rainfall modes and zonal wind at different time lag. The association between rainfall over east Africa and the zonal wind over the west Atlantic Ocean has been established. This relationship emphasizes the role of the Atlantic in the modulation of seasonal rainfall over East Africa.

The analysis in the following chapter concentrates on the intra-seasonal oscillations over tropical Africa.

(a) Monthly mean precipitation mm day $^{-1}$

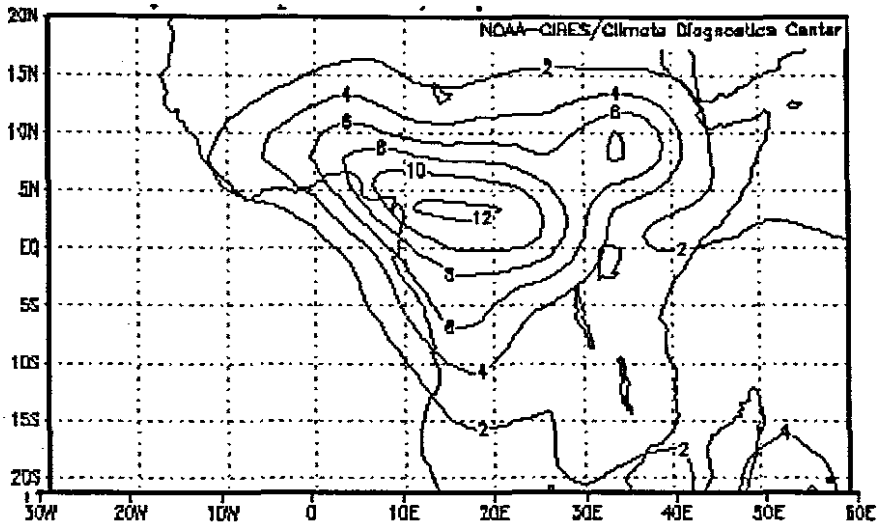

(b) Monthly mean OLR W m^{-2}

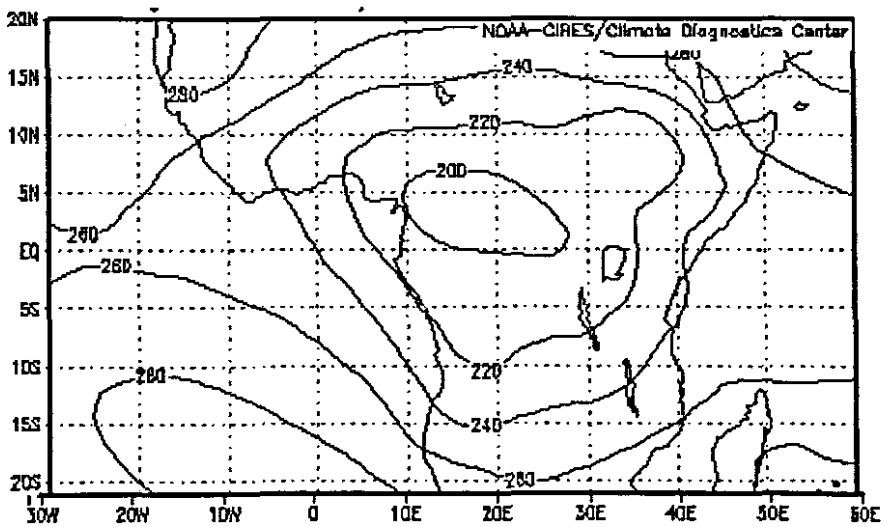

Figure 3.1. MAM mean (a) Precipitation (CMAP) mm day $^{-1}$ (b) Outgoing Longwave Radiation (OLR) W m^{-2}

(a) Monthly mean Omega Pascal s^{-1} (500hPa)

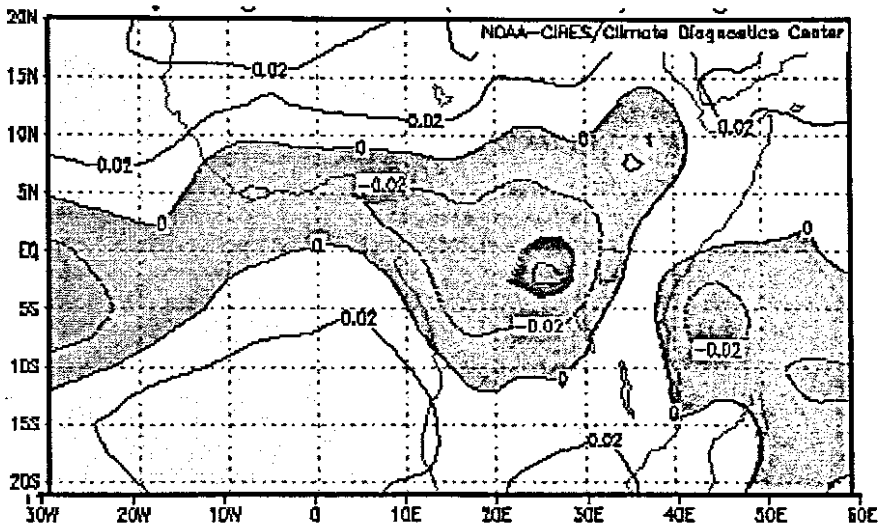

(b) Monthly mean Specific Humidity g kg^{-1} (500hPa)

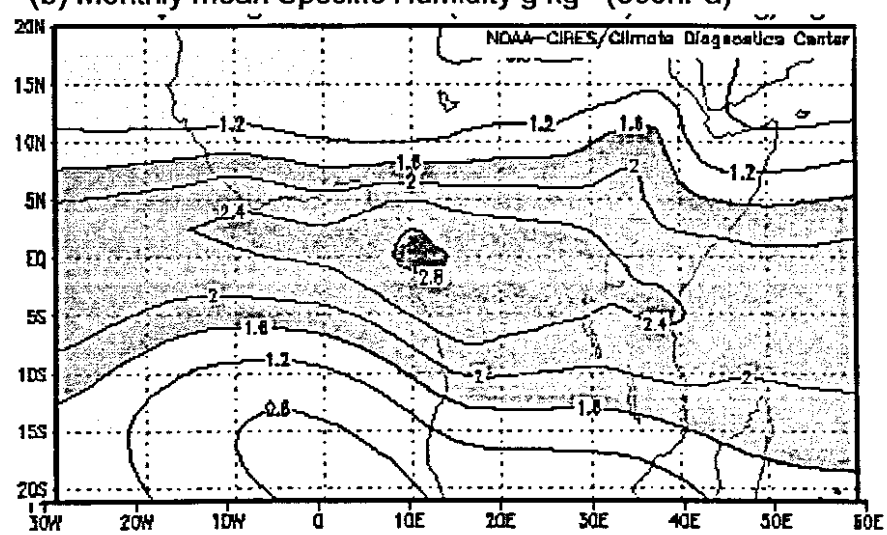

Figure 3.2 MAM (a) Omega Pascal s^{-1} at 500hPa, (b) Specific Humidity g kg^{-1} at 500hPa.

(a) Monthly mean precipitation mm day $^{-1}$

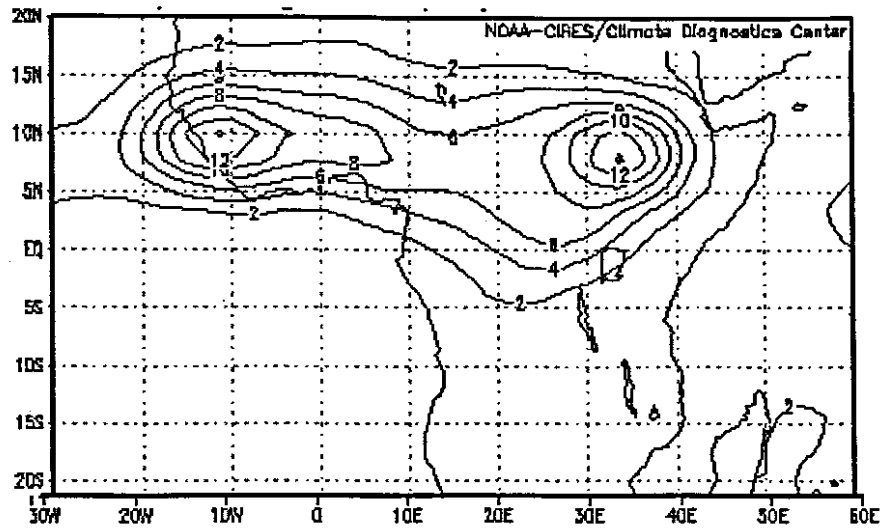

(b) Monthly mean OLR W m^{-2}

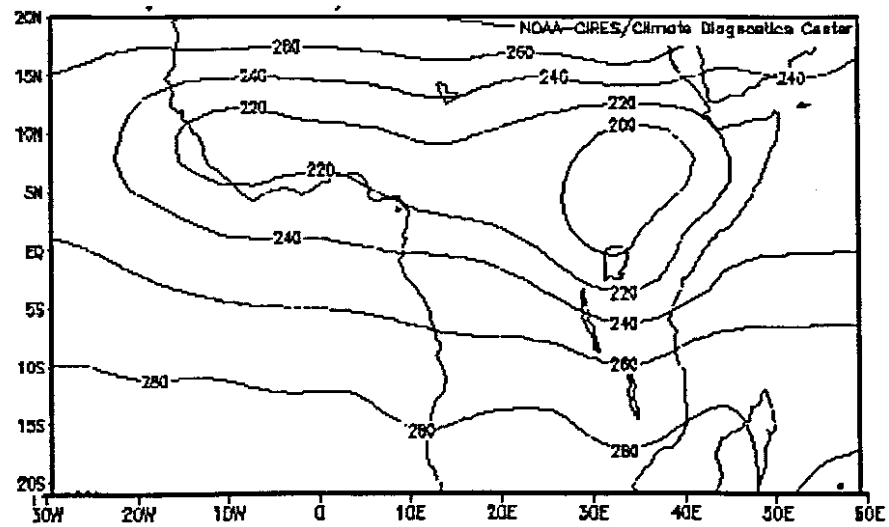

Figure 3.3. JJAS mean (a) Precipitation (CMAP) mm day $^{-1}$ (b) Outgoing Longwave Radiation (OLR) W m^{-2}

(a) Monthly mean Omega Pascal s^{-1} (500hPa)

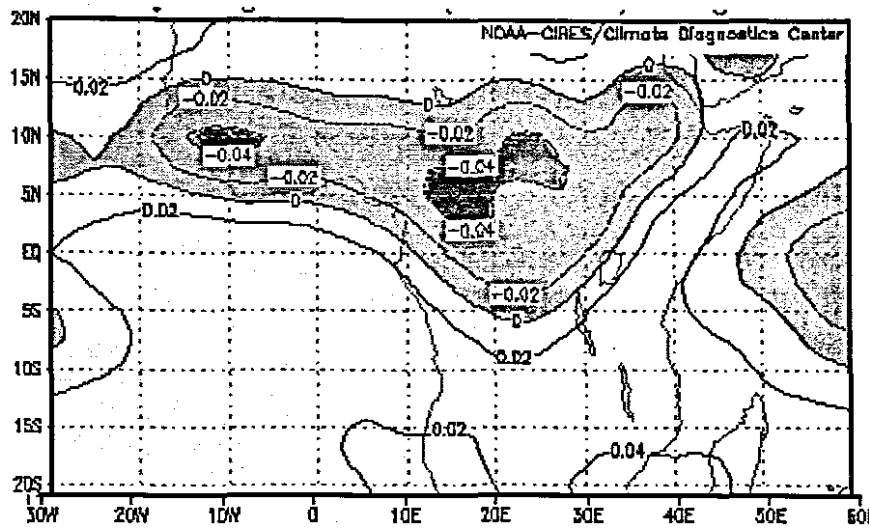

(b) Monthly mean Specific Humidity g kg^{-1} (500hPa)

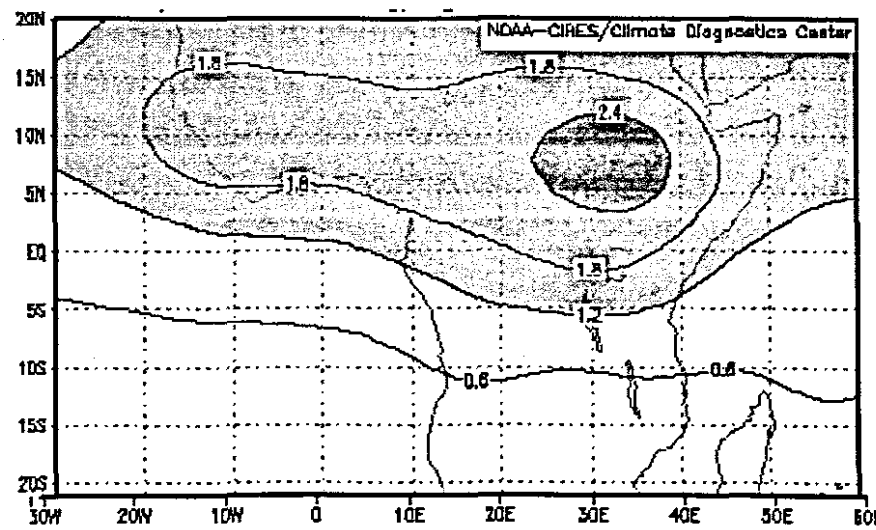

Figure 3.4 JJAS (a) Omega Pascal s^{-1} at 500hPa, (b) Specific Humidity g kg^{-1} at 500hPa.

(a)

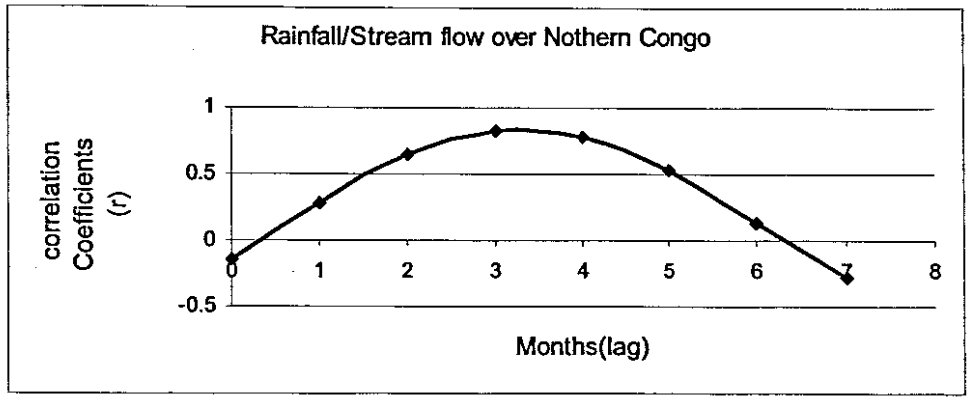

(b)

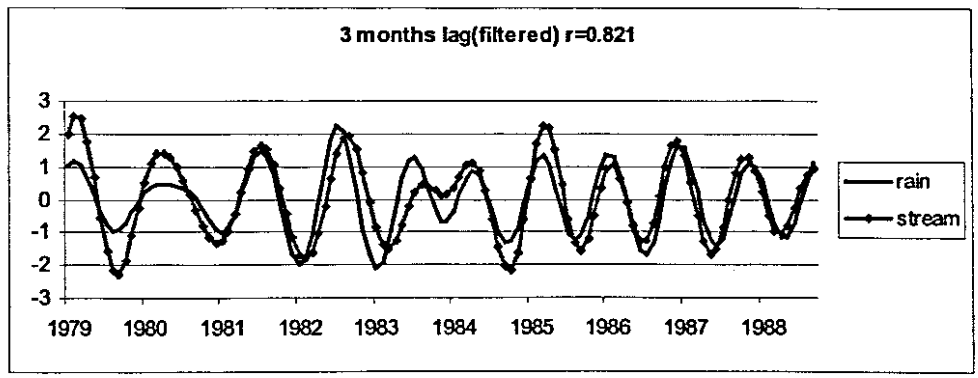

Figure 3.5 (a) Lag -correlation of wavelet-filtered seasonal CMAP rainfall over northern Congo and Congo River flow at different. (b) Monthly rainfall and stream flow shifted to the lag of maximum correlation.

(a) Precipitation mm day $^{-1}$

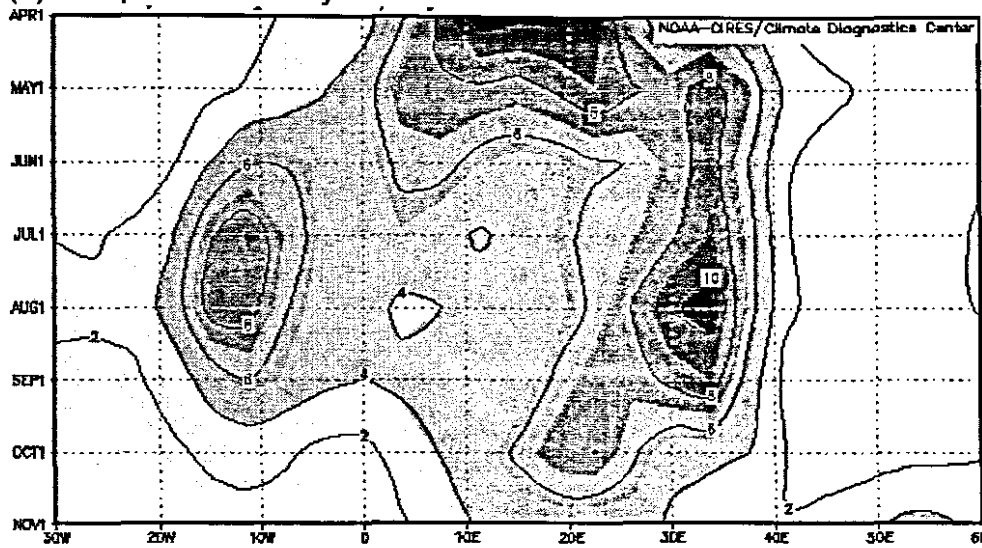

(b) Outgoing Longwave Radiation W m^{-2}

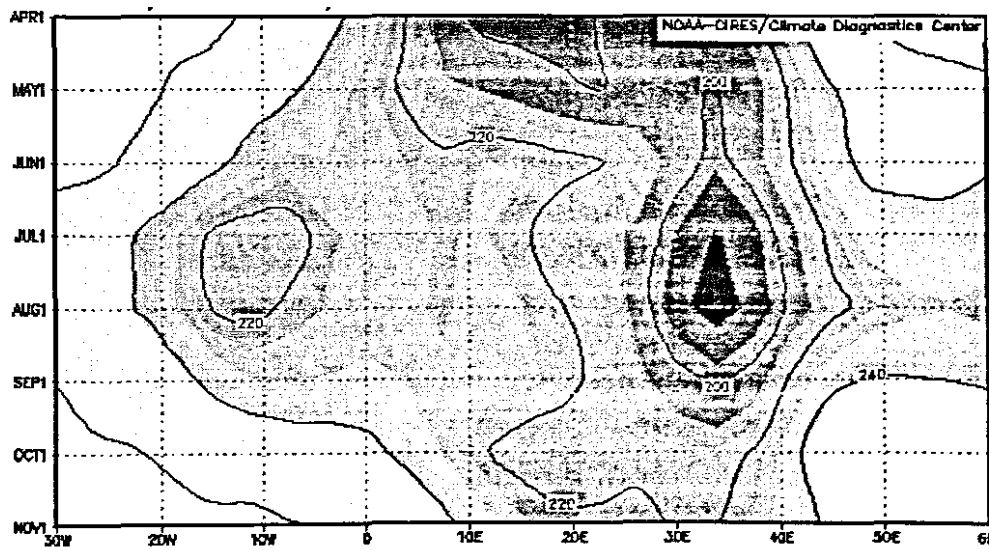

Figure 3.6 Monthly climatological mean CMAP rainfall and Outgoing long wave radiation (OLR) averaged from 2.5S to 12.5N.

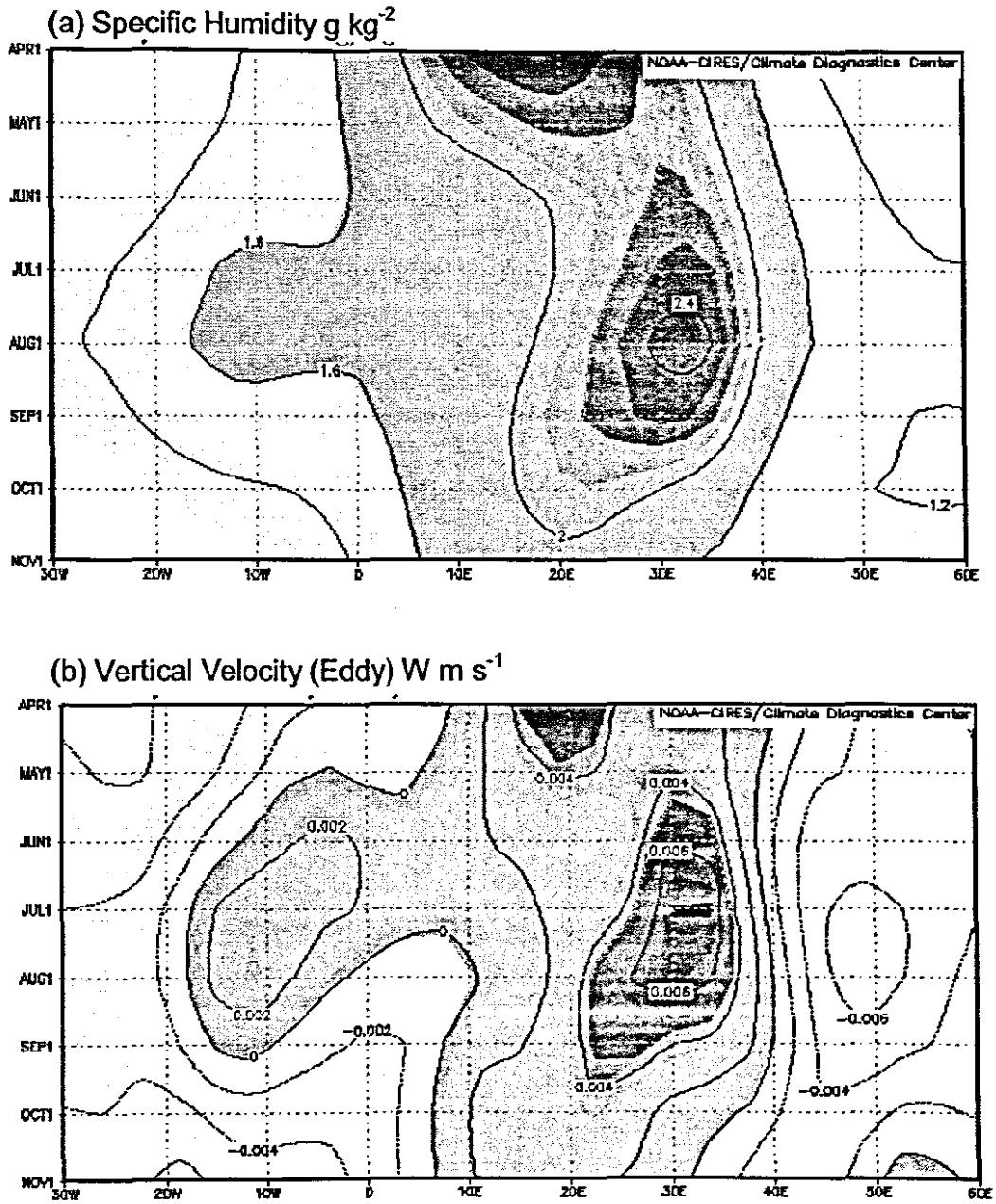

Figure 3.7 (a) Monthly climatological mean Specific humidity at 500hPa (b) monthly mean Vertical velocity at 700hPa averaged from 2.5S to 12.5N.

(a) Zonal wind at 850 hPa ($m\ s^{-1}$)

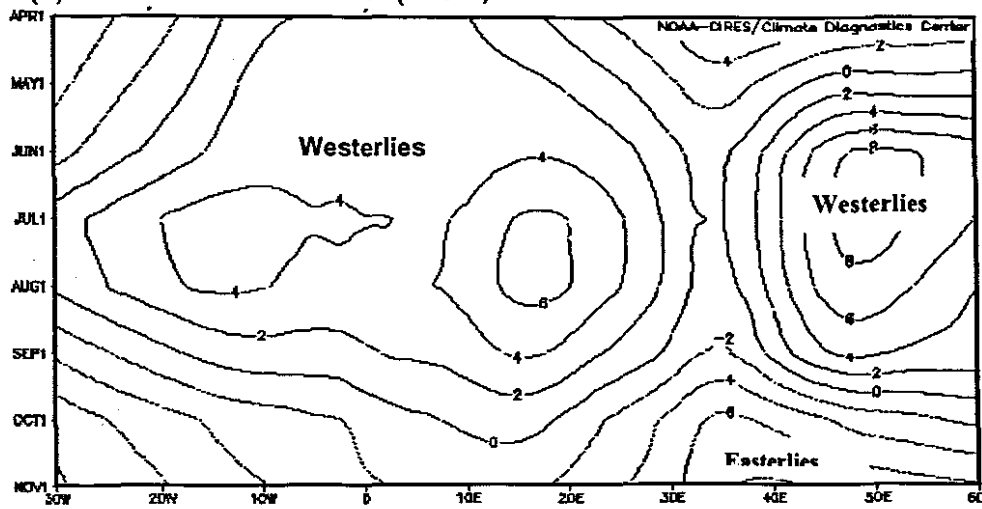

(b) Zonal wind at 200hPa ($m\ s^{-1}$)

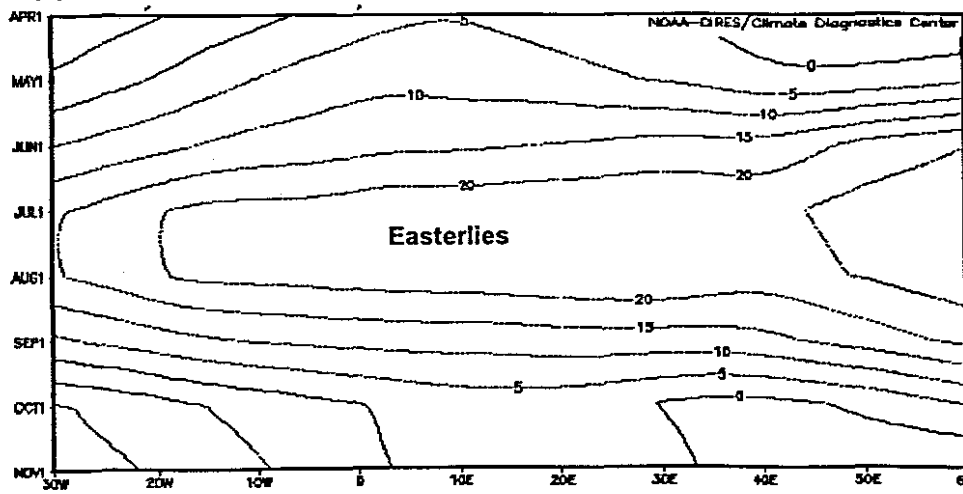

Figure 3.8 (a) Monthly climatological mean zonal wind at 850hPa and (b) at 200hPa respectively averaged from 2.5S to 12.5N.

(a) Zonal wind m s^{-1}

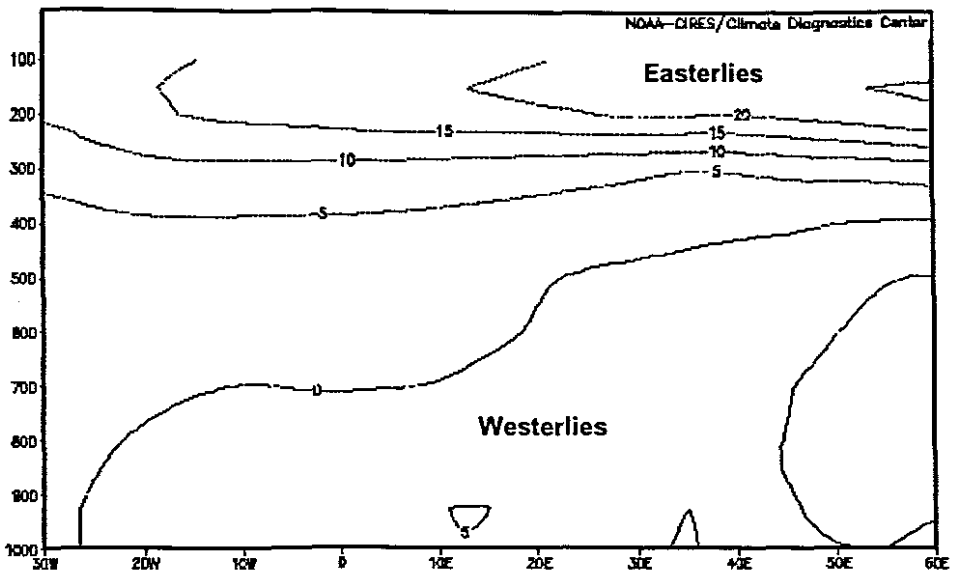

(b) Meridional wind m s^{-1}

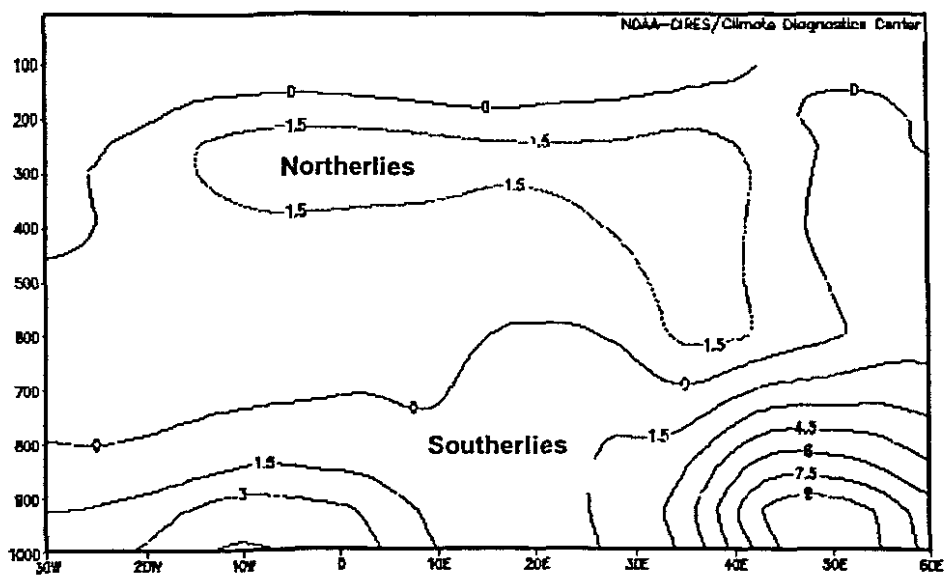

Figure 3.9 Cross section of Zonal and Meridional wind averaged over –2.5S to 12.5N for JJAS.

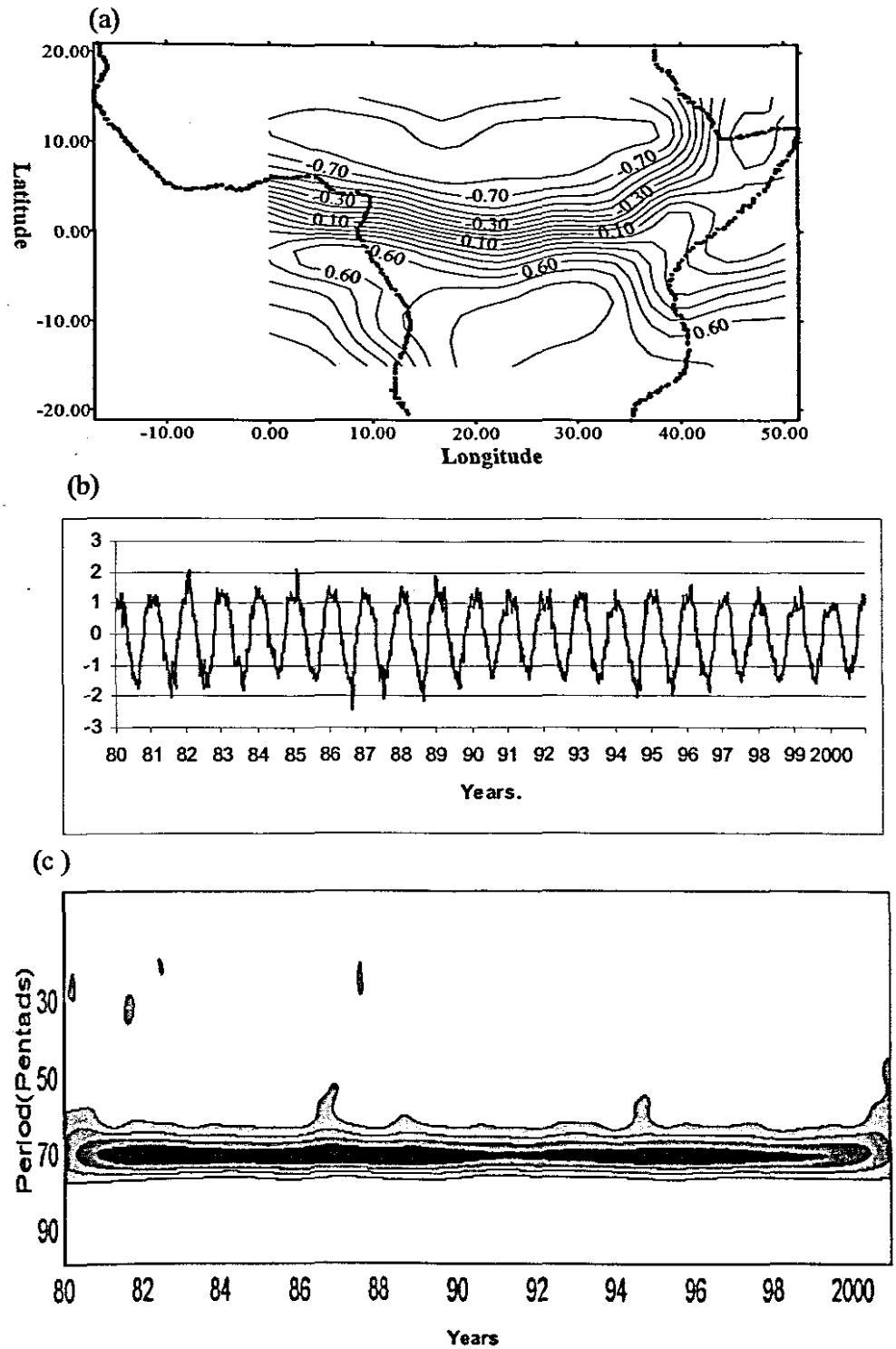

Figure 3.10 (a) Spatial loading (b) Time scores (c) Modulus spectrum for (unfiltered/unrotated) seasonal rainfall for the first Principal Component PC1 (36% of total variance).

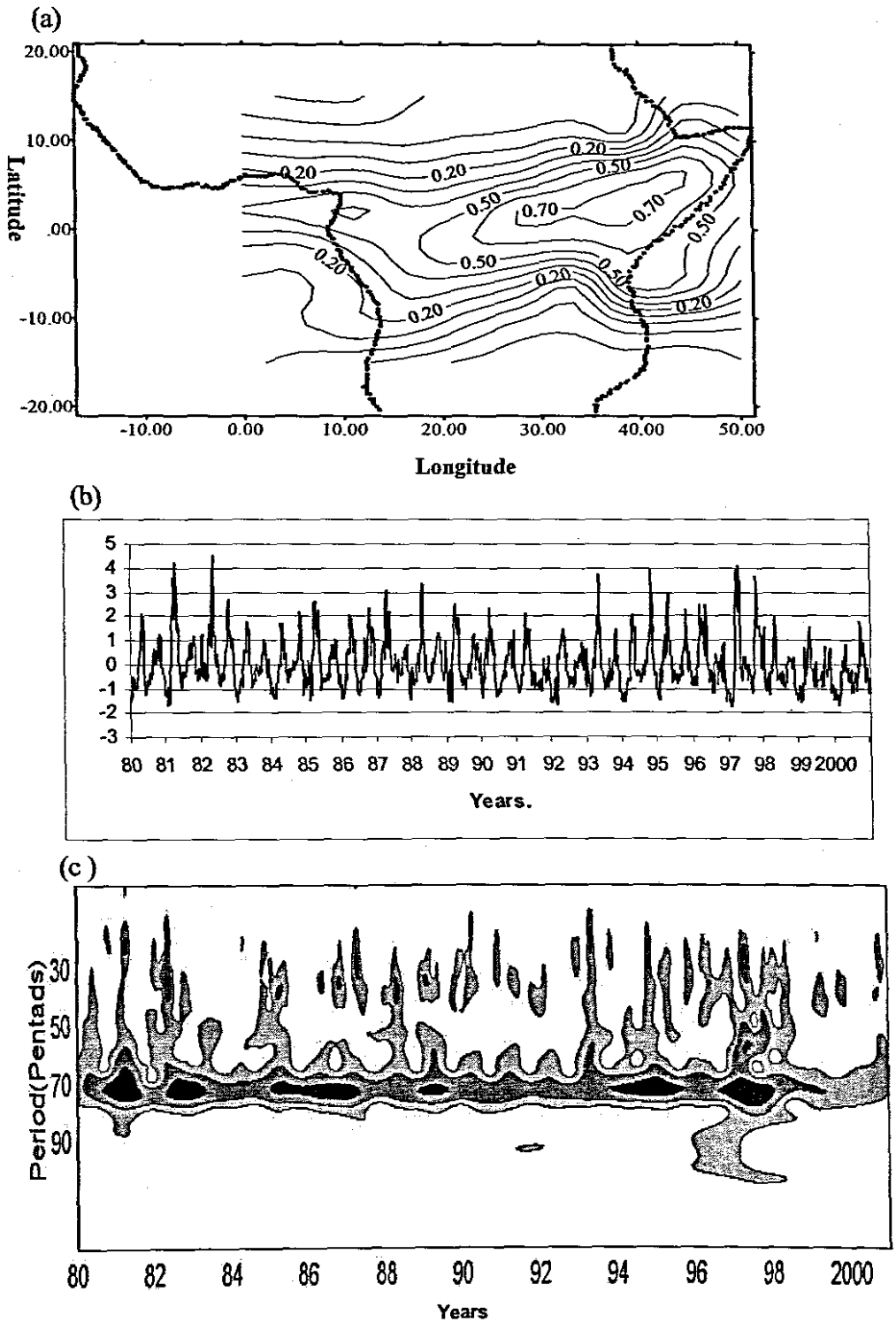

Figure 3.11 (a) Spatial loading (b) Time scores (c) Modulus spectrum for (unfiltered/unrotated) seasonal rainfall for the second Principal Component PC2 (12.5% of total variance).

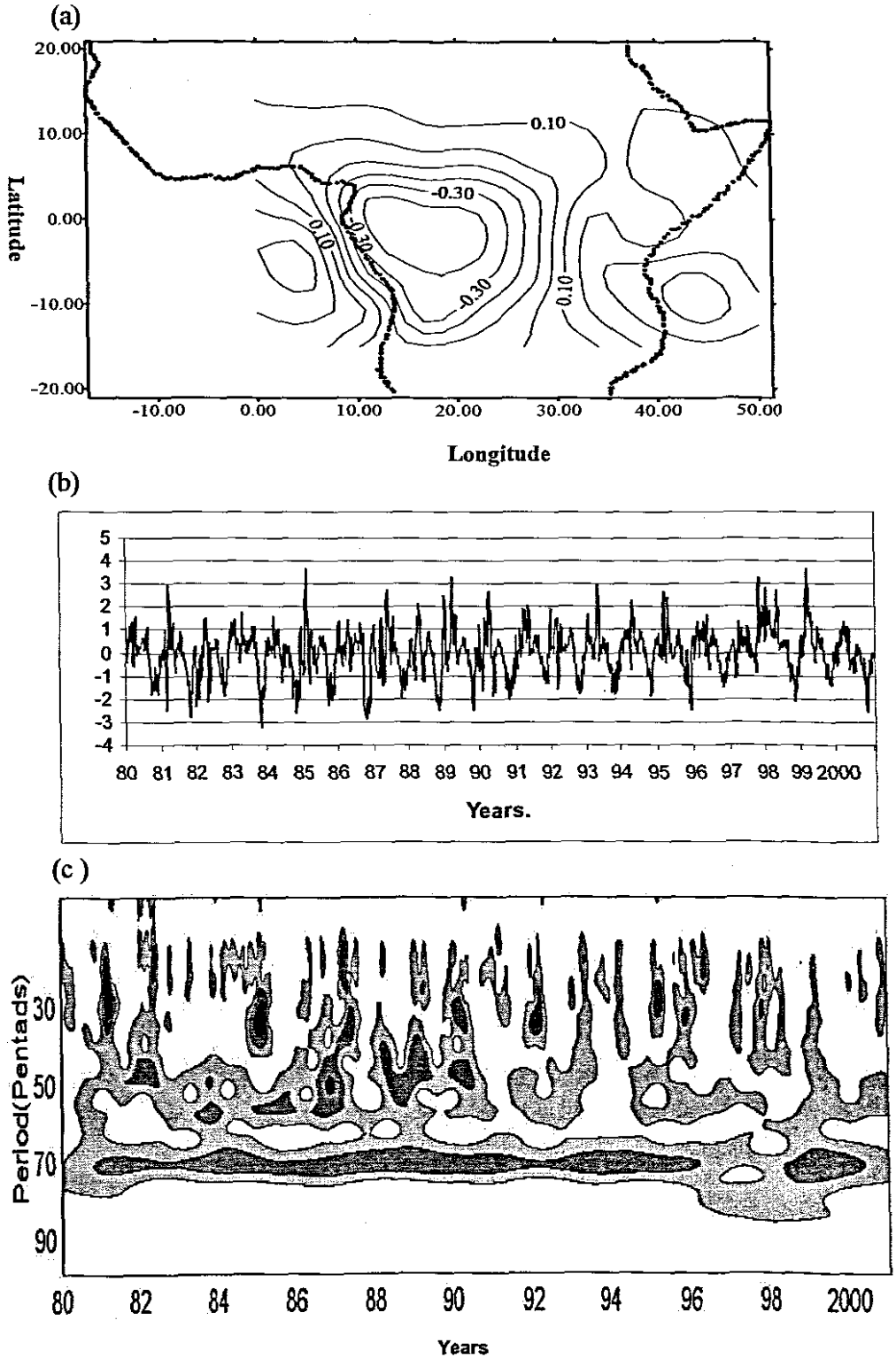

Figure 3.12 (a) Spatial loading (b) Time scores (c) Modulus spectrum for (unfiltered/unrotated) seasonal rainfall for the third Principal Component PC3 (5.8% of total variance).

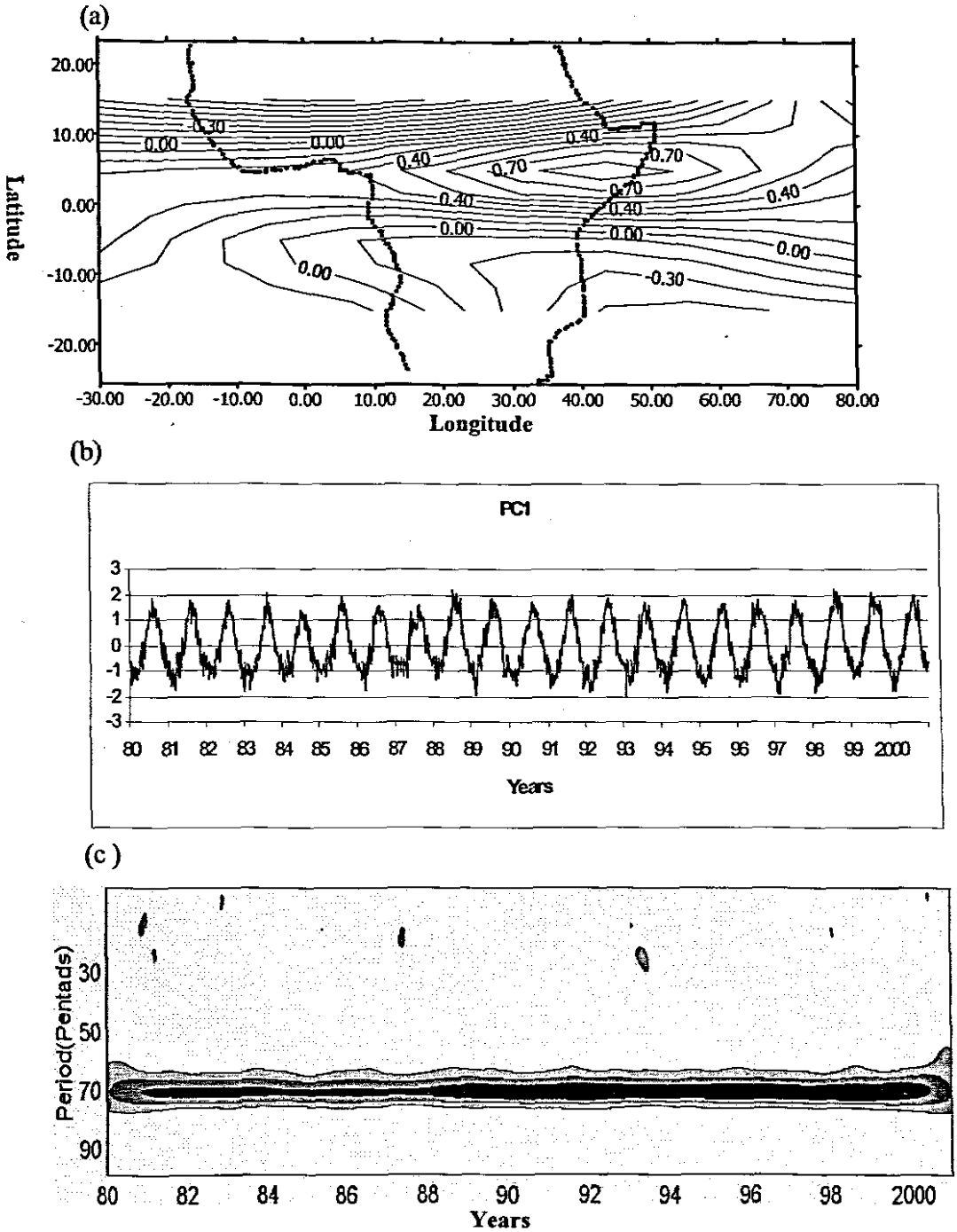

Figure 3.13 (a) Spatial loading (b) Time scores (c) Modulus spectrum for (unfiltered/unrotated) seasonal zonal wind for the first principal component PC1 (25.8% of total variance).

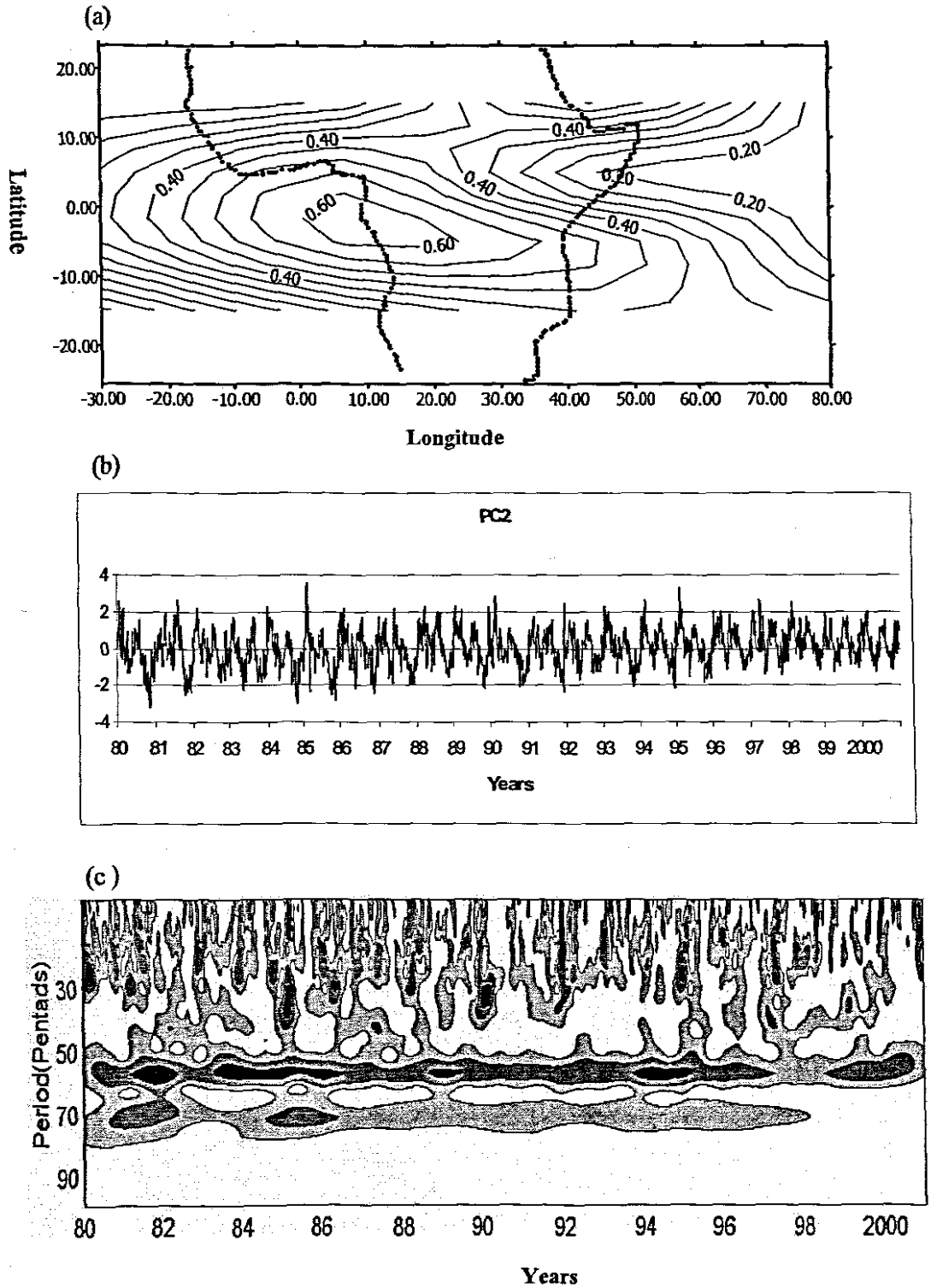

Figure 3.14 (a) Spatial loading (b) Time scores (c) Modulus spectrum for (unfiltered/unrotated) seasonal zonal wind for the second Principal Component PC2 (18.7% of the total variance).

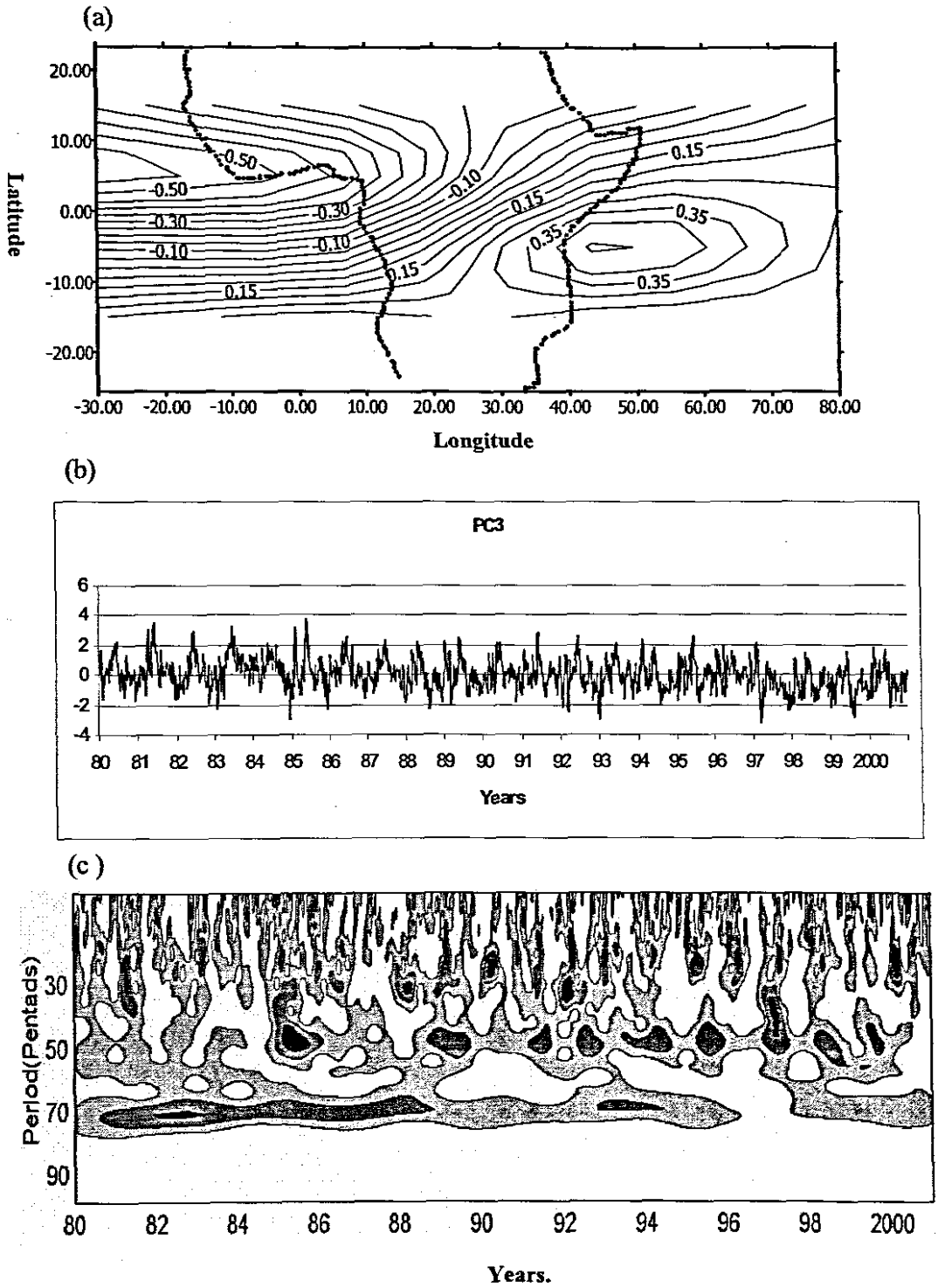

Figure 3.15 (a) Spatial loading (b) Time series (c) Modulus spectrum for (unfiltered/unrotated) seasonal zonal wind for the third principal component PC3 (10.9% of the total variance).

(a)

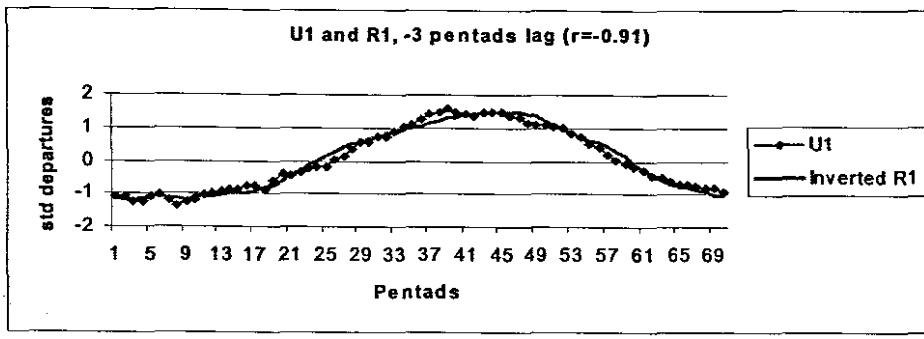

(b)

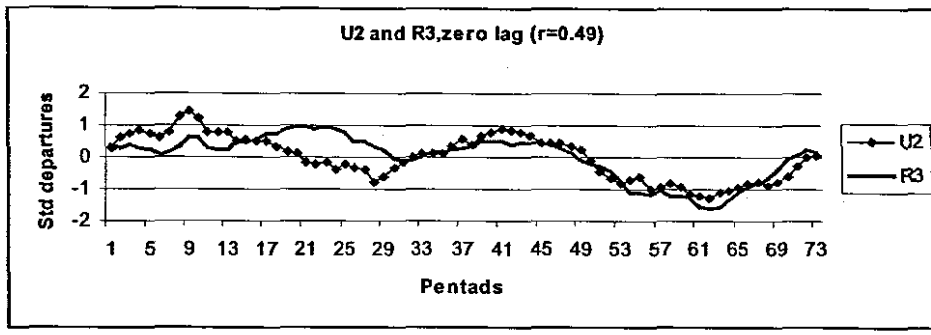

(c)

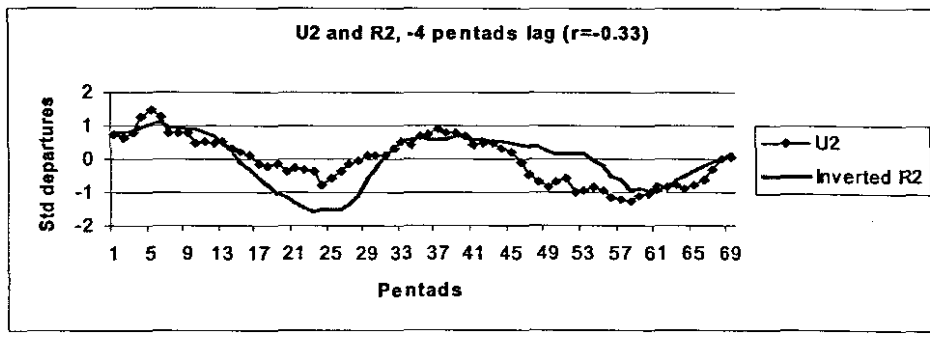

(d)

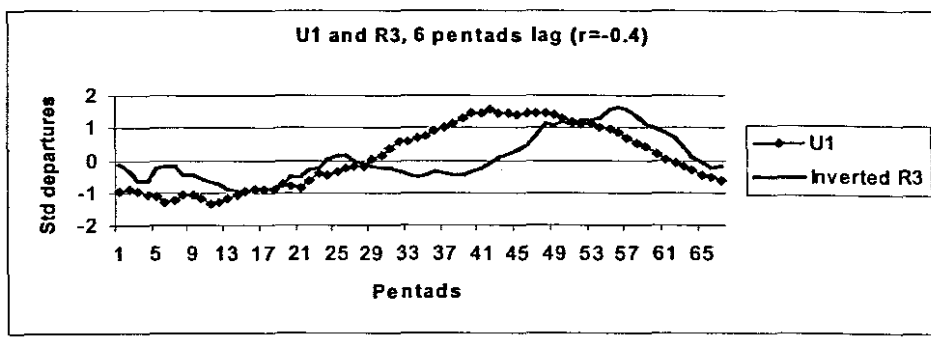

Figure 3.16. Seasonal rainfall and zonal wind modes shifted to the lag of maximum correlation based on the cumulative average of 21 years.

Chapter Four

Intra-seasonal oscillations over tropical Africa

4.0 Introduction

Tropical intra-seasonal oscillations have attracted much attention, ever since its discovery in the early 1970s (Madden and Julian, 1971, 1972, 1994) for reasons of both scientific and practical interests. Traditionally, climate research in Africa has tended to focus on seasonal mean area-average rainfall totals guided partly by available data and by a desire to diagnose the large-scale relations as a first step (Mutai and Ward, 2000). However, it is now clear that for a full understanding of a maximum predictive utility, there is need to study spatial and temporal variability within a season.

Utilization of climatological information and prediction in agricultural management has become popular in most tropical African countries. Farmers and policy makers need to know when dry spells within the rainy season are likely to occur to prepare for deficits that may arise. A dry rainy season in tropical Africa may mean famine, but too much rain at the wrong time can cause crops to rot, soil to waterlog and rivers to flood. Therefore the study of intra-seasonal rainfall variability is most appropriate.

Intra-seasonal variability during the rainy season is an integral part of each season's character. These oscillations can be viewed as the link between individual weather events and the seasonal climate anomaly; hence the dynamics of intra-seasonal variations can be instrumental in setting up the seasonal anomalies. Diagnostic studies of dynamical instabilities in different parts of tropical Africa and its adjacent oceans are required to assess interaction of continental convection with the regional circulation at intra-seasonal scales. A key question is whether their source is internal to the African continental

monsoon, or whether the disturbance propagates across the tropical African sector from the adjacent oceans.

The data sets (CMAP rainfall and zonal wind at 700hPa) described in chapter three are also used here. However wavelet filtering is applied to the data sets to retain cycles between 4-14 pentads (20-70 days) thereby eliminating cycles below 20 days and above 70 days. The data sets were then subjected to Principal Component Analysis with varimax rotation and the first three principal components were considered. Further, rainfall and zonal wind scores were cross-correlated.

Results of principal component analysis for the intra-seasonal oscillations

Table 4.1 displays the principal component analysis (PCA) modes and the associated percentage variance explained by each mode. The first three Principal Components (PC's) account for about 71% and 37.4% of the total variance of CMAP rainfall and 700hPa zonal wind respectively. Hence the convection reveals a larger intra-seasonal signal for standing modes, whilst the wind systems are less coherent and may propagate.

CMAP rainfall Modes	Approximate Position	Variance Explained (%)
PC1	Northern Congo	29
PC2	Northeast Angola	22
PC3	East African highlands	20
Zonal wind Modes		Variance Explained (%)
PC1	Equatorial east Atlantic Ocean	14.3
PC2	West Indian Ocean	13.3
PC3	Southeast Atlantic Ocean	9.8

Table 4.1 Intra-seasonal principal components.

4.1 Rainfall Modes

Figure 4.1 shows the spatial loading, the associated time series and the modulus spectrum for the first principal component (PC1). It has large positive loading over the northern Congo. It reflects low-pressure and uplift over this region. The water vapor that maintains the rainfall originates mainly from the tropical Atlantic Ocean. Evapo-transpiration from the dense vegetation also provides an important local source of water vapor (McGregor and Nieuwolt, 1998).

The northern Congo receives rainfall almost throughout the year with a peak season from June to September and minima during December/January. Strong oscillations (wet/dry spells) are revealed during the years 1981,1982, 1986, 1988,1987,1993 whereas in 1990 and 2000 they are weak. The oscillations attain a peak during May/June and appear to be weakest in December/January (exhibiting seasonality). These findings are consistent with the results of Madden (1986) and Cook and Wang (2001) among others. Generally strong Intra-seasonal oscillations are revealed in the 80's than in the 90's.

PC2 (Figure 4.2: a-c) has large positive loading over northeast Angola. This mode reflects the influence of both the Congo and Angola lows during the austral summer (Mulenga, 1998). Rainfall pulses are noted during March/May season while minima occur in the June/July season. The time coefficients associated with this mode have large amplitudes during the years 1981, 1982 and 1992.

PC3 (figure 4.3: a-c) has high positive loading over the east African highlands. The main source of rainfall in east Africa is the ITCZ. The zone of maximum rainfall follows the latitudinal position of the over- head sun with a time lag of about 4-6 weeks (McGregor and Nieuwolt, 1998). The time coefficients associated with this mode have large amplitudes during the years 1980, 1985, 1988, and 1990. The ISO peak is during March/May season and weak during the

rest of the year. It is notable that the Intra-seasonal oscillations over east Africa are weak compared to the first two modes.

The modulus for all the three PC's show that spectral power is strongest in the 30-50 days period typical of the Madden Julian Oscillation. The ISO over this region exhibit annual and inter-annual variation as depicted by the time scores. The primary climatological factors determining the annual variability of the ISO have been recognized as annual variations of sea surface temperatures, wind, and convection (Madden, 1993). However, the magnitude differs from mode to mode and is optimum in different seasons.

Further investigation shows that the intra-seasonal oscillations and seasonal cycles are phase locked (figure 4.4 a-c). Intra-seasonal oscillations (ISO) of 40-50 days are observed within the season over northern Congo. Averaging the ISO scores over 21 years, the seasonal onset and decay is coherent for modes one and three. The ISO is affected by the seasonal cycle through one or more seasonally- dependent energy sources (Huang and Cho, 1998). The seasonal forcing changes the intensity of the intra-seasonal oscillations.

Over eastern Africa, intra-seasonal oscillations influence the first season (March/May) more, than the September/November season. Dry spells of about 20 days are observed within the first season (figure 4.4c). Inspection of rainfall sequences over this region reveal a tendency for a season to be made up of a few isolated rainfall events combined with a few more major rainfall spells punctuated by dry spells (Ward and Mutai, 2000). More work is needed to forecast the March to May rains and intra-seasonal oscillation dynamics could be a valuable consideration.

4.2 Zonal Wind Modes

The spatial loading, time scores and modulus spectrum for PC1 are presented in figure 4.5. The main loading is seen over the equatorial east Atlantic Ocean. An axis extends into the African continent. High spectral power between 30-60 days is notable but little locking to the seasonal cycle is evident. Westerly flow peaks in May /June season apart from 1993 when strong oscillations prevailed in the entire first half of the year. High amplitudes are revealed during 1981, 1987 and 1993.

PC2 has positive loading (westerlies) over east Africa extending up to the Indian Ocean south of the equator (figure 4.6a). Strong amplitudes are observed in 1981, 1985, 1988 and 1992. Oscillations peak in March and appear to be weak in the second half of the year (4.6b). Annual variations in the oscillations are observed and spectral energy is spread widely.

Figure 4.7a shows the spatial loading of PC3. Strong loading is found over the southeast Atlantic. This mode is driven by the quasi-stationary St. Helena anticyclone. This is more of a subtropical mode and influences the southern parts of the African continent. Weak easterlies prevail over central Africa and the Indian Ocean. Time scores reveal annual and inter-annual variability of ISO over this region.

The 21year mean reveals intra-seasonal oscillations of 30-60 days and shorter cycles too (figure 4.8:a-c). Organized oscillations are prevalent at the beginning and end of the year for all the three modes. This could be explained by their approximate location along the equator (Rui and Wang, 1990). Intra-seasonal oscillations over the Atlantic and the Indian Ocean are organized by the seasonal cycle. Strong westerlies are observed throughout the March to May and September/October seasons over the Atlantic (figure 4.8a). Over the Indian Ocean, ISO in the zonal wind are predominant in the March to May season as

compared to the rest of the year (figure 4.8b). Figure 4.8c reveals that westerlies over the St Helena mode are spread throughout the year yet amplitudes are seasonally dependent (Huang and Cho, 1998).

4.3 Cross Correlation Analysis.

To investigate the influence of zonal wind on rainfall at intra-seasonal time scale, cross correlation analysis was done for rainfall modes (R1, R2, R3) and zonal wind Modes (U1, U2, U3) at different time lags (Table 4.2).

Lags(Pentads)	U1/R1	U1/R3	U2/R3	U2/R2
-6			-0.27	
-5			-0.24	
-4	-0.2	-0.25		0.18
-3		-0.23		0.25
-2			0.3	0.17
-1	0.23		0.41	
0	0.3	0.3	0.35	-0.25
1	0.2	0.25		-0.34
2			-0.2	-0.21
3			-0.4	
4	0.18		-0.3	
5				0.22
6				0.23

Table 4.2 shows correlation coefficients for intra-seasonal rainfall and zonal wind modes. Weak associations ($r < 0.15$) are omitted.

A strong relationship between U1 and R1 is observed as well as U1 and R3 (Table 4.2). The strong association between U1 and R1 at zero-lag depicts the

influence of the Atlantic Ocean on the rainfall variability over the Congo (figure 4.0). McGregor and Niewolt (1998) observed that the rapid turnover of moisture between the earth's surface and the lower troposphere is not sufficient to maintain high rainfall over this region, as exhibited by the general decrease of rainfall with distance from the Atlantic.

The relationship between U1 and R3 clearly emphasizes the association between surface westerly anomalies over the Atlantic and rainfall in eastern Africa (Okoola, 1999). Wet spells in eastern Africa are often associated with synoptic disturbances that propagate eastward into the region in association with westerly low-level wind anomalies.

The correlation at lag –4 pentads (table 4.2) suggests westerlies surge over the Atlantic 20 days before the rain event over eastern Africa. The above results are consistent with findings of Mutai and Ward (2000). A lead-lag structure of intra-seasonal teleconnections with eastern African rainfall suggested that 10-20 days before the rainfall event, low level westerlies develop in the equatorial Atlantic, and penetrate across Africa during the event.

Relatively high correlation coefficients between U2 and R3 are observed at different lags. The highest correlation coefficients are –0.4 at lag –1 and 0.4 at lag +3. This positive relationship emphasizes the role of local westerly wind anomalies in rainfall events over east Africa. Agumba (1985) suggested that the introduction of deep westerlies to eastern Africa associated with a barotropic structure over northern Africa cause synoptic scale lifting in east Africa, hence increased rainfall. Waliser et al (1999) observed that before the rainfall event, anomalous surface easterlies grow over the Indian Ocean, giving the NE and SE trades a stronger onshore component as they approach East Africa. During the event these wind anomalies weaken.

A strong negative correlation is observed between rainfall over northeast Angola and the Indian zonal wind mode. This relationship implies that increased surface westerly flow over the Indian Ocean reduces rainfall over northeast Angola.

4.4 Summary

Principal component analysis has revealed important spatial and temporal patterns for non-transient intra-seasonal oscillations over the study region. The dominant rainfall mode is over northern Congo where maximum upward motion occurs possibly in relation to forest vegetation. The third mode emphasizes the role of mountainous topography in the modulation of rainfall over eastern Africa. Spectral peaks of 30-50 days were revealed particularly during the rainy seasons.

The PCA for the zonal wind revealed important modes over the equatorial region. The dominant mode emphasizes the importance of the Atlantic moisture influx in the modulation of the intra-seasonal oscillations over tropical Africa. Cross correlation provided an insight to the role of the Atlantic and Indian Oceans in the modulation of intra-seasonal oscillations over tropical Africa.

The results above suggest that wet spells over the Congo and eastern Africa are triggered by increased westerly flow over the Atlantic. These start to develop a few pentads before the rainfall event over equatorial Africa (Mutai and Ward, 2000). Increased westerlies over the Indian Ocean reduce rainfall activity since they draw moisture away from the region.

The major non-transient ISO modes over tropical Africa have been revealed in this chapter. Chapter five examines the evolution and propagation of African intra-seasonal oscillations. In this case hovmoller and Composite results will be presented and discussed.

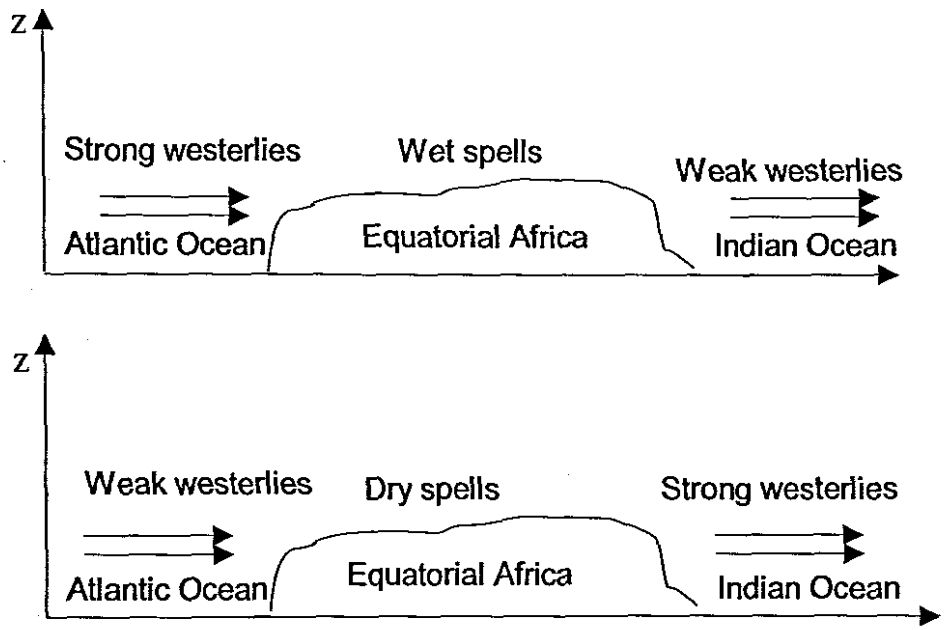

Figure 4.0 Schematic diagram showing the association of zonal wind and rainfall at intra-seasonal time scales.

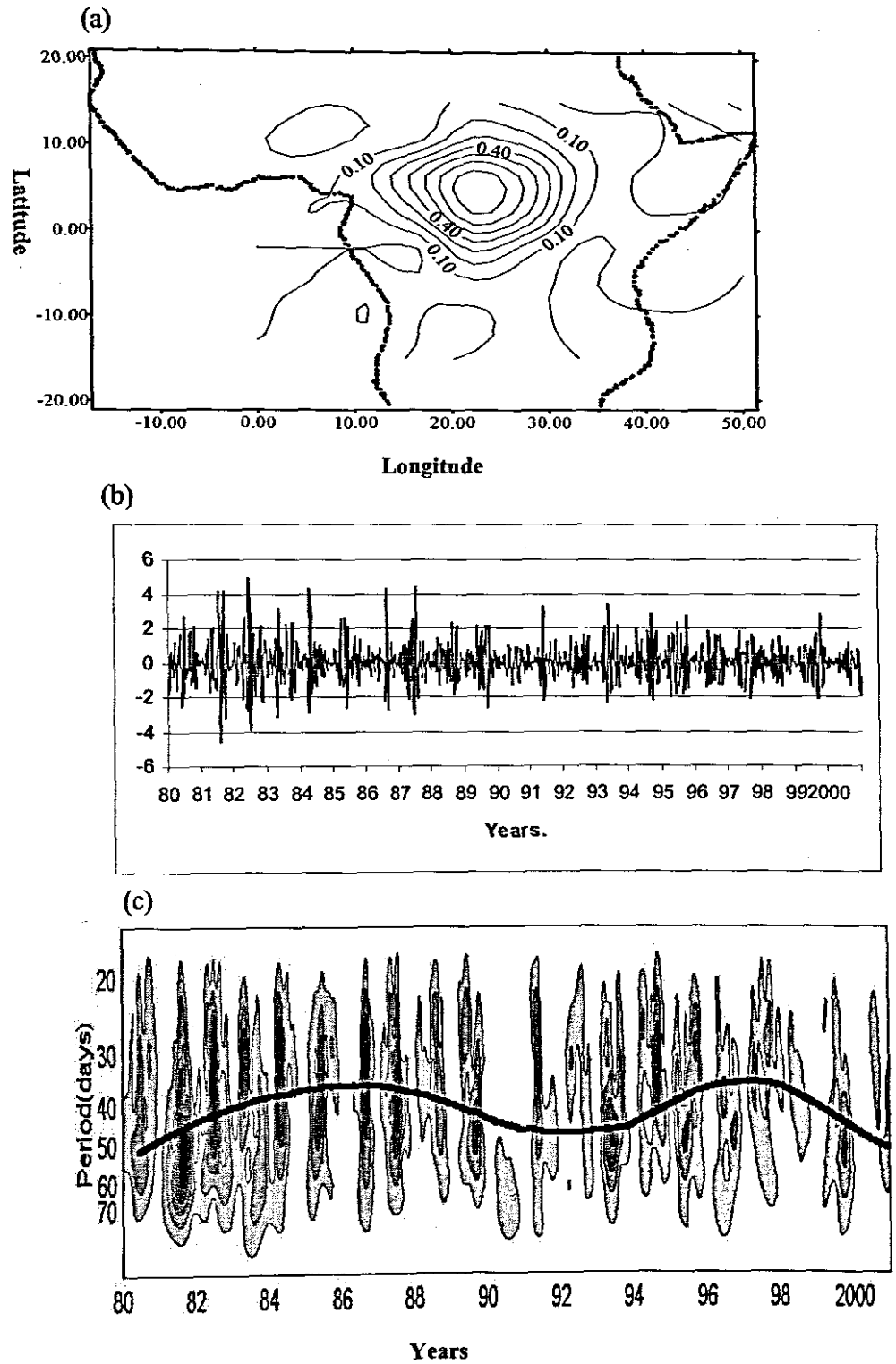

Figure 4.1 (a) Spatial loading (b) Time scores (c) Modulus spectrum for intra-seasonal rainfall for the first Principal Component PC1 (29% of total variance). Bold line represents dominant spectral cycle.

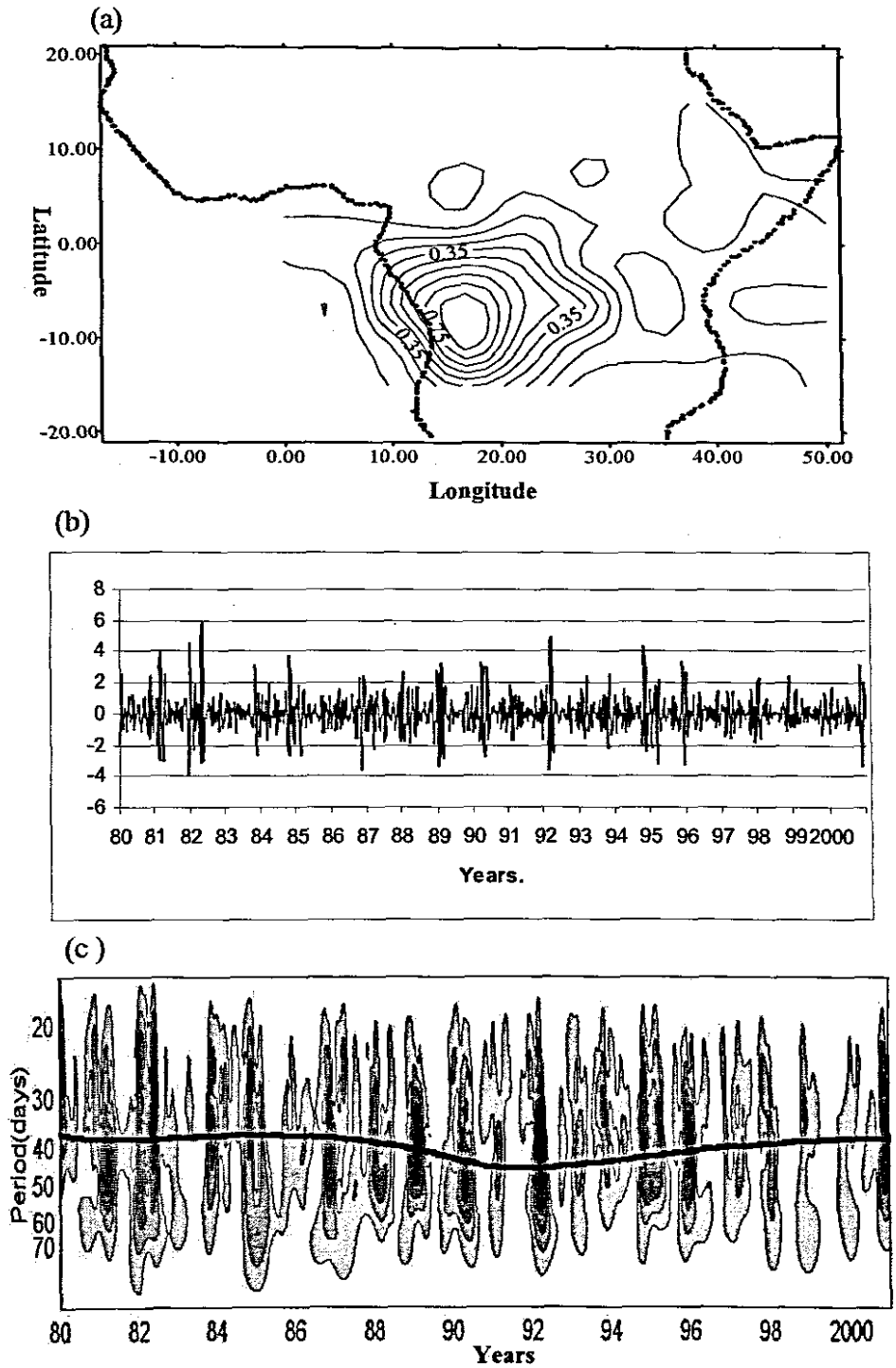

Figure 4.2 (a) Spatial loading (b) Time scores (c) Modulus spectrum for intra-seasonal rainfall for the second Principal Component PC2 (22% of total variance).

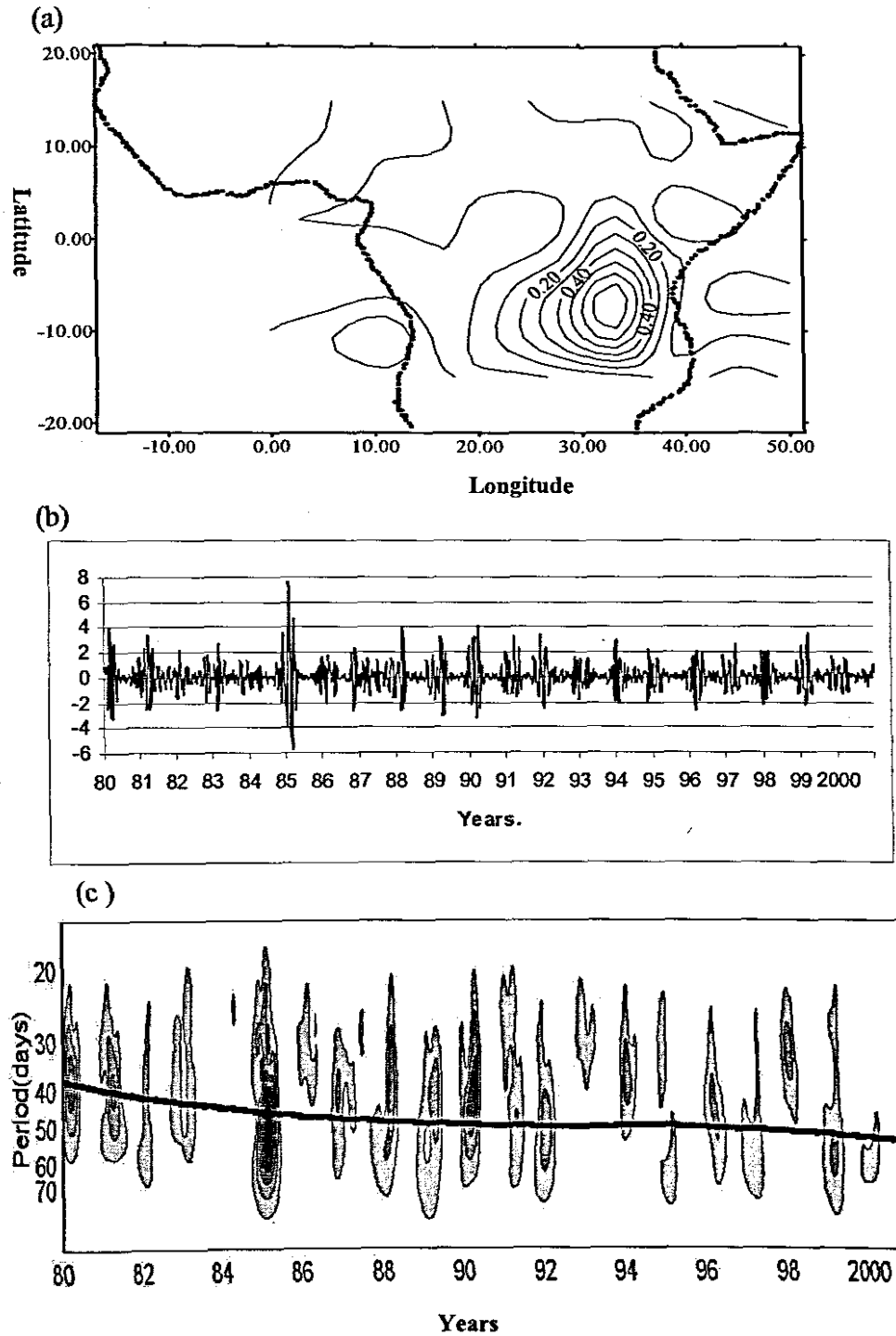

Figure 4.3 (a) Spatial loading (b) Time scores (c) Modulus spectrum for intra-seasonal rainfall for the third Principal Component PC3 (20% of total variance).

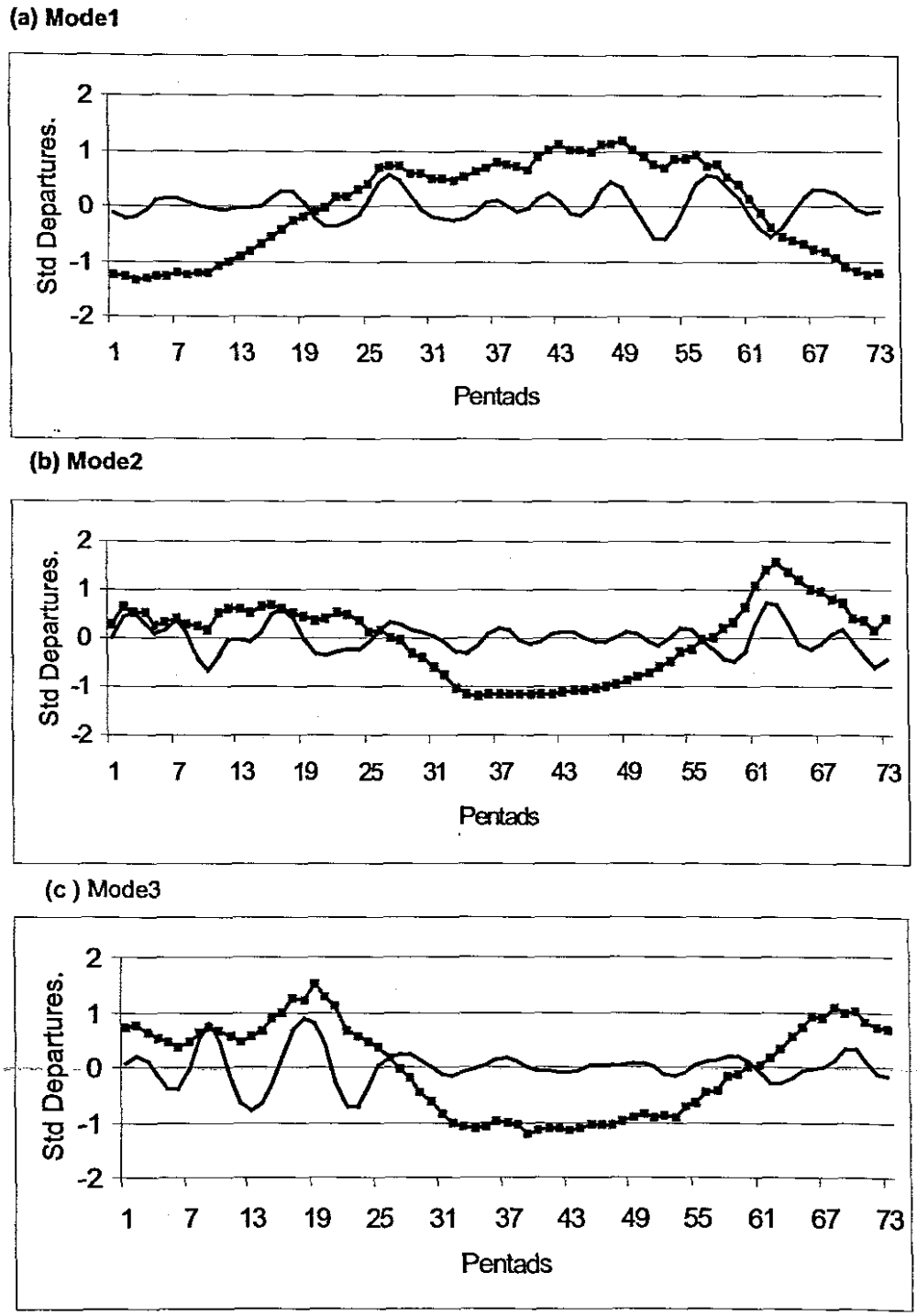

Figure 4.4 Intra-seasonal and seasonal cycles for rainfall for (a) PC1, (b) PC2, (c) PC3, averaged over a period of 21 years.

—♦— Seasonal cycle of rainfall

——— Intra-seasonal oscillations from time score

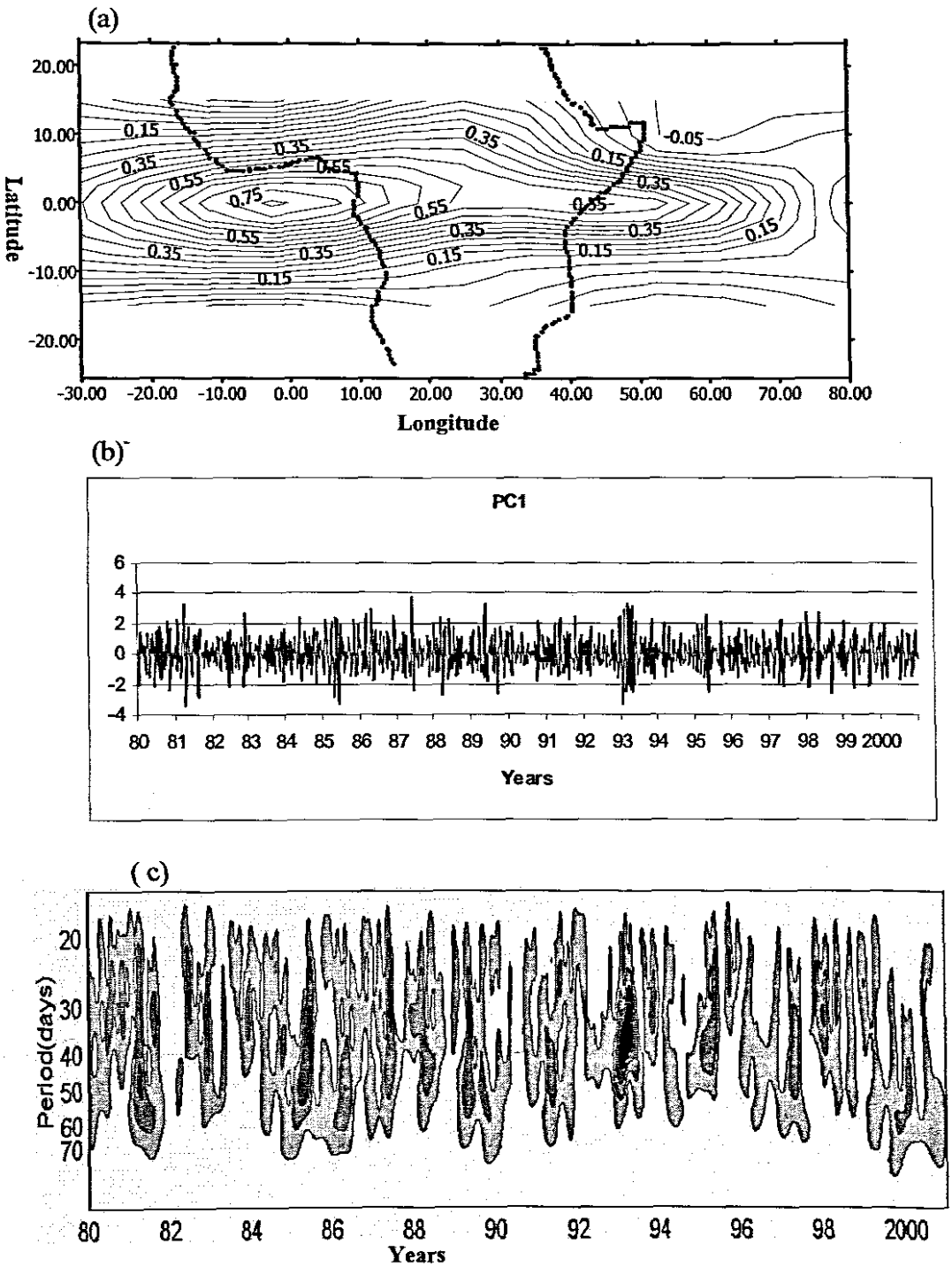

Figure 4.5 (a) Spatial loading (b) Time series (c) Modulus spectrum for Intra-seasonal Zonal wind for the first principal Component PC1 (14.3% of the total variance).

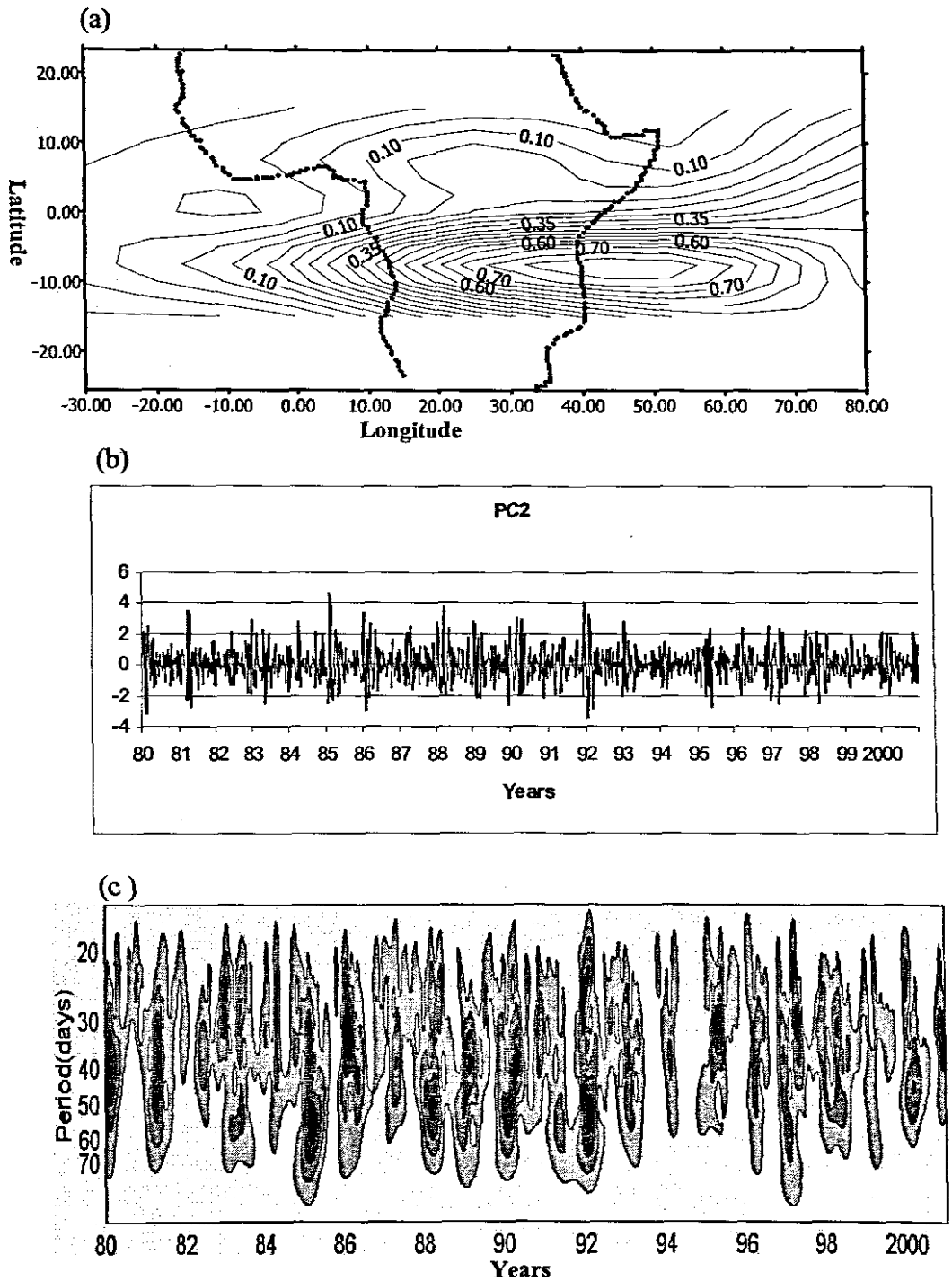

Figure 4.6 (a) Spatial loading (b) Time series (c) Modulus spectrum for Intra-seasonal Zonal wind for the second Principal Component PC2 (13.3% of the total variance).

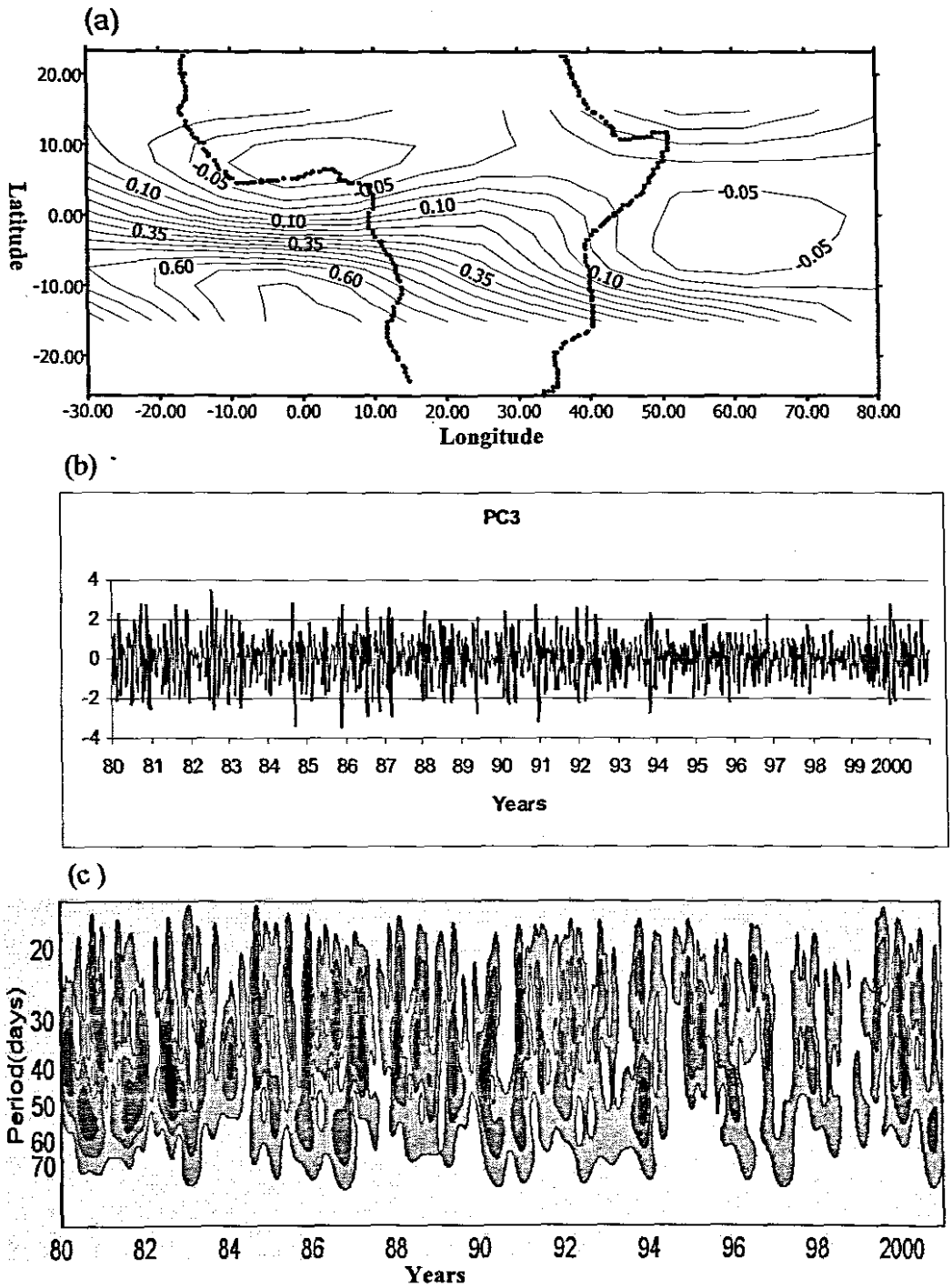

Figure 4.7 (a) Spatial loading (b) Time series (c) Modulus spectrum for Intra-seasonal Zonal wind for the third principal Component PC3 (9.8% of the total variance).

(a) Atlantic Mode

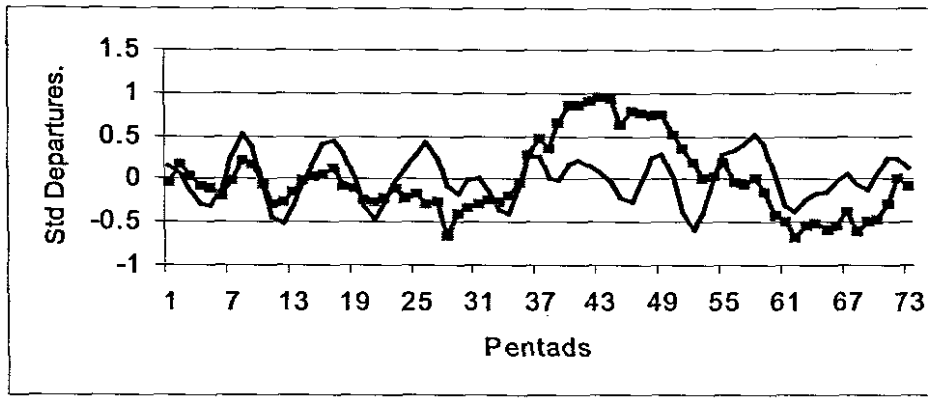

(b) Indian Mode

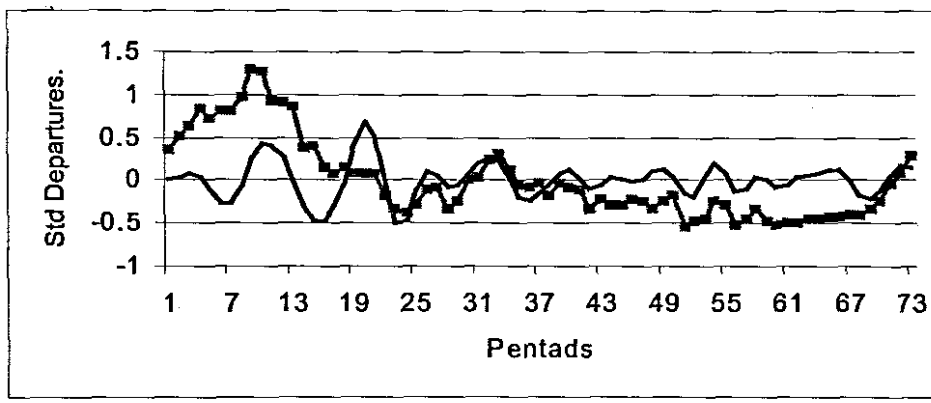

(c)St. Helena Mode

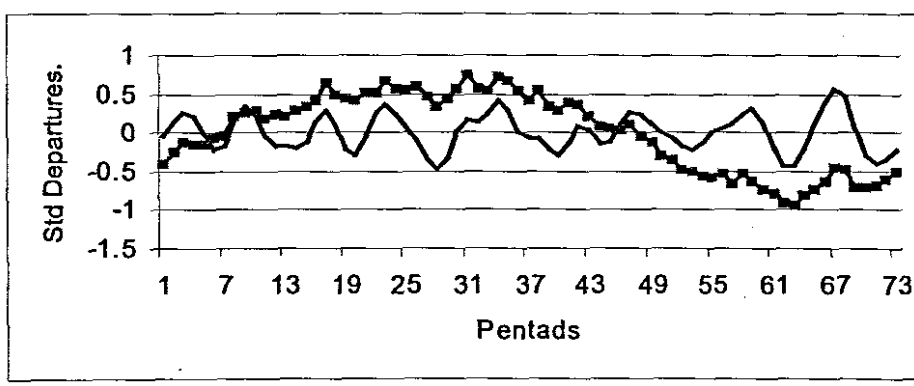

Figure 4.8 Intra-seasonal and seasonal cycles for 700hPa zonal wind for (a) PC1, (b) PC2, (c) PC3, averaged over 21 years.
—♦— Seasonal cycle of zonal wind where + =westerly
——— Intra-seasonal oscillations from time score

(a)

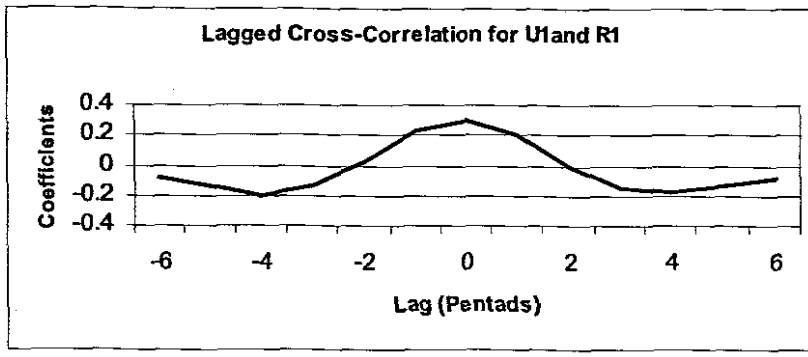

(b)

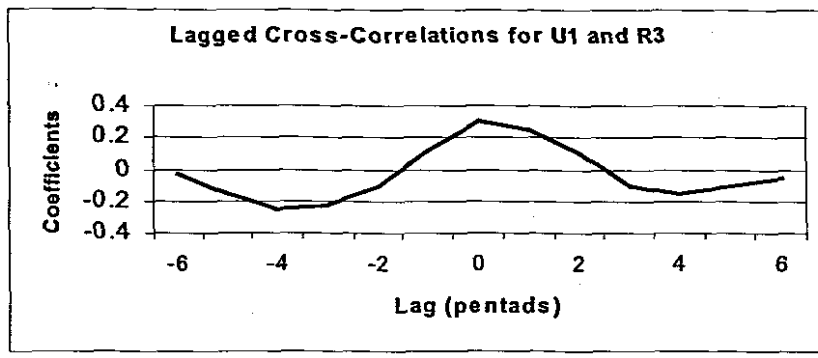

(c)

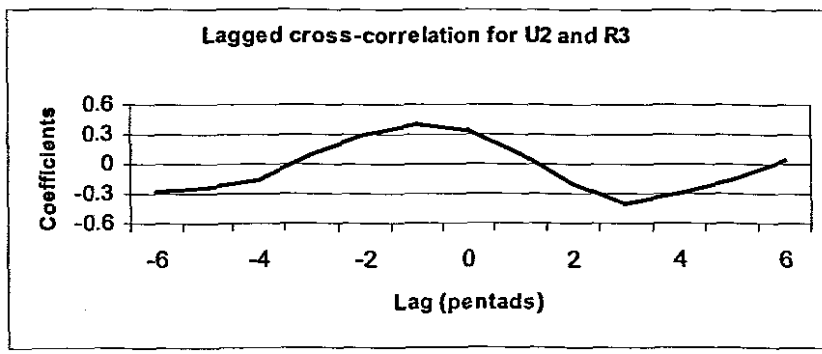

(d)

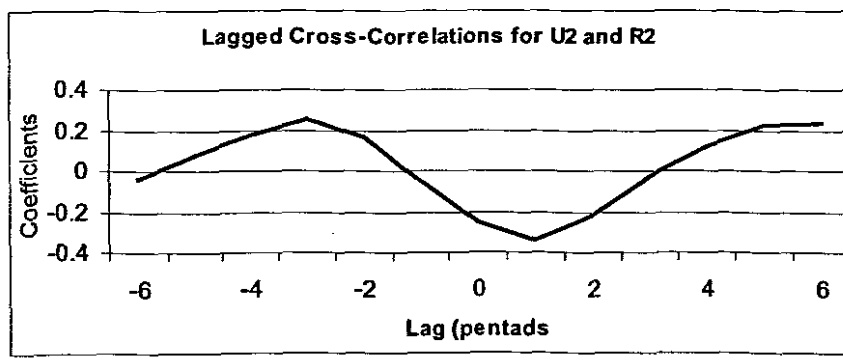

Figure 4.9 Cross Correlation of intra-seasonal zonal wind and rainfall PCA modes.

(a)

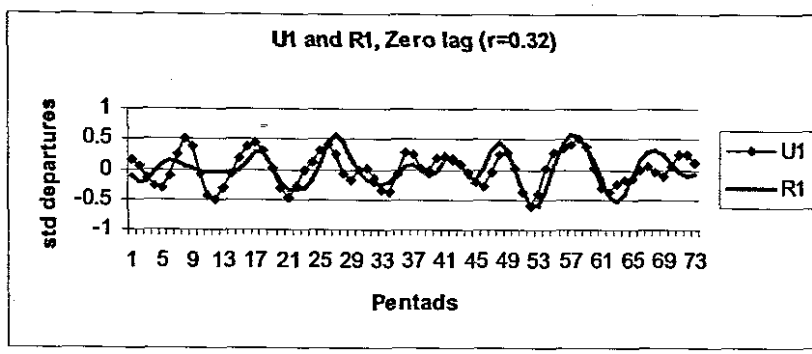

(b)

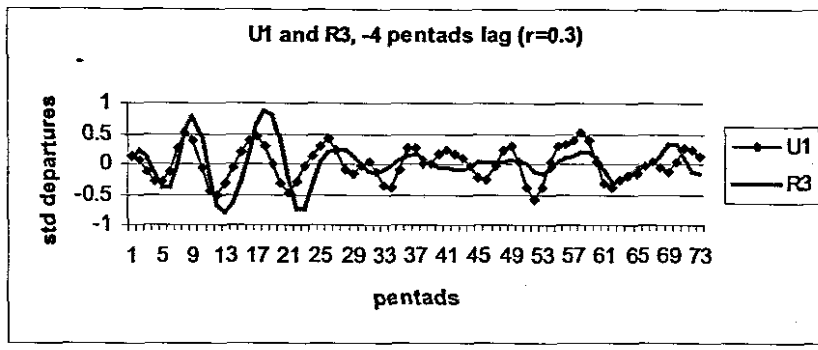

(c)

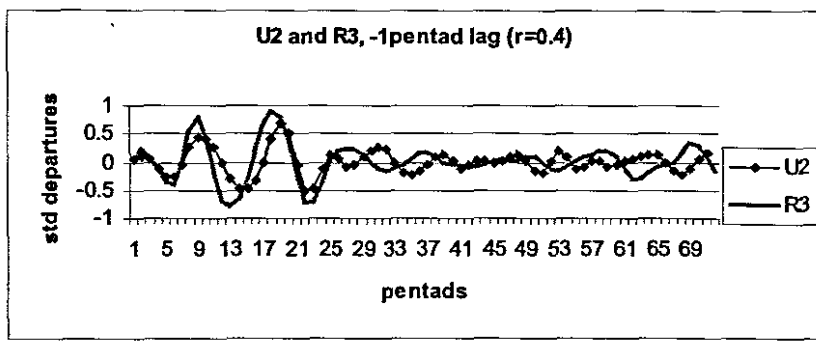

(d)

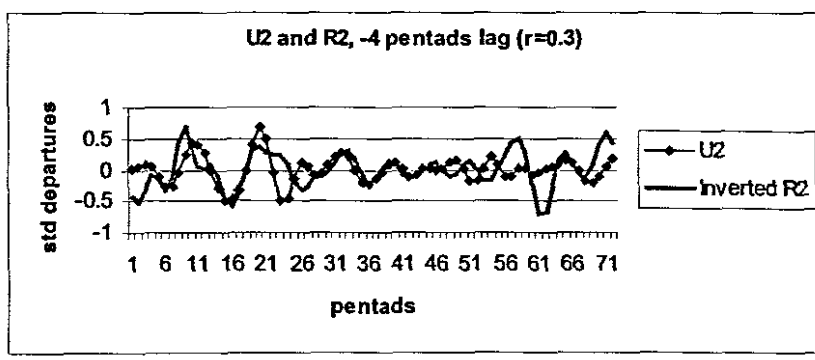

Figure 4.10 Lagged correlation for intra-seasonal rainfall and zonal wind modes.

Chapter Five

Evolution and propagation of African intra-seasonal Oscillations

5.0 Introduction

Whereas chapter four identified a static, pulsed convective system, this chapter will describe the evolution and propagation of intra-seasonal oscillations over tropical Africa. The dominant mode of rainfall (northern Congo) from the PCA analysis is considered here since it explains the largest percentage of total variance. This mode receives most rainfall during the June/September season.

Previous studies have examined intra-seasonal oscillations based on OLR data in areas where there is convective activity. In addition to OLR, velocity potential at upper level is chosen as the dynamic quantity representing the intra-seasonal oscillations to investigate their evolution and propagation characteristics in this study.

Velocity potential is a measure of the divergent component of the wind. Regions with positive (negative) velocity potential indicate converging (diverging) winds. The 200hPa level (~10 km above the earth's surface) was chosen because at this level, converging (diverging) winds indicate downward (upward) vertical motion. It is also above the major topographic features of the earth's surface.

Hovmoller plots averaged from 2.5°S to 12.5°N for the rainy season, (April to November) of OLR and velocity potential anomalies are presented in section one and two of this chapter. Composite results for velocity potential and OLR anomalies are examined in section three.

5.1 Hovmoller results for OLR anomalies

The hovmoller plots (figure 5.1:a-d) for the years 1980-2000 demonstrate that there are eastward and westward propagating convective features as well as standing systems due to in-situ convection. Stationary convective features are revealed during 1981, 1984, 1985, 1992, and 1997. Some years exhibit ISO events of all the three characteristics mentioned above. For example, in 1988 a convective system developed in the Atlantic in June, propagated eastwards to the Indian Ocean. However, part of it propagated westward. Eastward propagation is also revealed during 1987 and 1989, although more pronounced over the oceans (figure 5.1b). Westward propagation is observed in the years 1990 and 1995 (figure 5.1c).

During 1993 (figure 5.1c), a system developed near 25°E, propagating eastward at about 2 m s^{-1}. In 1999 (figure 5.1d), a convective feature developed at 30°W in the Atlantic in June and propagated eastwards to 10°E, becoming stationary up to mid October. In April 2000, another convective system developed at 30°W propagated eastwards at 5 m s^{-1} to 5°E in June becoming stationary till November. Further, stationary systems are observed from May to October between 12.5°E to 30°E during this year. Deep convection is also observed in the west Indian Ocean during 1997, which was actually an El-Nino year.

In general, eastward propagation is not well defined during the JJAS season in the 2.5°S-12.5°N band over the African continent. Standing systems are more prevalent. The non-propagating pattern of OLR could be associated with the African Monsoon. Some of the propagating OLR anomalies are seen to originate west of 0°. Results reveal some convective features developing over the Atlantic and over the Congo basin. Eastward propagating features are found to have different phase speeds in different years and over different areas. Sometimes the features move slowly, then become stationary and resume propagation in the same direction or in a different one.

Over East Africa, eastward propagation is weak and the strong meriodional circulation along the coast appears to suppress it. Results show that the May to June onset ISO shows strong eastward movement of convection along the equator, however, August to October has a weak eastward propagating signal being consistent with earlier studies (for example, Cook and Wang, 2001). The intra-seasonal oscillation is found to influence the onset, break and retreat of the Indian monsoon (Chen et al., 1988).

5.2. Hovmoller results for velocity potential anomalies at 200hPa

Velocity potential anomalies are presented in figure 5.2, (a-d). Hovmoller plots show standing and eastward propagation of atmospheric divergence over the region. The circulation anomaly develops over the Atlantic and propagates eastward at 5 m s^{-1} to the Indian Ocean (for example, 1986, 1991,1999). The anomalies reveal that some features intensify as they cross the Congo basin with additional upward motion. For example, divergence developed over the Atlantic in 1983 in September, propagated eastwards, intensified over the Congo in October and proceeded to the Indian Ocean.

Results reveal that the Congo basin intensifies the intra-seasonal oscillation (for example, 1981, 1988, and 1997). Atmospheric upper level divergence is seen to develop over the Congo basin and propagates to the equatorial Indian Ocean at 3-5 m s^{-1} where it intensifies due to the warm waters (Salby and Hendon, 1994)

Percentages of standing, eastward as well as westward propagating systems were computed for cases recorded in the period 1980-2000. Results (table 5.1) strongly imply that the dominant mode of intra-seasonal convective activity and atmospheric circulation is predominantly an eastward propagating disturbance accounting for 44% and 95% of total cases in convection and velocity potential anomalies respectively. In addition to standing systems, westward migration was

observed in convection but the spatial distribution is limited and the strength of systems is weaker compared to the eastward propagation.

Parameter	Standing features (%)	Eastward propagation (%)	Westward propagation (%)
OLR	31	44	25
Velocity Potential	5	95	Nil

Table 5.1 shows percentage of stationary, eastward and westward propagating systems using OLR and velocity potential anomalies.

5.3 Composite results for OLR and 200hPa Velocity Potential

To understand the evolution of intra-seasonal oscillations, three pentad phases were selected for analysis. Considering that the deep convection phase is p0, then two pentads p-2 and p-1 prior to deep convection were analyzed. Composites were drawn from seven years when strong wet spells (anomalies of rainfall > 2 mm day^{-1}) were recorded over the northern Congo region during the JJAS season. Table 5.2 gives the years and the pentads used in the analysis.

5.3.1 Outgoing long wave radiation anomalies

Figure 5.3 shows the composite OLR anomalies. At p-2, a convective activity is observed over the northern Atlantic, western Africa, and northern Congo and in the Indian Ocean. Negative anomalies are also seen over some parts of the southern Atlantic, southern Africa and Madagascar. The system shifts from west to central Africa at p-1 with even lower values (deep convection) than before, revealing eastward propagation characteristics of the ISO. The feature over South Africa reaches the coast extending towards the Indian Ocean, while over Madagascar, convective activity propagates to the east of the island.

At p0, convection intensifies over northern Congo covering some parts of Sudan and Uganda. Though it's fully established at p0, little apparent propagation is found at this stage.

Years	p-2	p-1	P0
1981	50	51	52
1986	46	47	48
1987	38	39	40
1988	45	46	47
1989	45	46	47
1993	47	48	49
1994	48	49	50

Table 5.2 shows the years and pentad numbers used in composite analysis for the strong wet spells in the June-September season over northern Congo.

5.3.2 Velocity potential anomalies

Figure 5.4 shows the evolution of ISO using velocity potential anomalies at 200hPa level. At p-2 there is strong divergence (convergence) over the Atlantic Ocean and the southwestern Indian Ocean while convergent (divergent) flow dominates the African continent at the upper (lower) levels. At p-1 the circulation propagates eastward to the African continent. Strong divergence is over central Africa at upper levels. Over the Indian Ocean, propagation is noted as the system shifts east of Madagascar. At p0, divergent flow is well established over the Congo basin and the adjacent Indian Ocean. However, the reverse occurs over western Africa and the east Atlantic Ocean.

Intra-seasonal variability during boreal summer, while locally exhibiting spectral peaks over the Indian Ocean, does not exhibit pronounced eastward propagation

over the highlands of eastern Africa. This is explained by the strong meridional flow over the east African coast as earlier discussed and shown in chapter 3.

5.4 Summary

The above results reveal that intra-seasonal variability within the equatorial troposphere is characterized by eastward propagating, stationary and westward planetary-scale disturbances. Eastward propagation is more pronounced in the velocity potential anomalies than in the OLR anomalies (table 5.1). This is explained by the nature of the OLR data and the influence of land-atmosphere interactions on intra-seasonal oscillations. It appears that the thermodynamic component is more stationary and the kinematic component more transient.

Hu and Randall (1994) suggested that the local interactions between convection, evaporation and radiation produce a local standing oscillation in convection with a 50 days period. Motivated by the possibility that intra-seasonal perturbations in circulation are induced by standing oscillations in convection, numerical simulations have been conducted in which spatially confined, stationary forcing oscillating with a given frequency is prescribed to stimulate intra-seasonal perturbations in circulation (Hendon and Salby, 1994). However, such simulations fail to capture eastward propagation of the Rossby gyres, which accompany the convective anomaly.

Here in this diagnostic study intra-seasonal oscillation exhibit maxima over the oceans and minima over land as revealed by the hovmoller plots. This characteristic of intra-seasonal oscillation is explained by the following:
(i) The local energy supply by turbulent moisture fluxes from the ocean surface is diminished over the land surface.
(ii) The remote energy supply by large-scale moisture convergence is reduced because the topography frictionally retards the circulation in the boundary layer.

(iii) Convection variability over land is dominated by a vigorous diurnal cycle maintained by various local mechanisms (for example surface diurnal heating and sea breezes) that are unrelated to ISO.

In view of the fact that intra-seasonal variations are linked to a variety of fundamental physical processes, a through understanding of the phenomenon has potential impact on prediction of long-range variations of the tropical atmospheric circulation.

Much of the data used in this study is derived from satellite observations due to the scarcity of conventional data over some parts of Africa. The next chapter is dedicated to calibration and validation of satellite rainfall over Uganda to assess the reliability of these estimates.

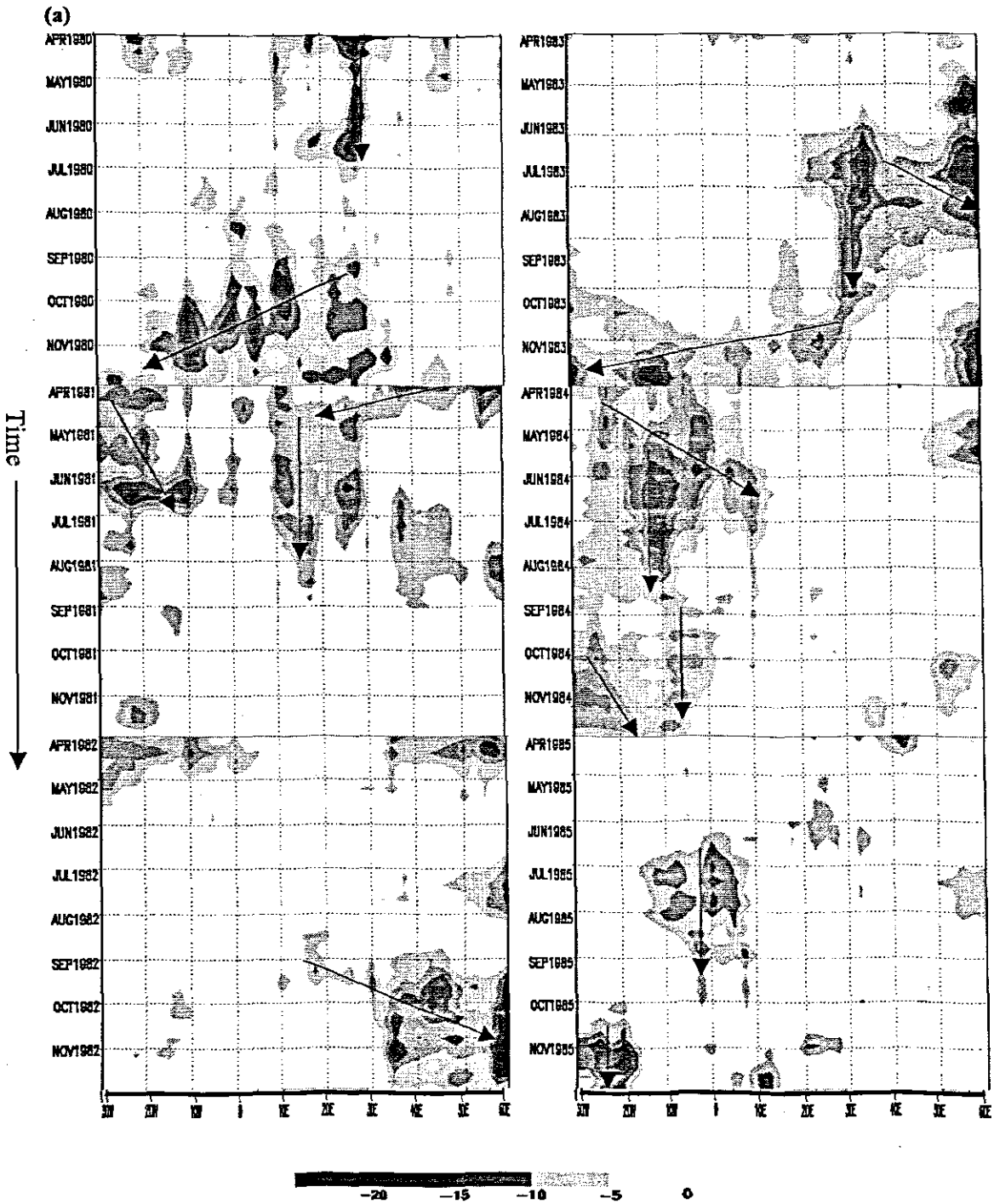

Figure 5.1 shows hovmoller plots for OLR Anomalies averaged from 2.5°S to 12.5°N for the years 1980 to 1985. Note the temporal discontinuity from November of previous year to April of the following year here and in the following hovmoller plots.

(b)

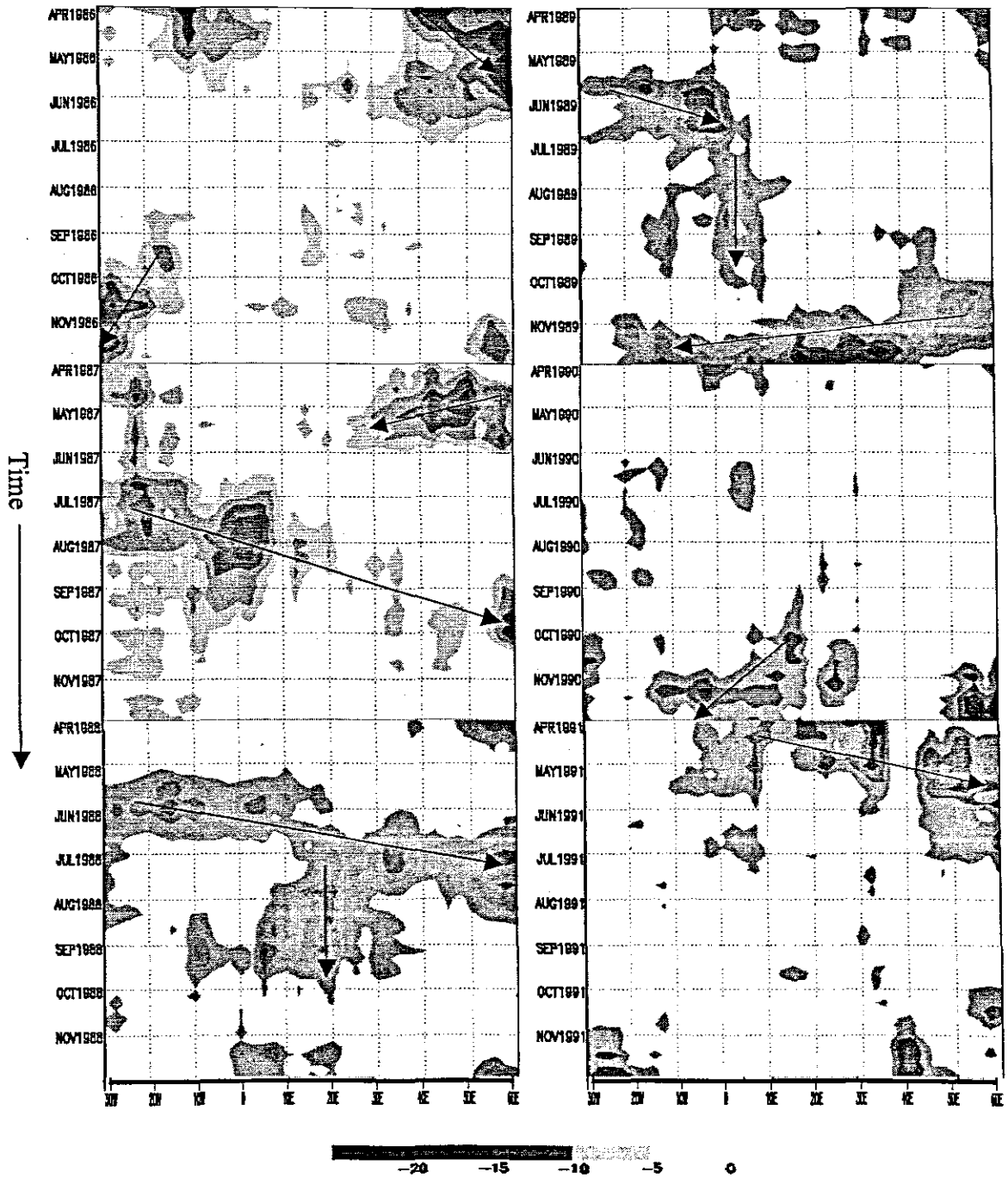

Figure 5.1 (continued) shows hovmoller plots for OLR Anomalies averaged from 2.5°S to 12.5°N for the years 1986 to 1991.

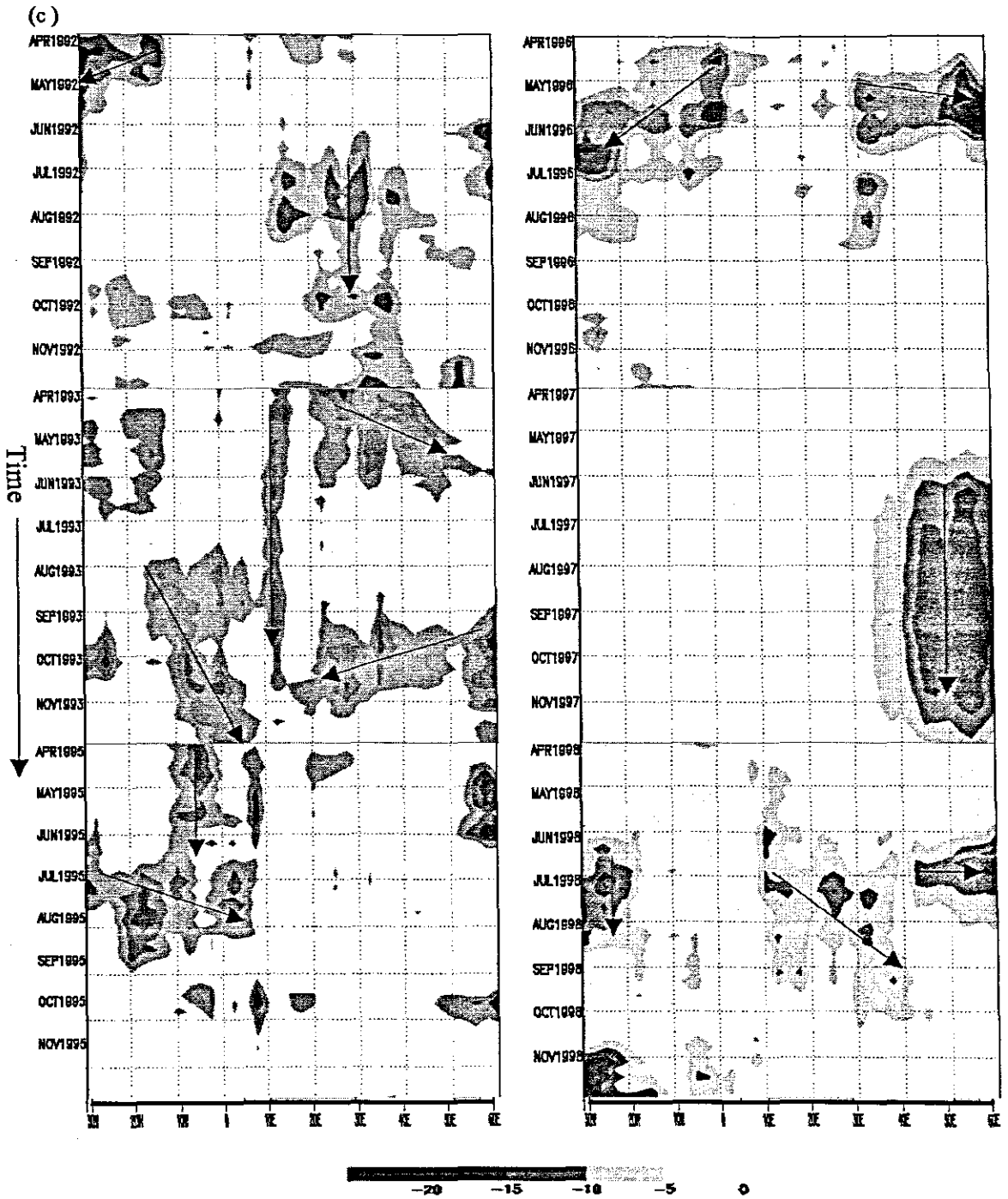

Figure 5.1 (continued) shows hovmoller plots for OLR Anomalies averaged from 2.5°S to 12.5°N for the years 1992 to 1998

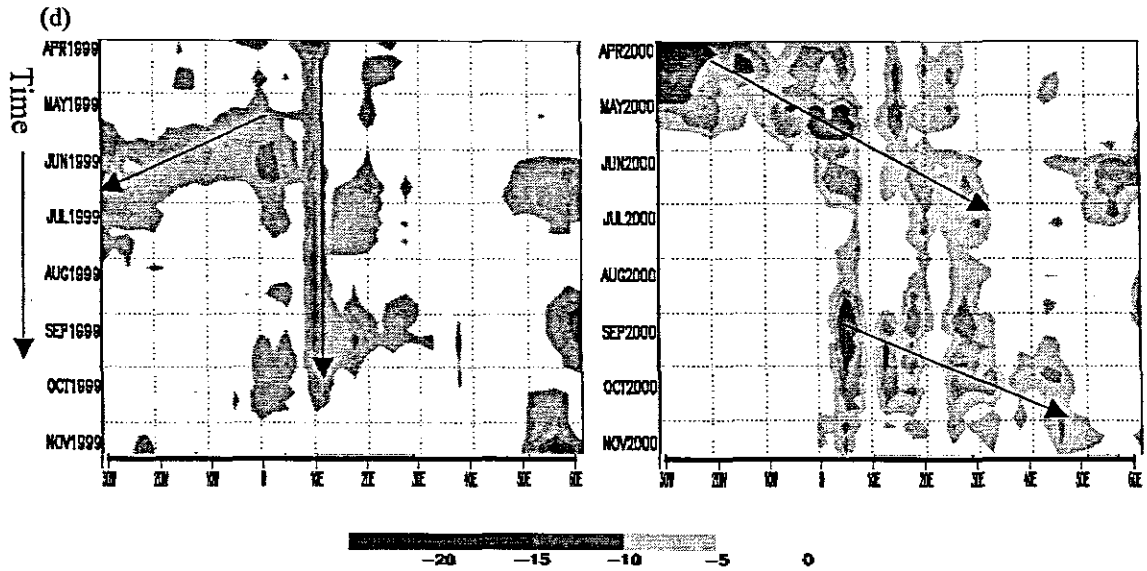

Figure 5.1 (continued) shows hovmoller plots for OLR Anomalies averaged from 2.5°S to 12.5°N for the years 1999 to 2000

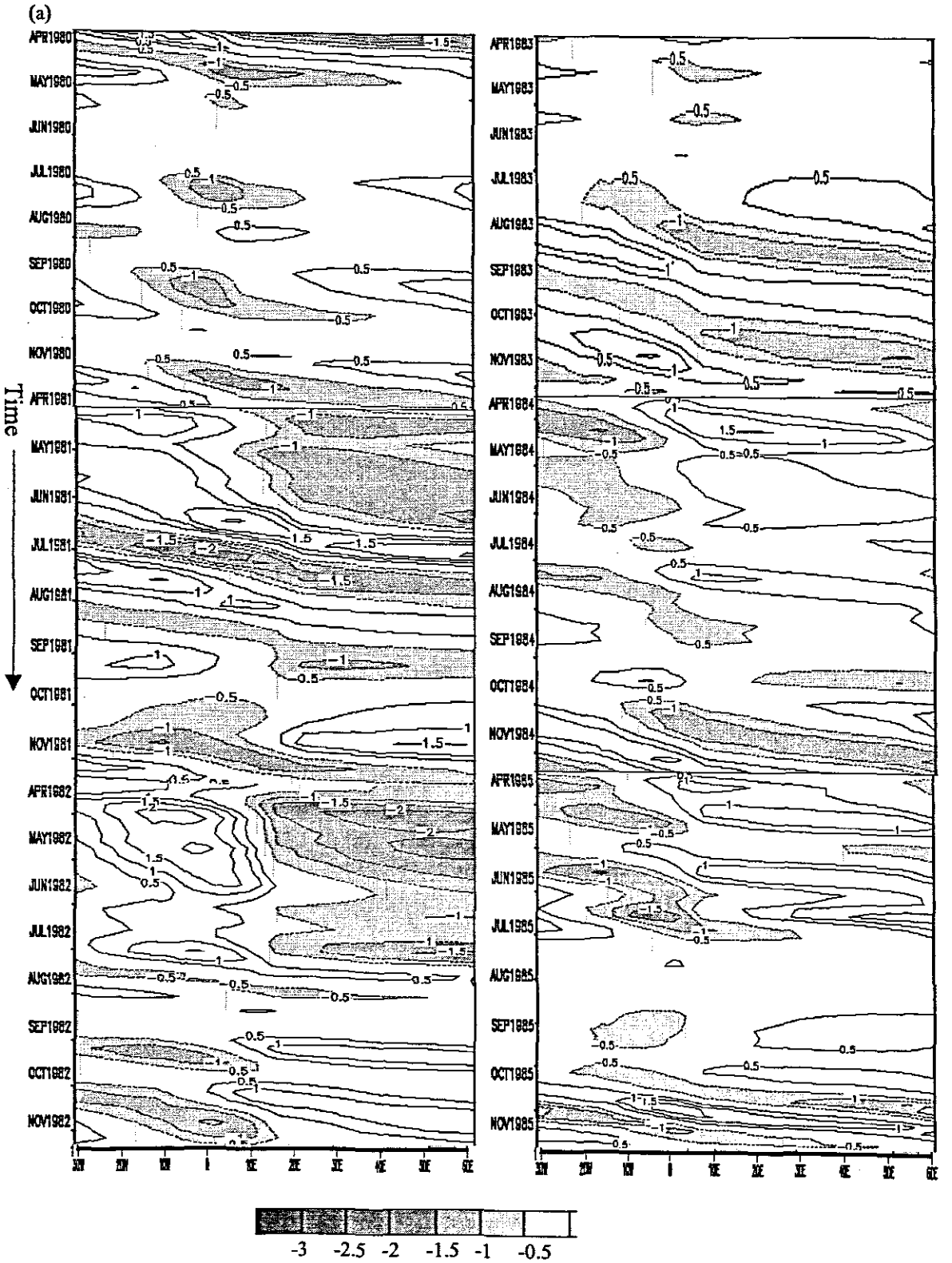

Figure 5.2 shows hovmoller plots for velocity potential anomalies averaged from 2.5S to 12.5N for the years 1980 to 1985.

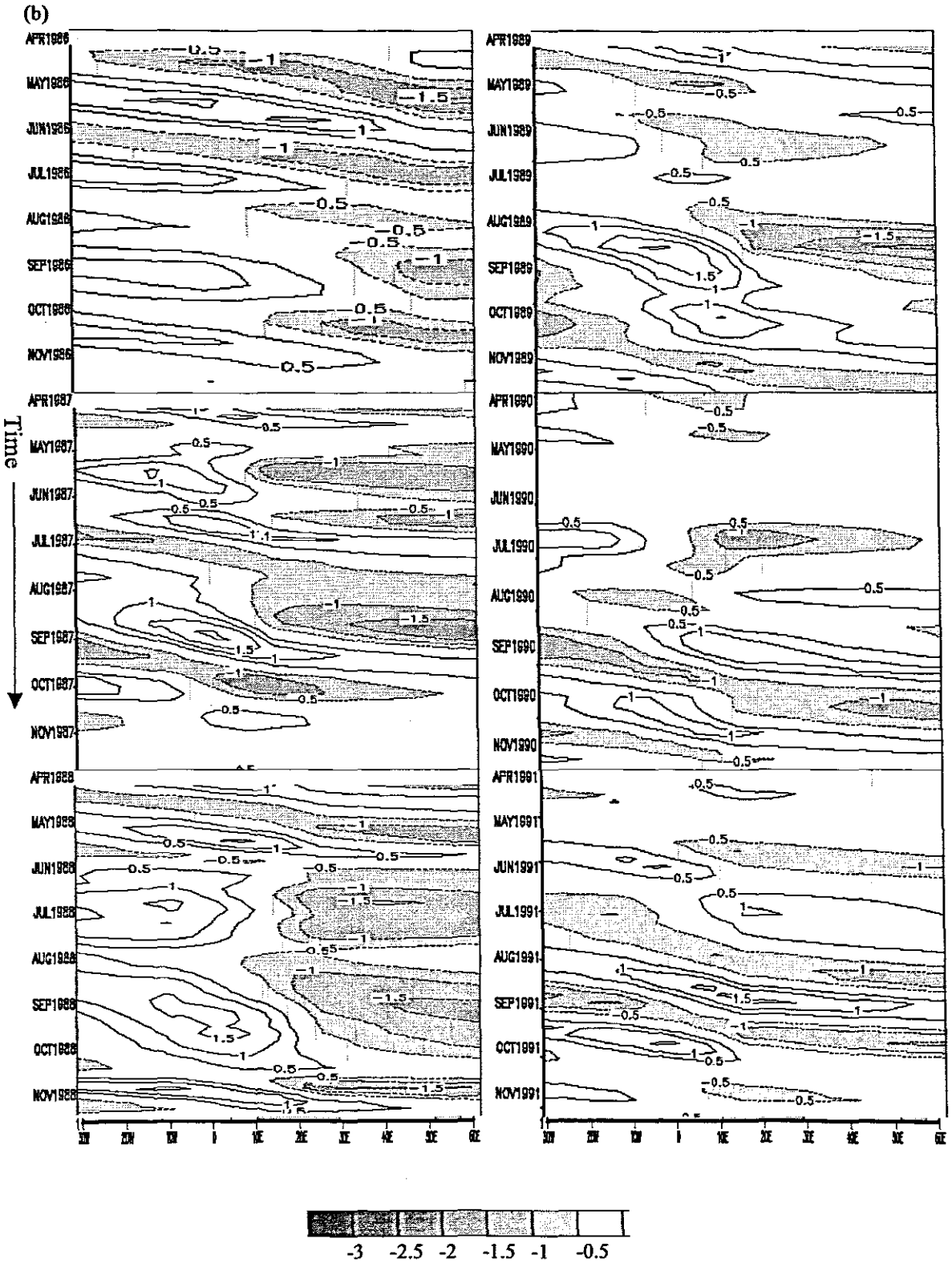

Figure 5.2 (continued) shows hovmoller plots for velocity potential anomalies averaged from 2.5S to 12.5N for the years 1986 to 1991.

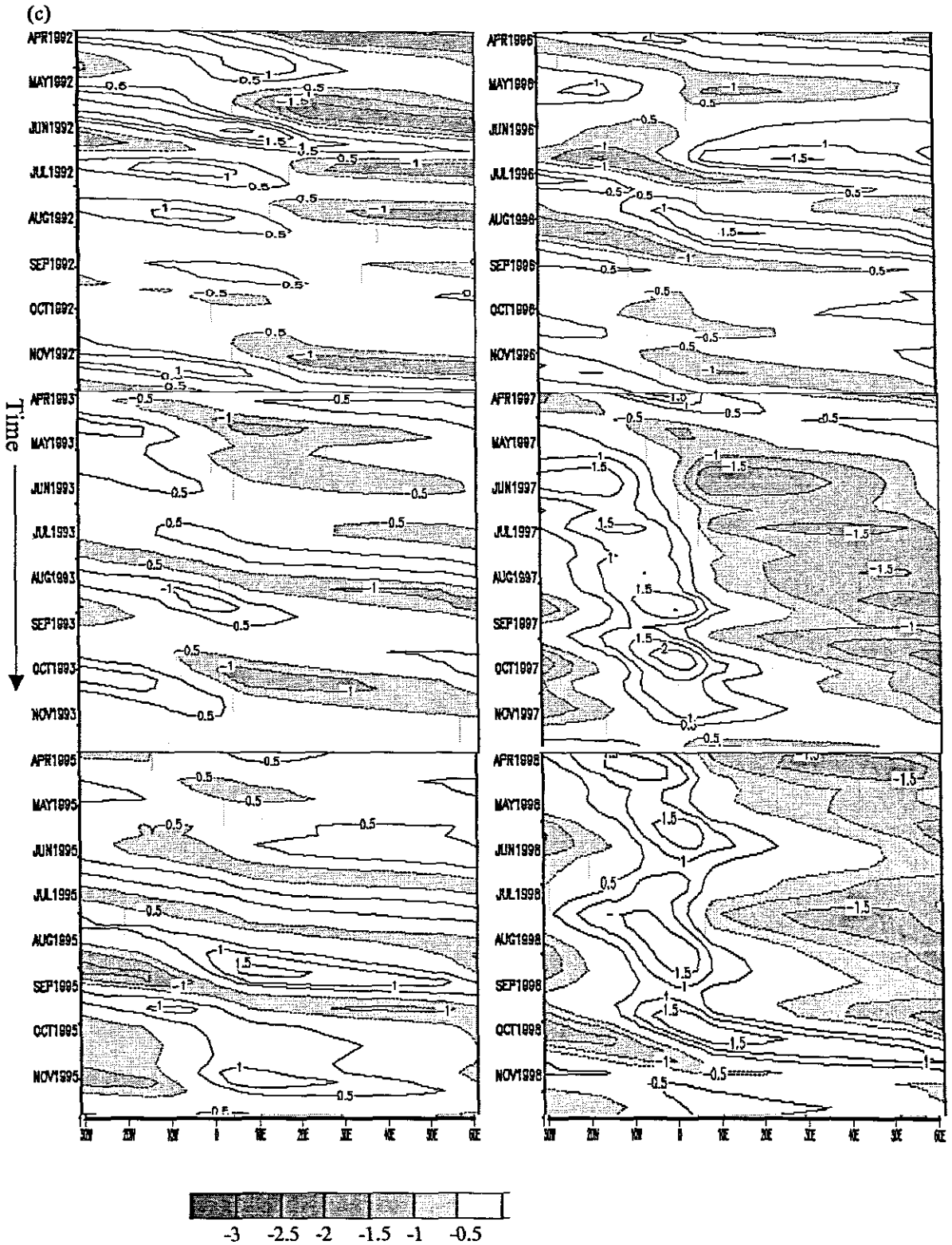

Figure 5.2 (continued) shows hovmoller plots for velocity potential anomalies averaged from 2.5S to 12.5N for the years 1992 to 1998.

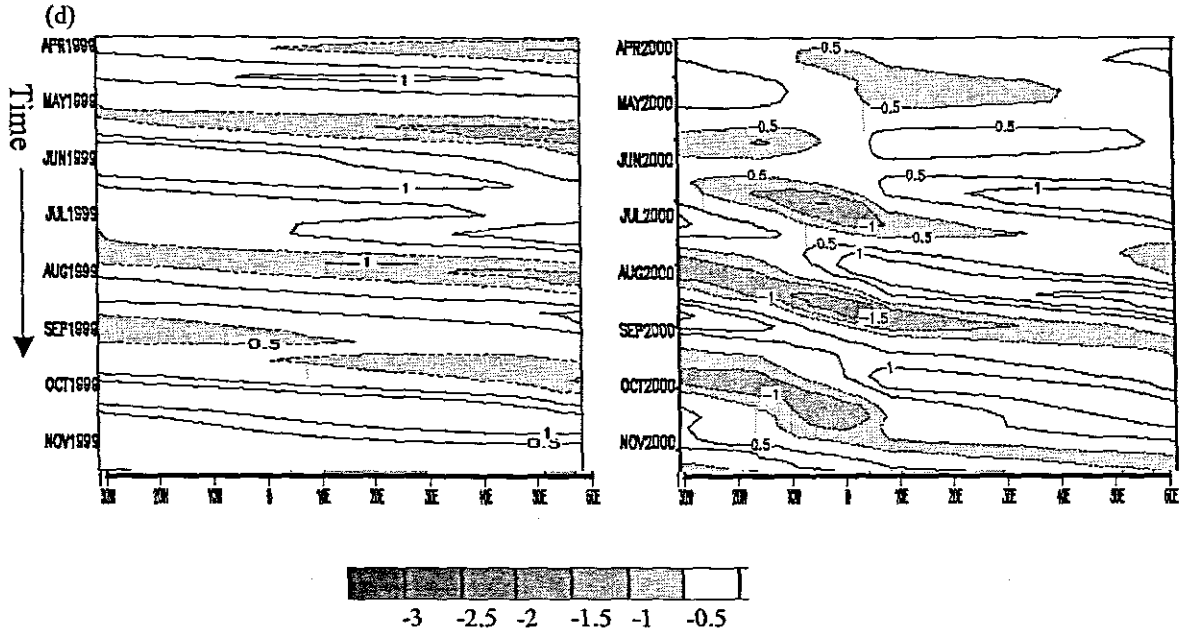

Figure 5.2 (continued) shows hovmoller plots for velocity potential anomalies averaged from 2.5S to 12.5N for the years 1999 to 2000.

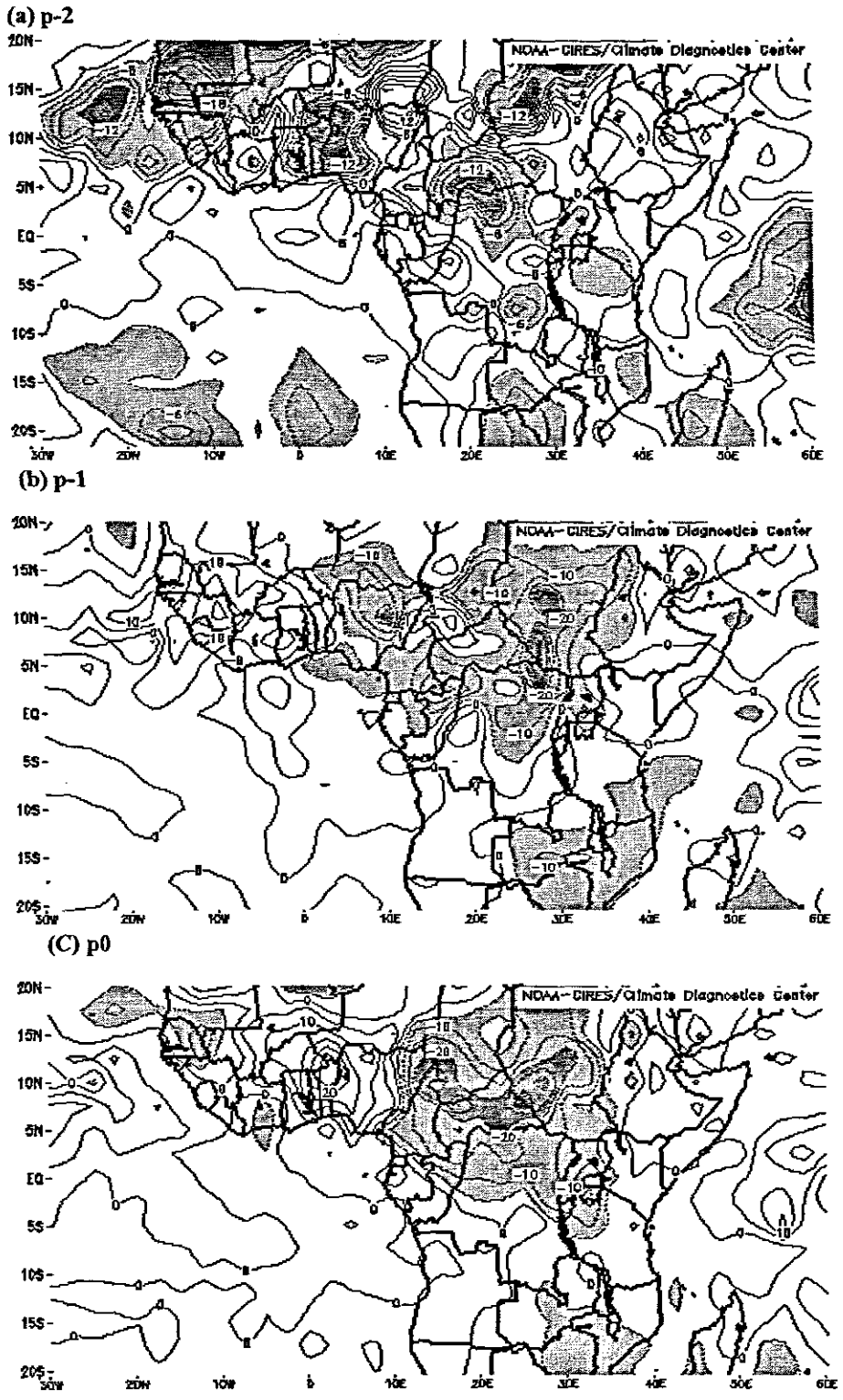

Figure 5.3 shows outgoing longwave radiation composite anomalies for p-2, p-1 and p0. Features appear strongest in the 5°-15°N band.

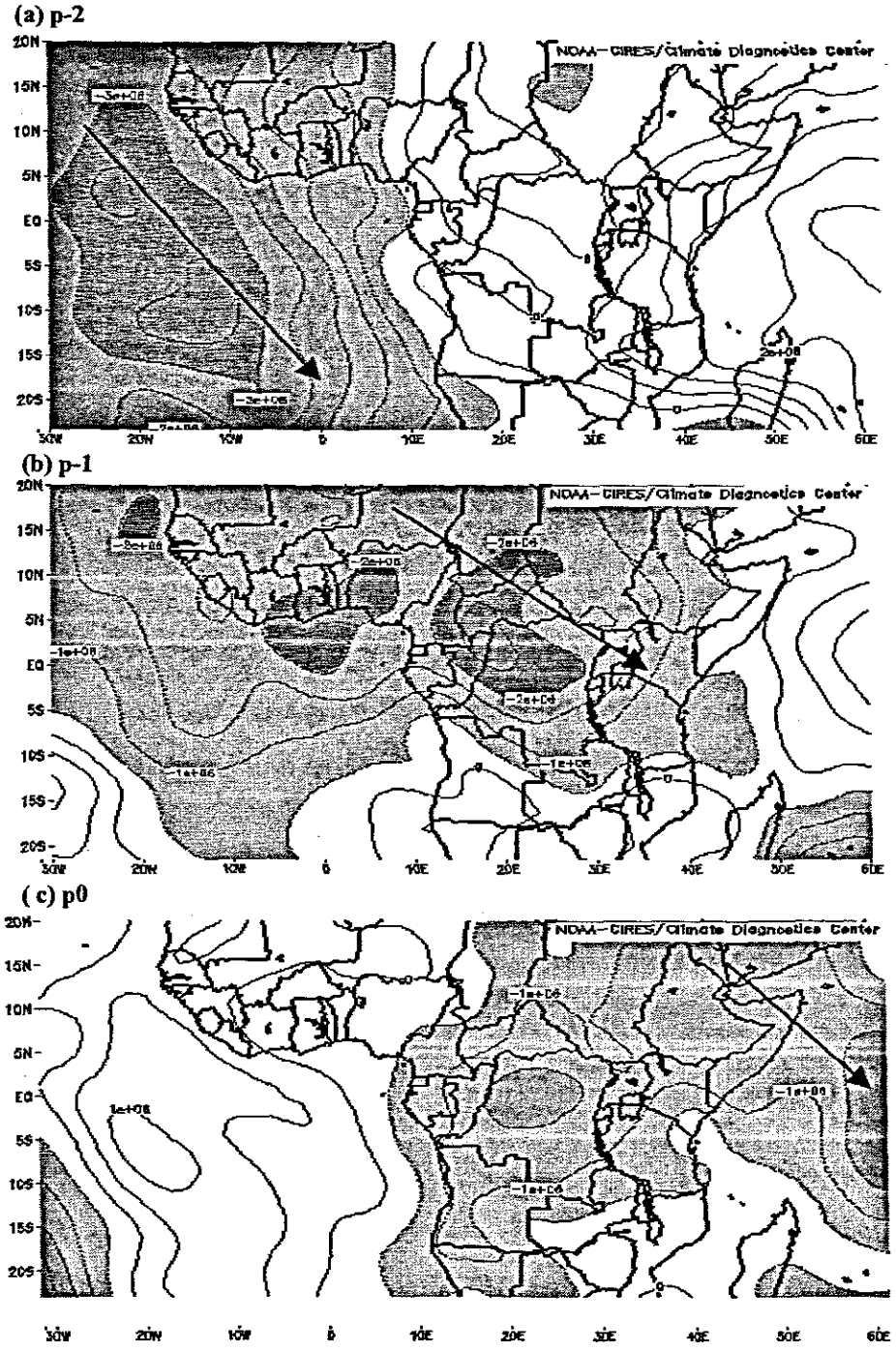

Figure 5.4 shows velocity potential composite anomalies at 200hPa for p-2, p-1, p0.

Chapter Six

Satellite Rainfall Estimation

6.0 Introduction

The first section of this chapter discusses some of the algorithms used in the development of satellite rainfall estimates over tropical Africa. Section two presents the results of satellite rainfall calibration and validation over Uganda using TAMSAT and historical gauge data for Uganda.

6.1 Satellite Rainfall Estimation Algorithms

Several algorithms of rainfall estimation have been developed using visible (0.4-0.7μm), infrared (10.5-12.5μm) and microwave (MW) radiance brightness temperatures from geostationary and polar orbiting satellites. They include the Orstom rainfall estimation technique, Climate Prediction Center (CPC) rainfall estimation technique, Combined satellite passive Microwave and Infrared Algorithm (MIRA), and TAMSAT rainfall estimation technique (discussed in chapter two). A detailed discussion of these techniques follows.

6.1.1 ORSTOM rainfall estimation technique

This technique uses ground surface temperature obtained from Meteosat images for estimating rainfall (Guillot, 1995). It was developed by the Lannion Centre De Meteorologie Spatiale (CMS) and tested in West Africa. The approach depends on the relationship between ground surface temperature and pluviometary and this is based upon the following two balances (Guillot, 1995): energy balance that links sensible heat flow to evapo-transpiration and water balance that links evaporation to rainfall. The sensible heat is also related to the ground surface temperature. The technique is based on the effect of the previous rainfall on the ground surface temperature. There is an inverse relationship between ground

surface temperature and the corresponding rainfall totals of the same period. However, local climatic factors may result in ground surface temperature gradient.

In Senegal a study of the relationship between rainfall totals and sum of ground surface temperature minus temperature gradient of the air was carried out (Guillot, 1995). The examination of the ground surface temperature showed that before the first rain there was a 3°-8°C south-north or west east gradient. The negative linear correlation between the rainfall totals and the mean temperature from June onwards indicated that the satellite estimated rainfall explained about 73% of variation of rainfall totals from end of July and for the three consecutive years period of 1984 to 1986 (Guillot, 1995). The comparison of the results obtained from the study with rainfall computed by kriging ground data showed greater accuracy in areas with sparse gauge distribution and an equal precision in regions with medium density of rain gauges. In order to do calibration using this technique contemporaneous data is required making its application difficult for African countries.

6.1.2 Climate Prediction Center (CPC) rainfall estimation technique.

The CPC technique was developed for estimating accumulated rainfall using satellite data, rain gauge data, model analysis of wind and relative humidity and orographic features (Herman et al., 1997). The United States Agency for International Development (USAID) developed the technique for drought monitoring purpose for Famine Early Warning System (FEWS) to assist the African continent. The technique estimates rainfall over tropical regions of the globe where more conventional surface observations are unavailable.

A preliminary estimate of accumulated precipitation is made based on the GOES Precipitation Index (GPI), an algorithm developed by Arkin and Meisner (1987). The GPI uses the duration of cold cloud tops over a region for the determination

of accumulated rainfall. The GPI estimate is corrected using a bias field that is calculated by incorporating the GTS observational data and fitting the biases to a grid using optimal interpolation producing an estimate of convective rainfall. It has been found that as compared to rain gauge reports, the GPI technique generally overestimates precipitation falling over land (Arkin and Ardanuy, 1989), while over tropical oceans the bias is near zero (Xie, 1995).

Over regions in which precipitation is due to orographic lifting and the clouds are relatively warm, an additional procedure is used which incorporates the local terrain features with numerical model analyses of meteorological parameters. The processes for estimation of rainfall from warm clouds takes into account surface wind direction, relative humidity, and terrain. Model analyses of surface wind and surface relative humidity are acquired from the environmental modeling center for global data assimilation system.

The CPC is advantageous that it can estimate precipitation from both cold and warm clouds. The technique incorporates rainfall from both the convective and stratiform cloud types producing a final estimate of total accumulated precipitation. The CPC technique for estimating rainfall from cold cloud is calibrated against contemporaneous gauge data rather than historical data. However there is sparse population of rain gauges in most African countries.

As earlier mentioned rainfall data that was used in the previous chapters were obtained from the CPC center. In order to ascertain the reliability of this data set, CMAP and gauge data are compared over Uganda. Results show a high correlation coefficient of 0.91. This means that CPC algorithm explains 82% of rainfall over Uganda. These types of comparisons should be handled with caution since CMAP rainfall is providing pixel values rather than point measurements as the gauges.

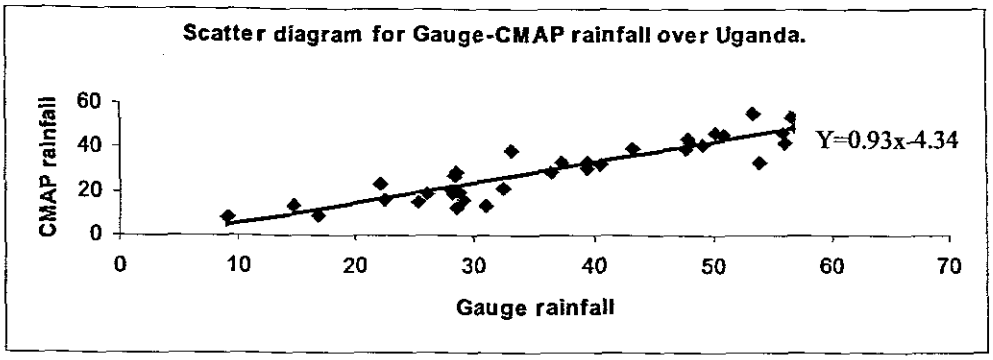

Comparison of gauge and CMAP rainfall over Uganda

6.1.3 Combined satellite passive microwave and infrared Algorithm (MIRA)

The combined passive microwave (PMW) and infrared (IR) satellite algorithm (MIRA) estimates rainfall at the smallest possible space and time scales. It is based on the assumption that PMW algorithms can provide accurate estimates of instantaneous rain rates, and that this information can be used to calibrate IR parameters, to improve rainfall estimates from IR data at high temporal frequency. It is widely accepted that satellite borne microwave sensors provide the most accurate estimates of rain rate currently available at quasi-global scales.

The frequency distributions of PMW estimated rain rate (R_{MW}) and IR brightness temperature (IR_{Tb}) values are derived from coincident satellite imagery, accumulated over some space and/or time domain large enough to ensure sufficient IR and PMW observations. To derive an optimised IR_{Tb}/ rain rate relationship for the calibration domain the Probability Matching Method (PMM) is used (Atlas et al., 1990). The IR_{Tb} threshold, which equates to the lowest measurable PMW rain rate (0.1 $mmhr^{-1}$,) represents the optimum IR rain/no-rain threshold ($IR_{Tb(T)}$), equivalent to the quantities derived by comparisons of IR and contemporaneous rain gauge data (Todd et al.,1995, 1999).

In this method an assumption is made that low (high) IR_{Tb} values are most likely to be associated with higher (lower) rain rates. It has long been known that there exists only a weak statistical relationship between IR_{Tb} and rain rate. In this case however, the relationship is derived only for the particular calibration domain, and is therefore variable over space and time, providing sensitivity to actual variations in cloud and rainfall relationships. The optimized IR_{Tb}/rain rate relationships resulting from the PMM procedure can then be applied to IR images to derive instantaneous rain rate estimates at the high frequency of geo-stationary IR sensor.

The satellite rainfall estimation algorithms discussed above are calibrated against contemporaneous gauge data that are very sparse in most of the African region. The radar and rain gauge network is in a sorry state due to lack of resources for maintenance. The communication system is unreliable leaving us with no choice but to rely on satellite algorithms calibrated against historical gauge data sets, for example the TAMSAT method.

6.2 Satellite rainfall estimation in Uganda using the TAMSAT method

The TAMSAT method of rainfall estimation as described in chapter two was used in the development of calibration equations for Uganda. Dekadal rainfall gauge data for the period 1993-2000 for fifty stations was obtained from the Department of Meteorology, Uganda while Cold cloud Duration (CCD) data at thresholds -30, -40, -50, -60 (°C) for the same period and area were obtained from the University of Reading (TAMSAT) UK for calibration purposes.

6.2.1. Calibration zones and parameters a_0 and a_1

Figure 6.1 shows the maps of the ratio of estimated rain days to actual rain days (bias) that are used for the determination of the optimum threshold temperatures. For April, bias was equal to 1 for most stations at threshold -40°C, hence the

optimum temperature threshold for that month. In March, the country is divided into two calibration zones at 1.6°N (figure 6.2a). This is because the satellite underestimates rainfall for the northern region at -40°C though it performs better for the southern region.

Table 6.1 gives the calibration parameters for all months. N is the number of dekads available, N_r corresponds to the number of rainy dekads on which the regression is based, and T_t is the optimum CCD temperature threshold. a_0 and a_1 are the intercept and slope of the regression/calibration plots respectively as in figure 6.3

Results show that the optimum temperature threshold for the dry months of January and February is -50°C (Table 6.1). During this time of the year little rainfall occurs. The ITCZ lies to the south of Uganda. Rainfall comes from relatively cooler clouds. However, the optimum temperature threshold for the rainy season is -30°C but in a few cases -40°C. Rainfall comes from warmer clouds with relatively higher temperature threshold. Because of favorable rain-giving mechanisms, the slight ascent of air leads to saturation and convective rainfall.

Month	Zone	N	N_r	T_t(°C)	a_0(mm h^{-1})	a_1(mm)
January	All Uganda	722	539	-50	-0.11	1.77
February	All Uganda	715	464	-50	-0.39	1.78
March	R1 (Latitude<1.6°)	487	461	-40	18.19	0.67
	R2 (Latitude>1.6°)	177	157	-30	-3.77	0.85
April	All Uganda	486	461	-40	14.47	0.83
May	All Uganda	743	706	-30	1.85	1.31
June	All Uganda	692	578	-30	3.73	0.82

July	R1 (Latitude<1°)	392	274	-40	0.5	1
	R2 (Latitude>1°)	220	211	-30	3.01	1.27
August	All Uganda	675	616	-30	2.56	1.02
September	All Uganda	655	615	-30	4.22	0.92
October		542	534	-30	6.24	1.11
November		816	773	-40	16.29	1.05
December		549	468	-30	-1.81	1.41

Table 6.1 Coefficients of calibration equations for the whole year. The country was divided into two regions at latitude 1.6°N in March and at 1°N in July (figure 6.2 a-b)

For some parts of the country, a warmer temperature threshold of –20°C would have been more effective in the calibration process. However, the data was not available. Apart from March and July, where the country was divided into two regions at 1.6°N and 1°N respectively, calibration equations could be applied to the wider area.

6.2.2 Validation of Satellite rainfall estimates

After the production of rainfall estimates for a region, it is important that some evaluation of the estimates are made. It helps in the identification of areas or periods for which the estimation algorithm is inappropriate, hence the need for modification. It also helps to quantify the accuracy (skill) of the technique, so that end-users and decision-makers are aware of the reliability and limitations of the estimates. In this study gauge rainfall data for the year 2000 was used for validation purposes.

Satellite rainfall estimates were produced for the year 2000 for validation of the algorithm. Results from the comparison between the gauge and satellite estimated rainfall data for year 2000 indicated a good agreement between the

two data sets with correlation coefficients greater than 0.85 i.e. $r > 0.85$ for the mean dekadal rainfall for the year 2000.

Figure 6.4a for mean gauge and satellite estimated rainfall reveal that the satellite persistently under estimates rainfall for most dekads of the year but with small values. Underestimation is likely due to the different shapes of the rainfall and CCD histograms and calibration which is based on the median instead of the mean gauge value. This "tailing off" of the rainfall estimates is a recognised problem with most TIR based technique. As discussed earlier, the thermal infrared images distinguish raining cloud from non-raining cloud on the basis of their observed cloud top temperature assuming that all rainfall comes from deep convective clouds with cold, high tops. However, wetlands, lakes and mountains may experience rainfall from clouds that have not formed from vigorous heating. Consequently they do not reach high enough into the atmosphere to register as cold clouds. In such cases rainfall would occur but would not appear in the satellite rainfall estimate, hence the under estimation of rainfall figures by the satellite.

On the other hand, the satellite over estimates rainfall for some dekads for example the first dekad of March, the first two dekads of November and the last dekad of May as indicated in figure 6.4a. Some of these are the seasonally phase-locked intra-seasonal oscillation events that "bracket" the rainy season. Over estimation of rainfall by satellite may also be due to the presence of very high, wispy cirrus clouds especially after a storm. The wispy appearance of cirrus clouds is due to the fact that they are high enough in the atmosphere to be composed of ice crystals rather than water droplets. Such clouds appear as very cold to the satellite and therefore would indicate the presence of rain. However, these clouds are not deep enough for rainfall to develop and this results in over estimation of rainfall by the satellite.

Results indicate that the gauge and estimated rainfall values are in phase for most dekads of the year, and in many cases, similar amounts of rainfall were registered for both gauge and satellite. The satellite was able to register most peaks of dekadal rainfall apart from the onset events.

In figure 6.4b, the satellite persistently underestimates rainfall as shown by the cumulative dekadal rainfall curve. However, for the standardized values where above or below normal rainfall are considered, the accuracy of the satellite is high (figure 6.4c). The number of dekads of gauge and satellite estimated rainfall with equivalent values is 58% of the total dekads in the year.

Spatial analysis for satellite and gauge data was performed. Figure 6.5(a-b) show the spatial distribution of gauge and satellite rainfall data for the year 2000 respectively. The satellite rainfall distribution for the year 2000 portrays excessive aridity over the northeastern parts of the country compared to the gauge distribution.

The influence of the Congo air mass on the total amount of rainfall received in the year over western Uganda is well captured in the satellite spatial distribution. As discussed earlier, the western parts of the country receive more rainfall in the September-November season while the eastern part gets more during the March-May season. This is demonstrated in figure 6.6b and 6.7b. The density and distribution of the gauges influence the spatial distribution, unlike the satellite.

The main problem with the estimates produced above is that no allowance is made for the accuracy of the rain gauge data as estimators of pixel rainfall. Satellite estimates are essentially averages over an area of the satellite pixel, whereas gauges provide measurements made at a point. Often there is no alternative method of comparison. There is an implicit assumption that averages over a sufficient number of gauges will limit the discrepancy between the mean

gauge value and the true area average. Therefore satellite rainfall estimates are basically reliable if averaged over large areas and if the amount of cirrus and warm raining clouds are not significant. A rain gauge gives an accurate reading of rainfall at a particular point but this may well be very different from the average rainfall over a large area.

For meaningful comparison between the two data sets, one must either derive point values from the satellite pixels or compute pixel averages from the rain gauge data. In this study the latter was attempted using block kriging to calculate the 'best' mean rainfall estimates for the rain gauges. Dekadal rainfall for the year 2000 was used to compute pixel averages from the rain gauge data (refer to chapter two). Comparison between the kriged and satellite values shows correlation of 0.9. This means that the satellite estimates explain 81% of rainfall in the year 2000.

6.3 Summary

The most dominant optimum temperature threshold was –30° for most months of the year. The satellite overestimates rainfall at onset and cessation periods. This is due to the influence of intra-seasonal oscillations at the beginning and end of the season. Under estimation is seen during the seasons due to rainfall from the warm clouds

Satellite rainfall estimates are useful particularly in the water management sector to provide a means of rapidly identifying areas experiencing below/above normal rainfall that may affect resources. The estimates can also be used side by side with the gauge rainfall data for drought monitoring, to give timely warnings for better planning and management of the economy and improve the quality of human life. Although satellite measurements can not substitute ground observations, they can provide a supplementary data set for climate monitoring where conventional data are sparse. Merging of satellite data sets with the

available ground observations can provide better global data sets for climatological research.

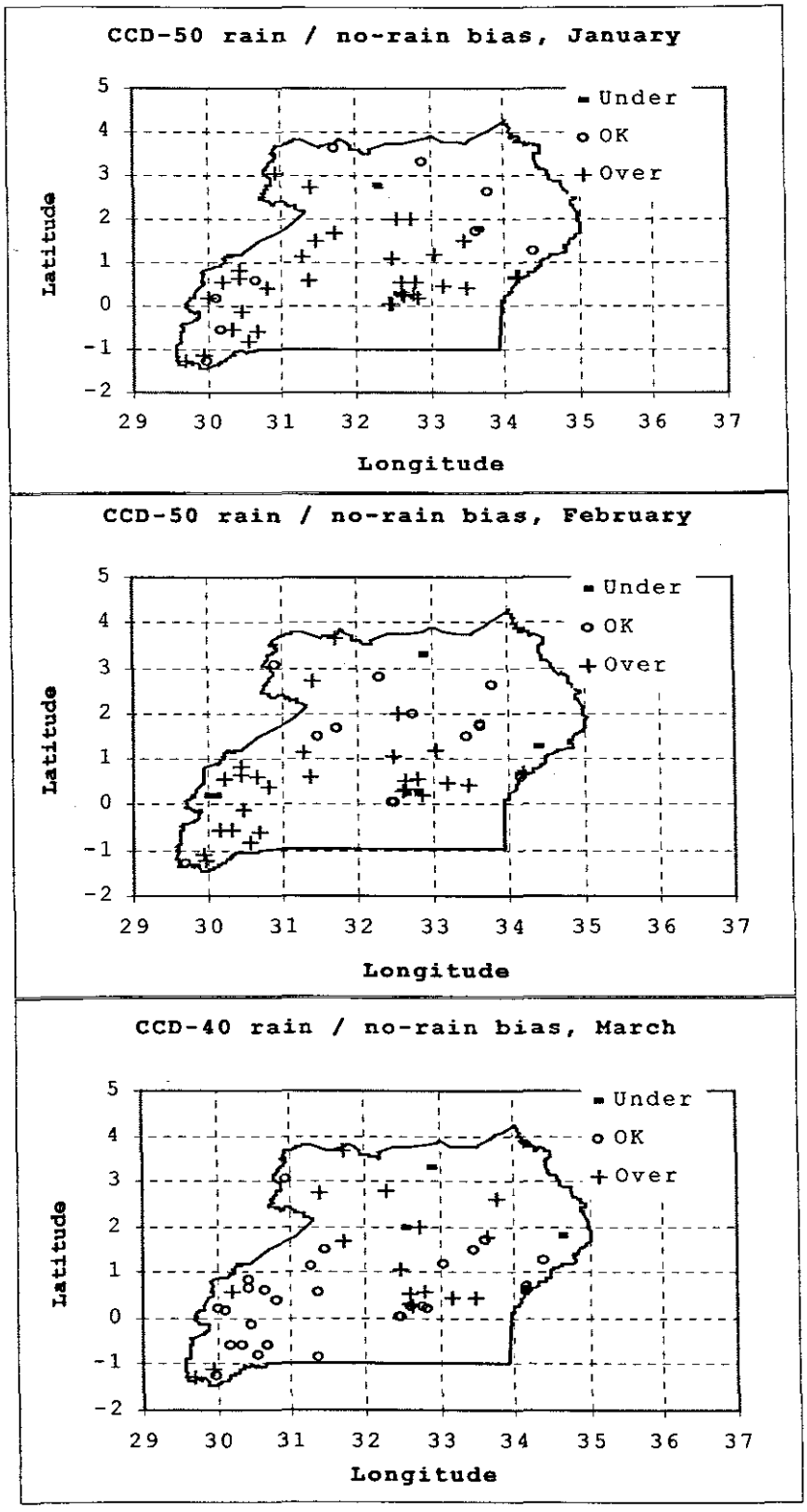

Figure 6.1 Maps for selection of optimum temperature thresholds.

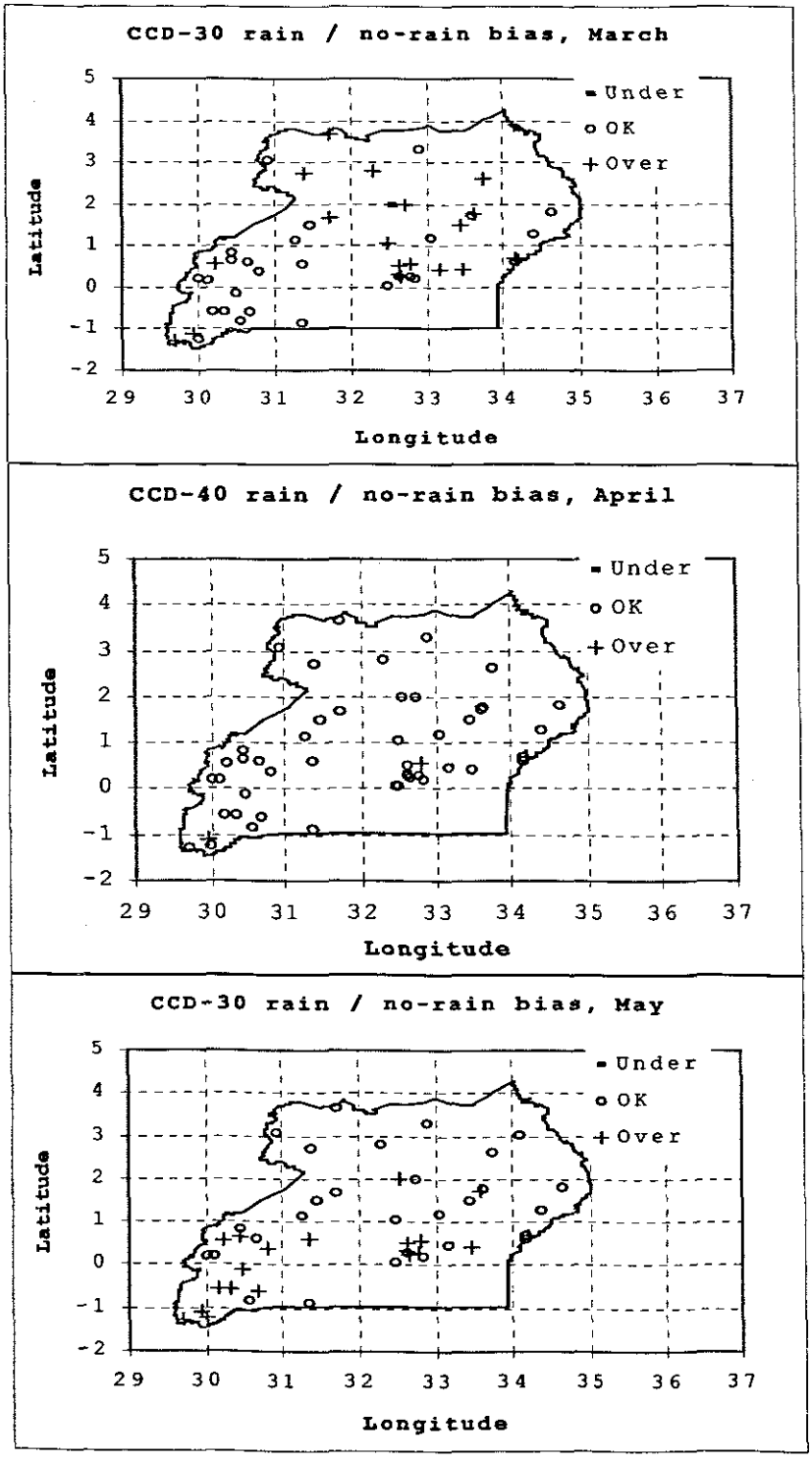

Figure 6.1 continues.

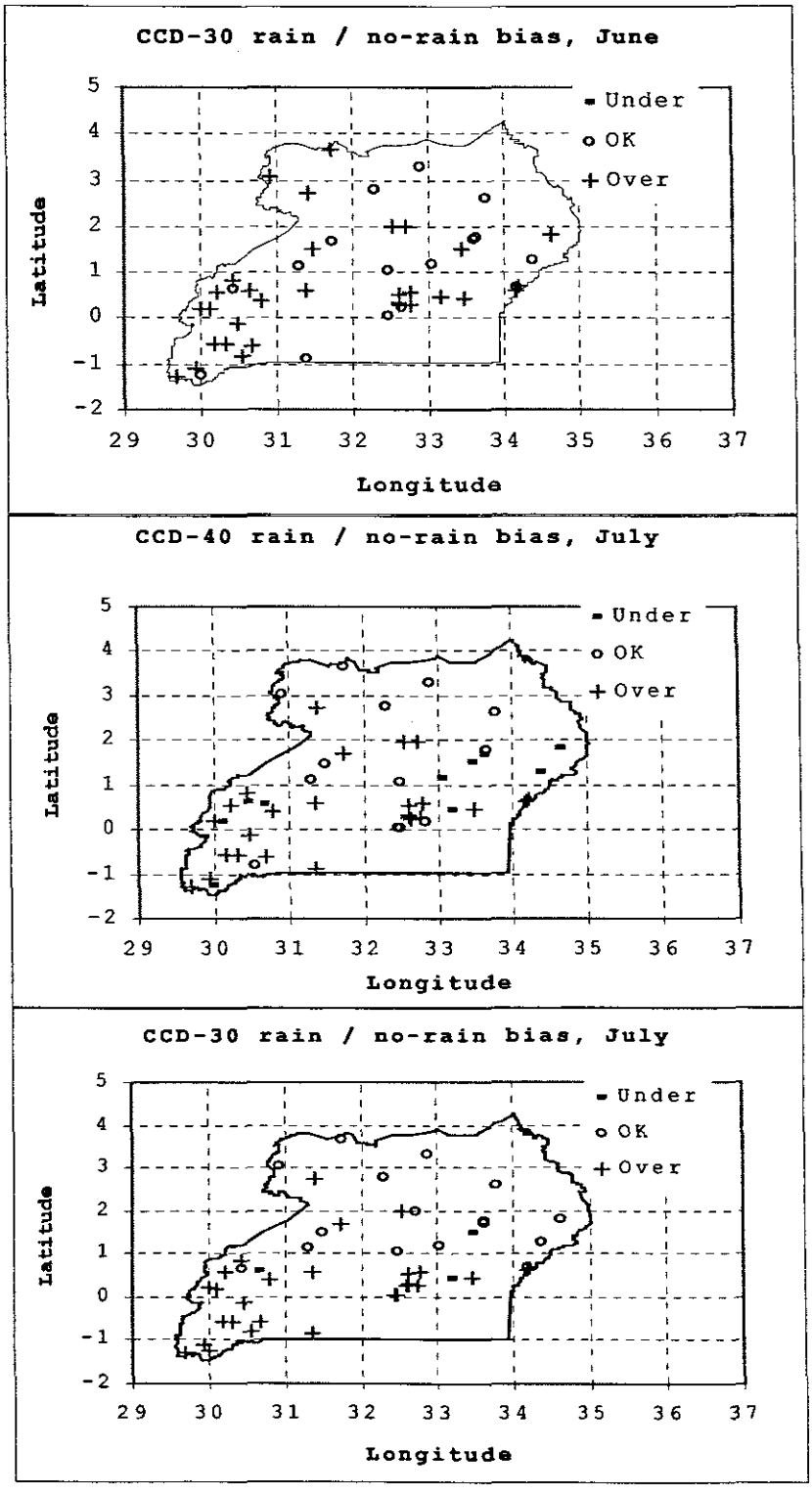

Figure 6.1 continues.

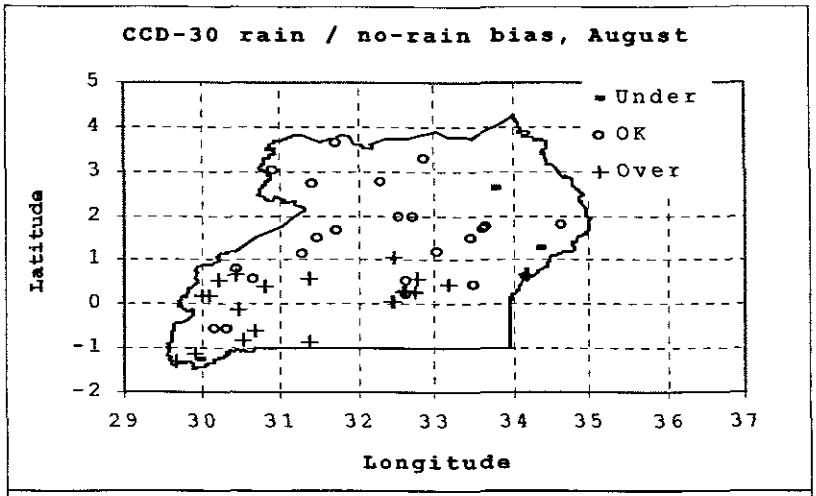

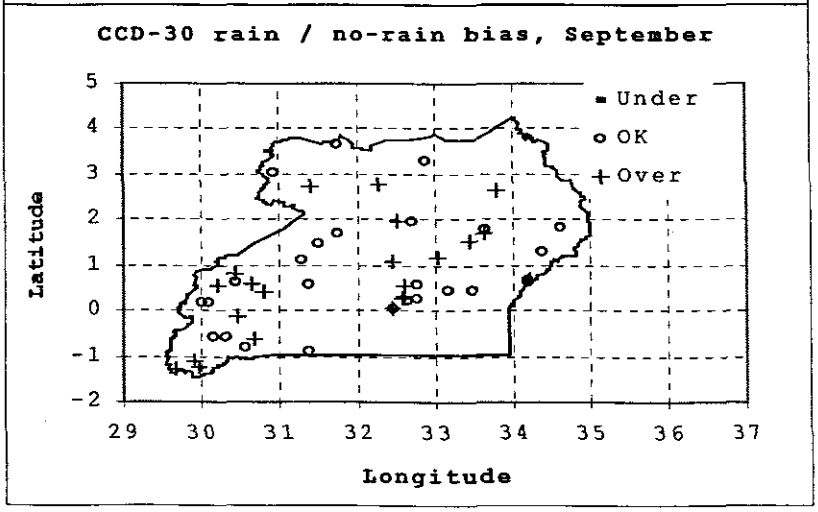

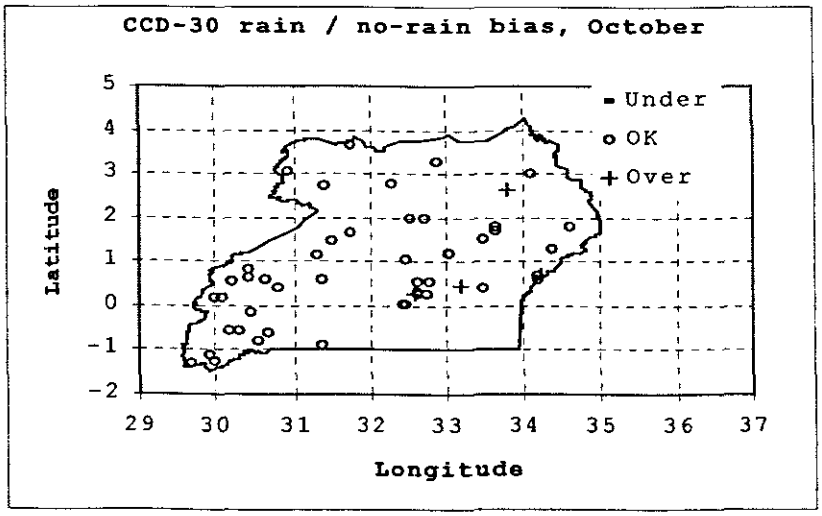

Figure 6.1 Continues

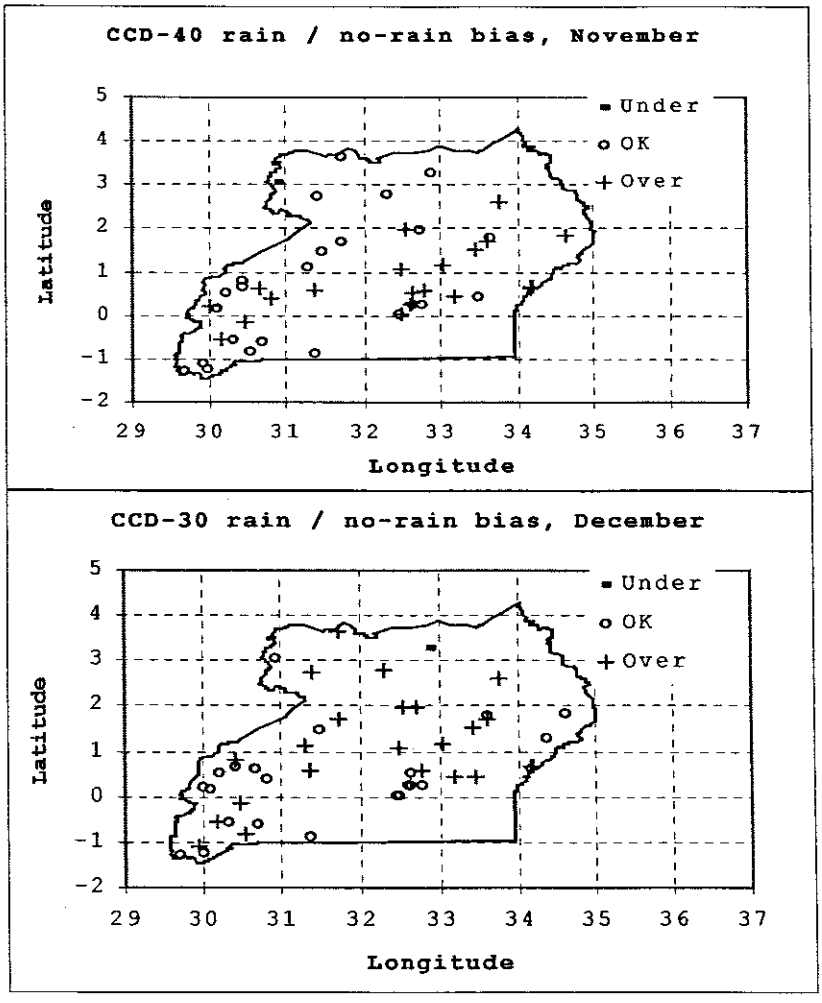
CCD-40 rain / no-rain bias, November
Under
OK
Over
Latitude
Longitude
5
4
3
2
1
0
-1
-2
29
30
31
32
33
34
35
36
37
CCD-30 rain / no-rain bias, December
Under
OK
Over
Latitude
Longitude

Figure 6.1

(a)

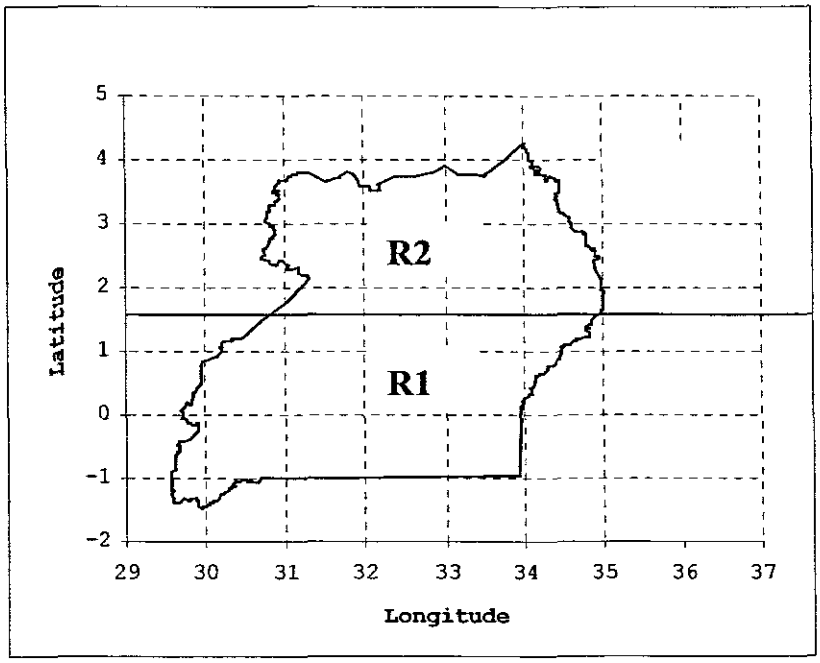

(b)

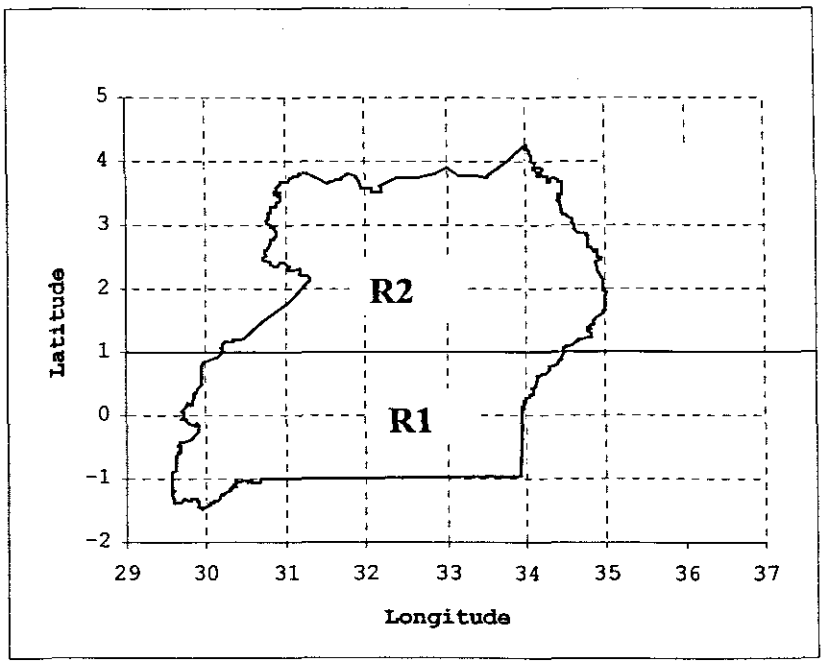

Figure 6.2 shows calibration zones for (a) March and (b) July.
The country is divided into two regions at latitude1.6°N in March and at 1°N in July.

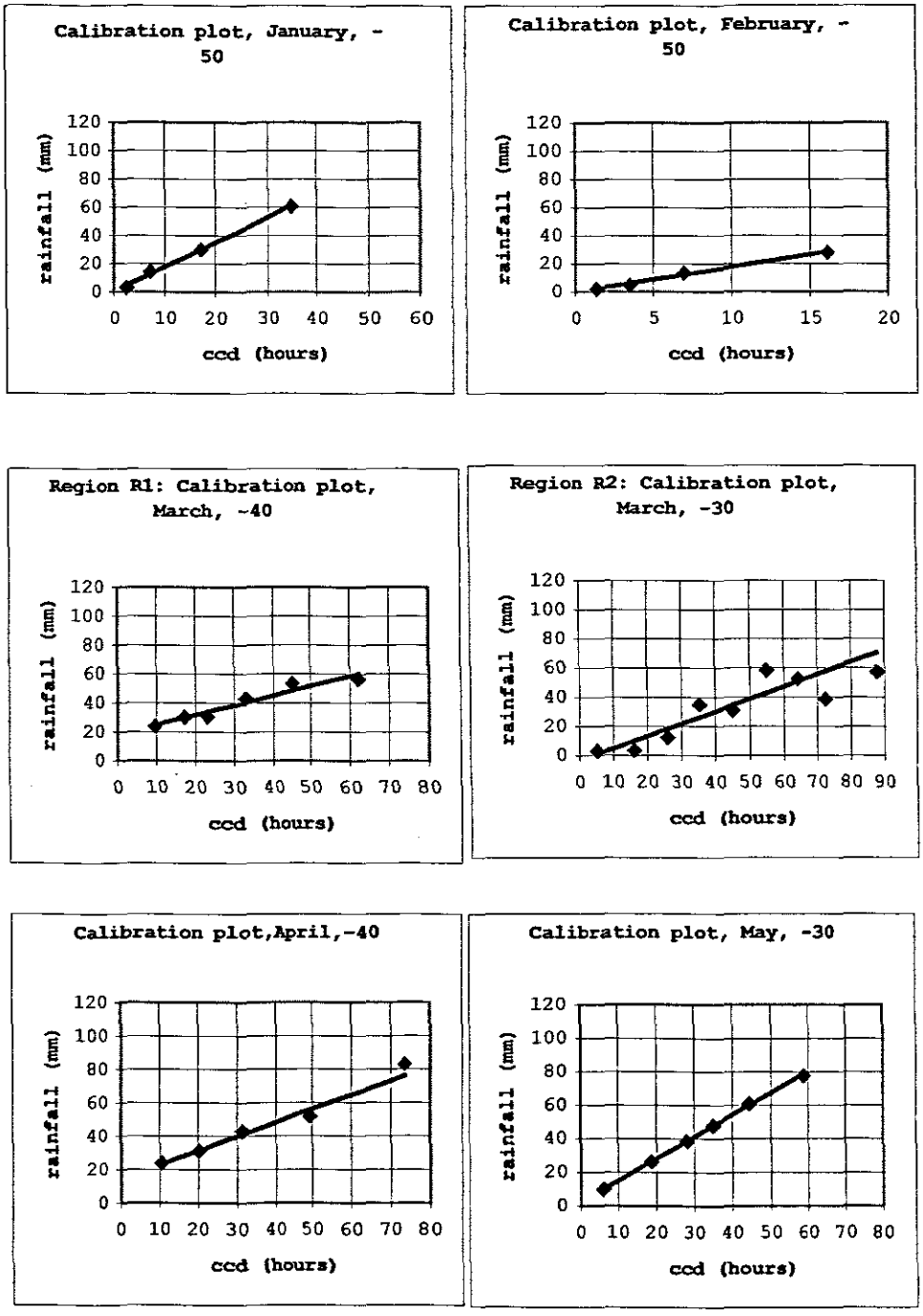

Figure 6.3 Shows calibration graphs for January to December for rainfall estimation.

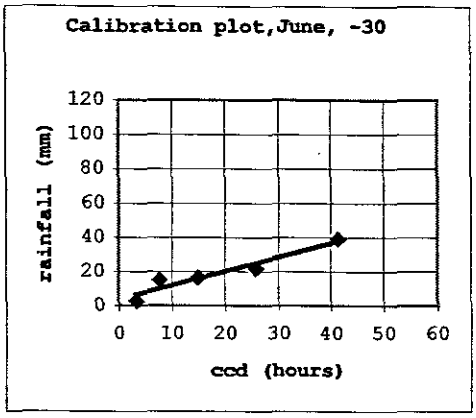

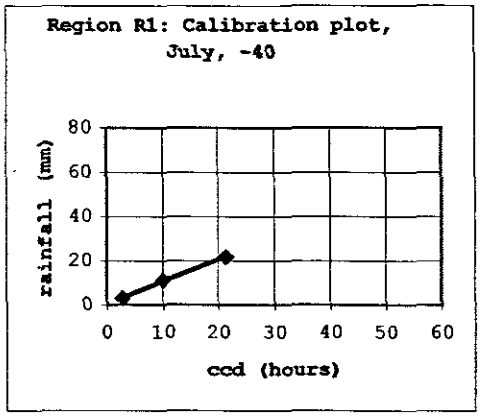

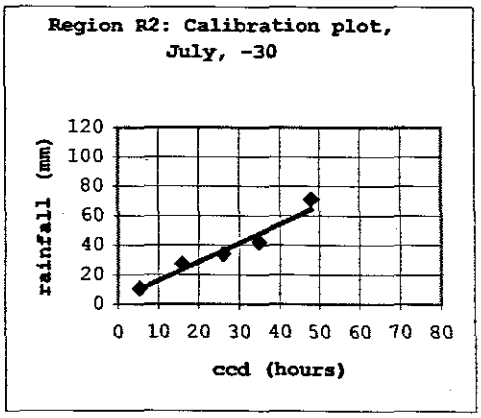

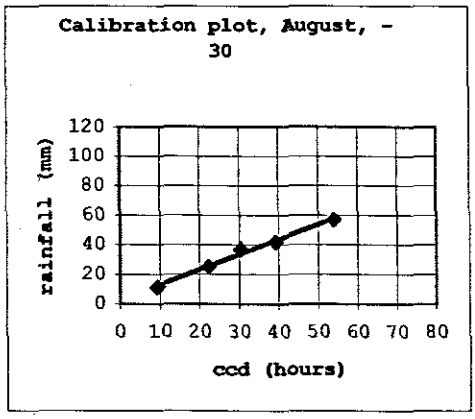

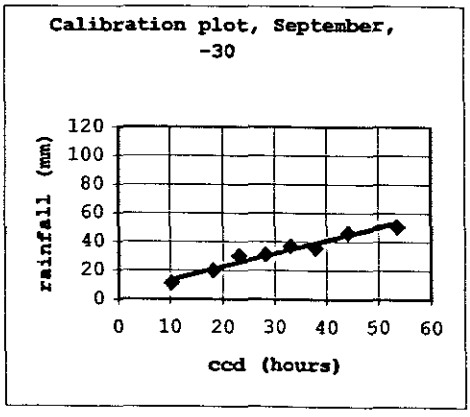

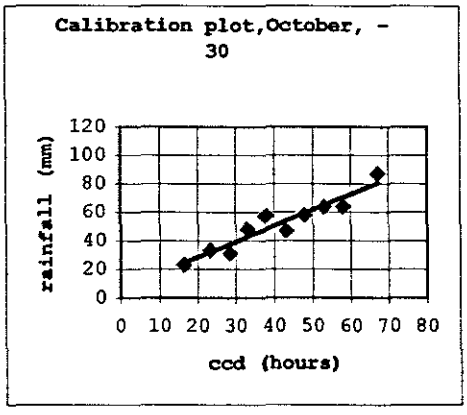

Figure 6.3 Continues

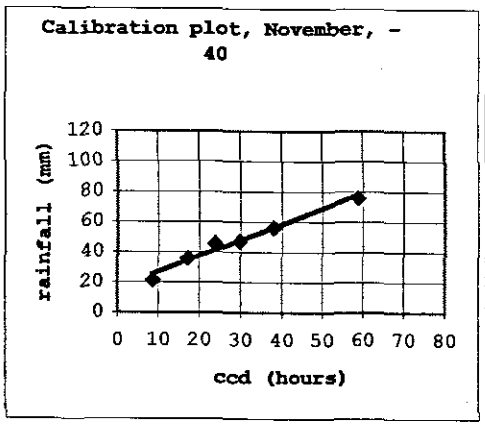

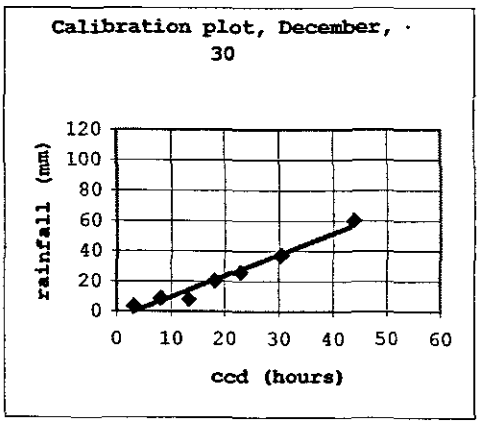

Figure 6.3 Continues

(a)

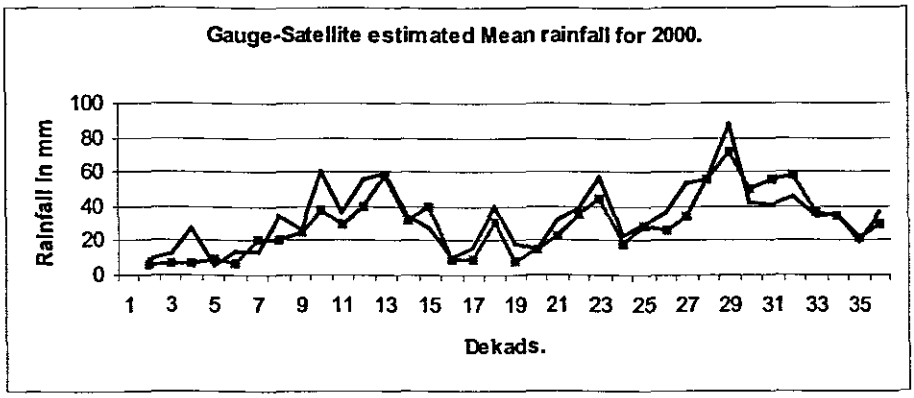

(b)

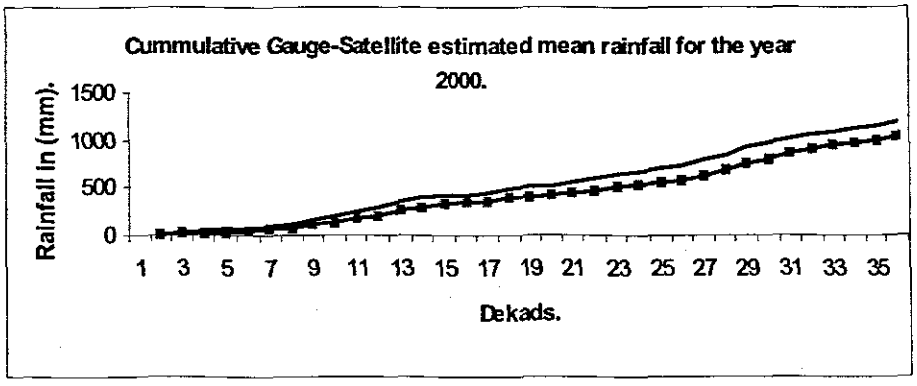

(c)

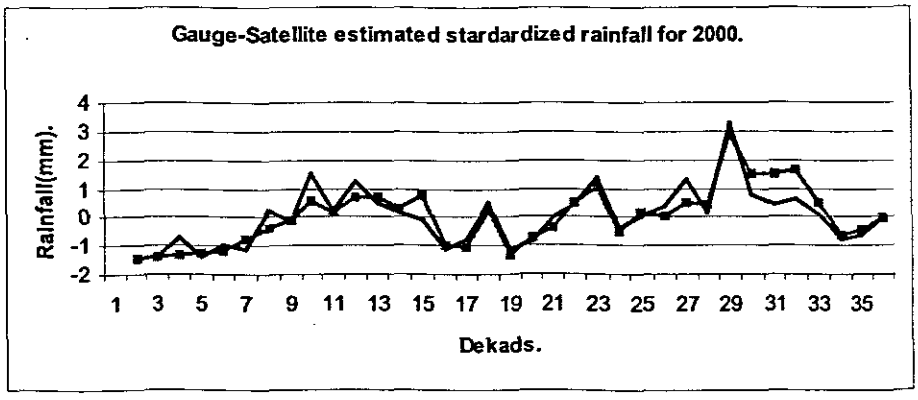

Figure 6.4 Gauge-Satellite estimated rainfall (a) mean rainfall (b) cumulative rainfall and (c) standardized rainfall for the whole country for the year 2000. Data for the first dekad of January was not available.

—♦— Satellite estimated rainfall.

——— Gauge rainfall.

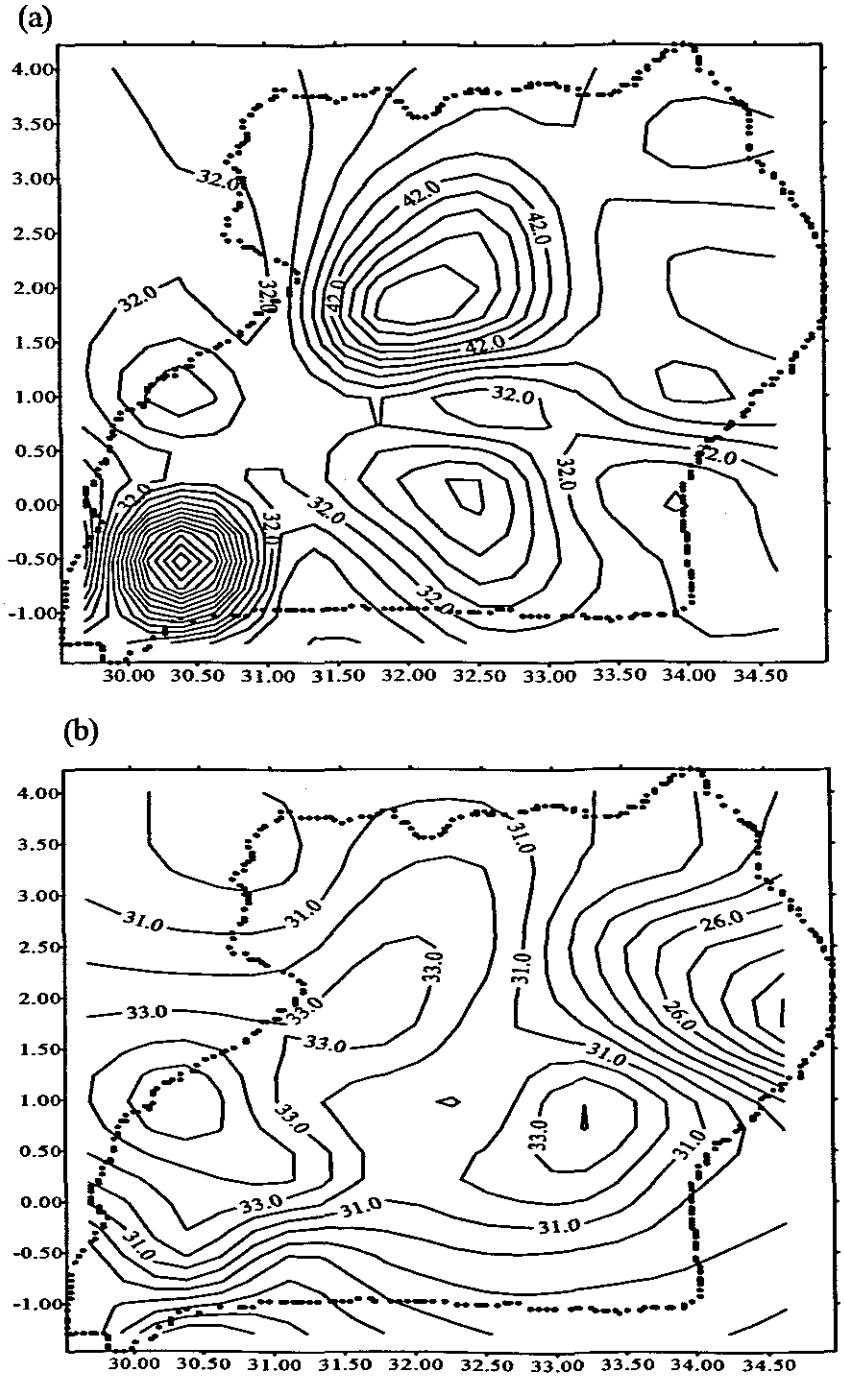

Figure 6.5 (a) and (b) are gauge and satellite spatial distribution of mean dekadal rainfall for the year 2000 respectively. The spatial pattern in (a) lower left is due to many gauges in a mountainous area.

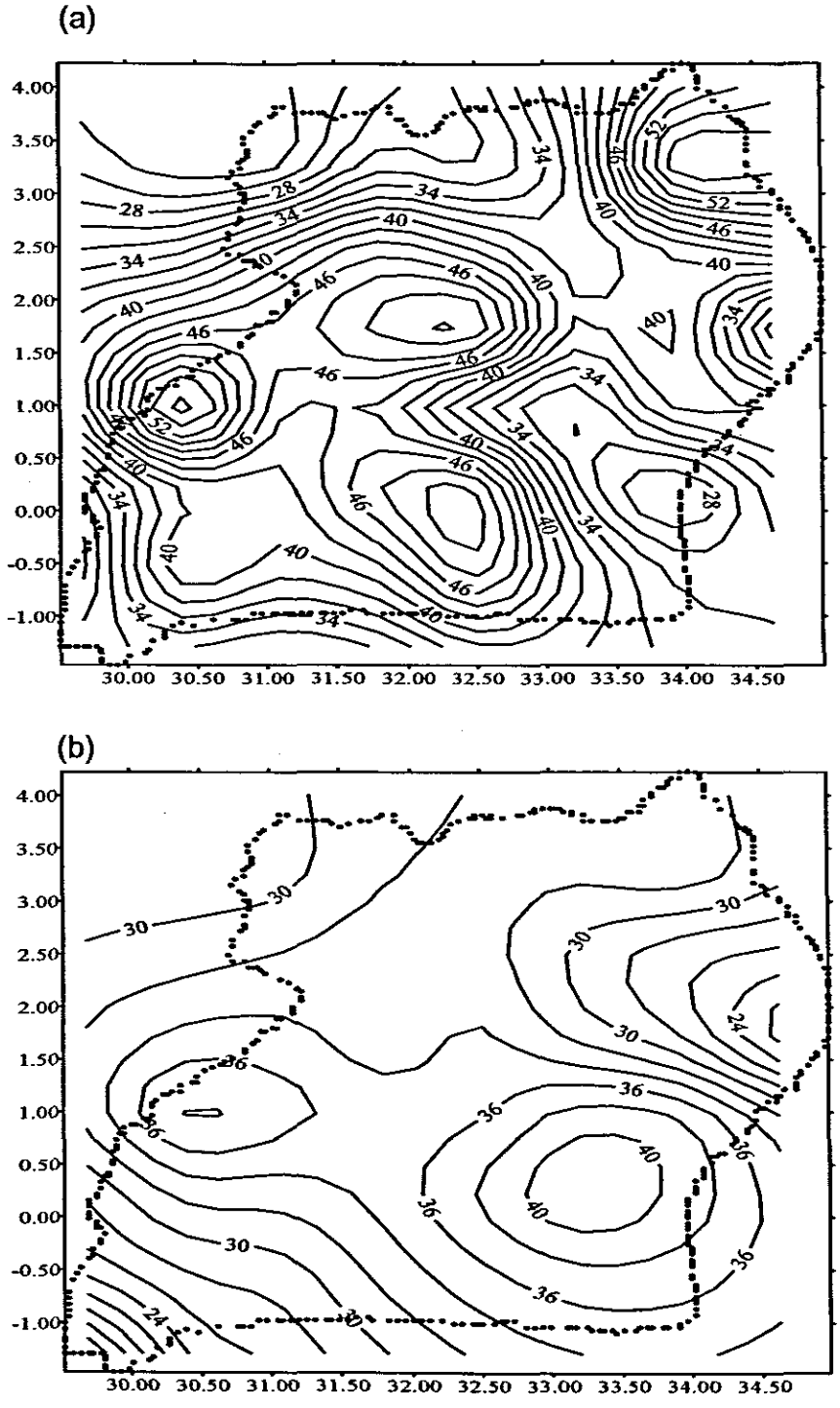

Figure 6.6 (a) and (b) are gauge and satellite spatial distribution of mean dekadal rainfall for the March-May season respectively.

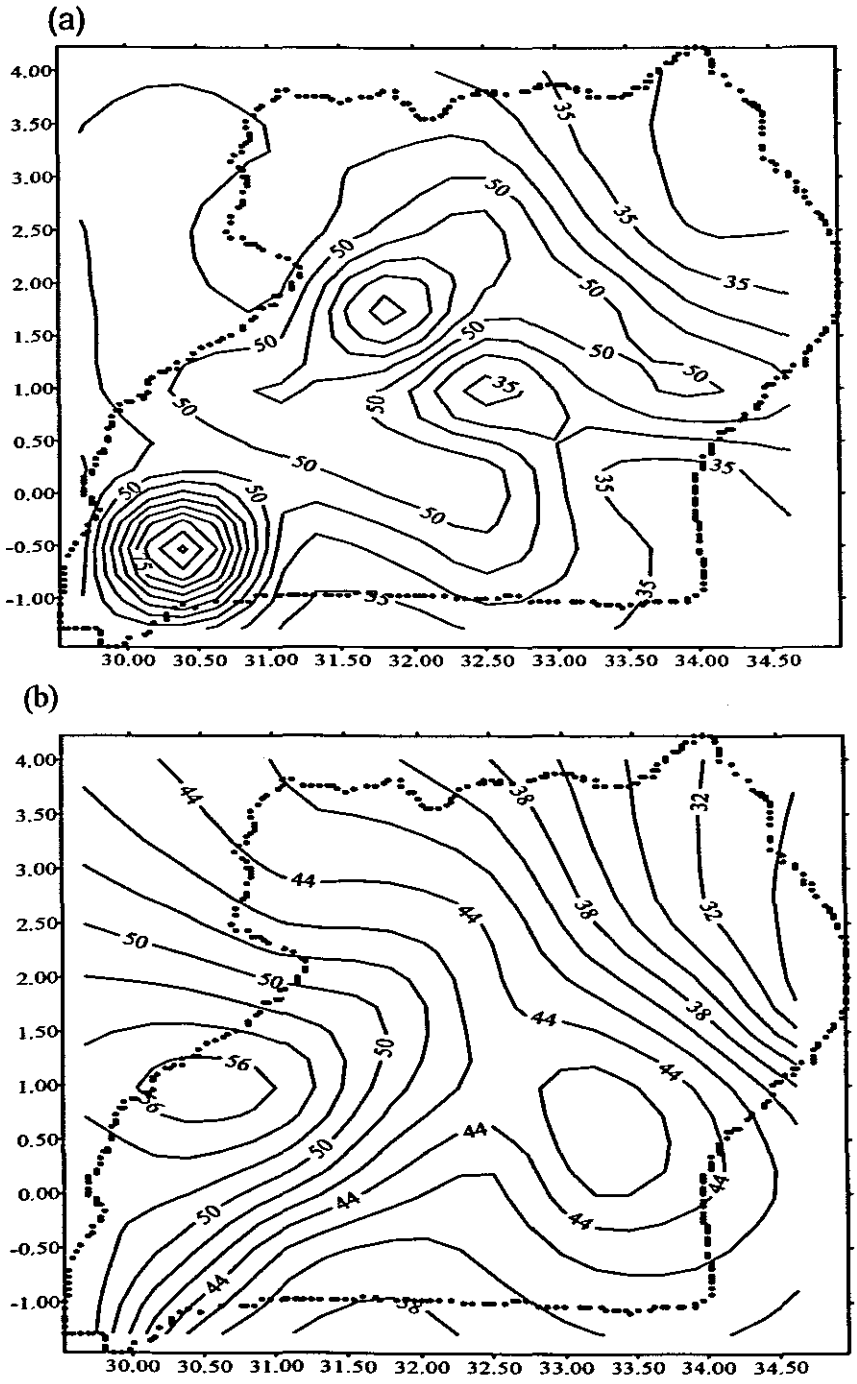

Figure 6.7 (a) and (b) are gauge and satellite spatial distribution of mean dekadal rainfall for the September-November season respectively.

Chapter Seven

An overview of data problems in Africa

7.0 Introduction

The economies of tropical Africa depend mainly on rain-fed agriculture that employs most of the workforce. To advance the understanding of rainfall variability, it is necessary to have a comprehensive observing system reliably producing high-quality data and products. Unfortunately, the station network over Africa is insufficient to adequately monitor rainfall (figure 1.3). Large gaps exist in the Angola-Congo-Sudan axis making it difficult to initialize regional models. In this chapter, the problems of data availability over Africa are examined and possible solutions to enhance the observational network over the region are recommended.

The climate monitoring and data collection infrastructure of most developing countries is constrained. This is due to limitations in resources, personnel, political instability and equipment. Keeping well-trained personnel in publicly funded institutions is difficult. In some cases, there is no organization mandated to collect and report data internationally on specific issues on a regular basis. The data management infrastructure of many African countries is weak and data reporting is fragmented. Without a central compiling system, data may remain scattered across many sectoral organizations and departments. Data are reported for different geographical areas by different agencies and organizations. As a result, it may be impossible to use and compare with otherwise valuable aggregated data sets in global and regional assessments.

Various statistical methods are used to fill data gaps and smooth curves. Although in the absence of real data these methods are necessary, the risk of using them should be understood. Furthermore, they are clearly not substitutes for monitoring, measurement and the verification of data obtained through remote

sensing and ground observations. Frequently, there are underlying differences in data collection methods for data with the same label from different sources. Without a detailed analysis of data collection and measurement methods and standards, there is a risk that incompatible data may end up in aggregated data sets.

7.1 Data quality and availability

The lack of relevant data is a common experience in Africa. Within the environmental domain there are still serious data gaps. There are inherent challenges in working with data sets on a global scale. Given that in general only data with the same definition, standards and date of measurement can be safely aggregated to a regional or global level, even small discrepancies or gaps can make data sets incomplete or otherwise deficient. On the other hand, even with good quality data, aggregation and averaging may mask important spatial and temporal diversity. In large-scale low-resolution aggregation, issues unique to smaller regions tend to disappear.

7.2 Data access

Data may be inaccessible because of copyright issues, high cost, professional jealousy or organizational competition. Although some parameters are accurately measured, the information may be classified or otherwise publicly unavailable. However, public and institutional attitudes towards access to data have changed noticeably during this decade. With Internet access becoming widespread, mass data processing is cheaper and easier, and cold war style security no longer necessary. The public has become more demanding and institutions more pro-active and open.

This opening up of data holdings and data exchange brings two potential problems for their use in broad assessments. First, access to essential data

which is currently taken for granted may become more commercialized and therefore more difficult for multilateral organizations and other compilers of environment assessments. In particular, this applies to satellite data and large integrated databases. Secondly, as data become more widely distributed and recycled, critical validation will become even more important than it is today.

7.3 Climatological data over Africa

African climatic variability is unique in many ways. There is a need to go beyond ITCZ movement to describe the characteristics of convection and links to surrounding monsoon circulation systems. The size of Africa brings unique land-atmosphere interactions particularly in the tropics. Its size and asymmetry around the equator are important factors. There is a need for regionalized studies to diagnose dynamical instabilities and their interaction with intra-seasonal variability that can assist capacity building efforts.

Successful research of African climate and weather requires several types of data, particularly historical daily observations for 30 years plus, metadata describing station events and ongoing daily data. However, the station network is too sparse to provide reliable data. The sparse station data suffer a host of problems such as station relocations, station environment, instrument changes, changes in time of observation, different lengths of observation, missing observations, and many others. The availability of data in the tropical Indian and Atlantic Oceans also remains a serious constraint to investigating the processes influencing African weather and climate.

Some climatological questions can be answered by processing the daily meteorological databases that are held within many of the National Meteorological Services of Africa. The atmospheric circulation, dynamic and convective instability issues are well-suited to study within reanalysis data sets, but the data sets need to be validated, preferably using data independent from

that used in the reanalysis process itself. This issue is particularly critical for decadal variability, which can be spuriously introduced into reanalysis products due to the evolving mix of observations that were available to force the reanalysis, which for the NCEP product, covers 1948 to present.

Maximum use of satellite data, such as the satellite derived OLR, NDVI, CMAP and many others, have facilitated climatological research studies. With the availability of new diagnostic data sets such as reanalysis and satellite based products, there is now the opportunity to study the sources of the rainfall teleconnections and work toward ensuring their accurate representation in global and regional models.

Geostationary visible and infrared data offer a unique opportunity to observe the location and movement of raining clouds at the synoptic scale with a temporal (30 minutes) and spatial (5km) resolution which is amenable to real-time operational monitoring and now-casting. Satellite data allow meteorologists to monitor weather systems long before they begin to affect a given region. The additional availability of a radar data network permits the more accurate detection over the more populated regions of meso-scale features associated with electrically active and potentially damaging storms as well as a more precise computation of the surface rainfall.

7.4 Re-Analysis Data sets.

Key questions revolve around the utility of the reanalysis data sets. Cross-validation of the reanalysis data sets with independent observations from Africa are needed to assess what extra input is necessary for reanalysis products to be useful at high spatial and temporal resolution. One reason numerical models may have difficulty with African climates is because their parameterization processes are often not suited to the African environment (Lebel et al 1997). The extreme northern and southern tips of the continent have winter rainfall regimes that bring

a new set of challenges to climate simulation. These rainfall systems are intimately connected to fluctuations in mid-latitude storm tracks and are governed largely by mid-latitude dynamics (Majodina and Jury 1996). For the northwestern tip of Africa, the systems are closely related to blocking episodes, which in turn are connected to the phase of the North Atlantic Oscillation (Lamb and Peppler, 1991).

The inadequacy of African climate processes in GCMs is often reflected in a model's inability to adequately represent the annual cycle. There is a need to examine the deficiencies and form hypotheses on the sources of the errors. It is necessary to gather observations as well as improve models, and key influences of the African regional climate not just the mean evolution of variables like rainfall but also moisture sources, fluxes and sinks (Cadet and Nnoli, 1987), heat sources and sinks, especially as they relate to the large African desert areas, and synoptic disturbances that move along their boundaries.

7.5 Recommendations for improving data availability in Africa.

Climate research and monitoring require an integrated strategy of land-Ocean-atmosphere observations, including both in situ and remote sensing platforms. In order to improve data availability in Africa, support through international programmes of the WMO for continuing the surface and upper air observing network is essential. Significant gaps in the surface network are apparent in Angola, the Congo basin, Sudan, and parts of the Sahel (see figure 1.3). The upper air network is in poor shape and this could be rectified through automated aircraft reporting systems for temperature, moisture and wind. Over the oceans, more attention needs to be paid to the tropical eastern Atlantic and western Indian Oceans adjacent to Africa. Oceanographic and air-sea interaction observations such as research ship cruises and ocean drifter deployments would enable the study of regional teleconnections between adjacent monsoon

circulation and convective anomalies over the continent. For predictive purposes these would need to be made available in near real-time.

Feasibility studies concerned with maintaining the network of observing stations in Africa should be established. Observational campaigns to fill gaps and closely monitor teleconnection sources that modulate the African climate should be strengthened. Monitoring and understanding land-sea-air interactions by remote sensing, local surface observations and numerical model data sets, focussing on feedback between the land surface, hydrology and overlying weather systems should also be emphasized.

A major need is the expansion of tropical ocean observations in the eastern Atlantic and western Indian Oceans consistent with anticipated predictive modelling activities and assimilation needs. In order to predict SSTs in key areas, sustained ocean measurements (moored arrays and profiling floats for subsurface structure, surface fluxes, etc) are required. An improved observational network on land to help better characterize continental scale convection, including a radiosonde network in data voids (e.g. Angola, Congo basin, Sudan) and wind profilers at near equatorial oceans islands to understand the origins of the MJO should be established.

Daily precipitation data are considered crucial for climate monitoring. A well-maintained station network will promote research data sets, while at the same time improve real time availability and model initialization. Proxies are needed for rainfall and surface fluxes to fill observational gaps; daily data should be archived to create long-term data sets particularly for hydrological conditions and their relation to the spatial coherence of climatic anomalies and stochastic processes.

There is a need to exploit remote sensing in diagnostic and predictive activities to take into account the large areas of Africa where sampling is sparse. Calibration and validation of remote sensing data is necessary to provide input to diagnostic

and predictive models. The tropical rainfall monitoring mission (TRMM) should consider African conditions in developing precipitation algorithms. The precipitation radar aboard TRMM is the first rain radar in space and most innovative equipment. Considerable success is likely in understanding convective scale-interactions using TRMM over central and eastern Africa where weather radar data are absent. Furthermore, the precipitation radar provides contemporaneous data, which could be used for calibrating satellite retrieved data sets.

The new and growing imperative for climate and weather observations arises from the recognition of their applications (refer to chapter 1). Governments and non-governmental organizations should give priority to funding National Weather Services in their struggle to maintain the observing network. The Global Climate Observation System through WMO should concentrate on the upper air and ocean observations. While the cost of a comprehensive observing system may appear to be a major obstacle, they are reasonable when placed in the appropriate context. The benefits are significant and make such a system worthwhile and cost effective for many areas of planning and decision making influenced by weather and climate.

In conclusion, the collection of data requires permanent monitoring networks with adequate geographical coverage and sufficient resources. Although the availability of remotely-sensed data has led to improvements in the cost, quality and availability of climatological data, remote sensing cannot entirely substitute for measurements on the ground. The use of satellite data has increased but the full potential remains untapped. The common belief that space observations will make ground-based measurements redundant is seldom justified. While space observations may reduce the need for conventional in situ measurements, they do not completely remove the need for direct reporting and ground truthing.

Chapter Eight

Discussion, Summary and Recommendations

8.0 Introduction

This study has identified the major spatial and temporal structures of seasonal and intra-seasonal rainfall and zonal wind variability over tropical Africa. The association of zonal wind and rainfall at seasonal and intra-seasonal time-scales has been examined. The evolution and propagation of intra-seasonal oscillations over the region have been investigated. Results of calibration and validation of satellite rainfall have been discussed. Below is the summary of the findings of this research.

Chapter 3

• During the MAM season, a zone of convergence develops over central and east Africa attracting moist westerlies from the Atlantic and easterlies from the Indian Ocean bringing wet conditions over the region. The convergence zone is associated with the ITCZ.

• During the JJAS season maximum upward motion is over the Congo due to strong convergence at the lower levels. This leads to wet conditions over this region. Over east Africa, dry conditions prevail due to the diversion of moisture by the SW monsoon component at the east African coast.

• Over northern Congo, peak rainfall is during the JJAS season whilst stream flow (Congo River) maxima is in the October-December (OND) season. Rainfall leads stream flow at two to four months. Rainfall in JJAS explains 81% of stream flow of the Congo in the OND season.

• The PCA results of rainfall and 700hPa zonal wind revealed the dominance of the annual cycle. However, shorter cycles for example six months also exist.

• The influence of the adjacent Indian and Atlantic Oceans on African seasonal rainfall is emphasized. This is due to the strong association revealed between rainfall and the zonal wind. Rainfall over central and east Africa is influenced by the westerly flow over the east Atlantic. Strong easterlies over the west Indian Ocean are associated with increased rainfall over tropical Africa.

Chapter 4

This chapter considered ISO filtered data and found that:

• The intra-seasonal signal for standing convective modes (71%) is stronger than for zonal wind (37.4%).

• The dominant mode of intra-seasonal rainfall is over the northern Congo (29%) while the second and the third modes are located over northeast Angola and east Africa respectively. The dominant mode for zonal wind intra-seasonal oscillations is over the east Atlantic Ocean (14.3%).

• Intra-seasonal oscillations of period 30-50 days are revealed and are phase locked to the seasonal cycle.

• Intra-seasonal oscillations influence the March-May season more than the September-November season over east Africa.

• Strong westerlies over the Atlantic favor wet spells over equatorial Africa whilst strong westerlies in the Indian Ocean reduce moisture transport to the region resulting in dry spells.

• Rainfall over the Congo responds immediately (zero lag) to westerly flow over the Atlantic, however east Africa rainfall lags westerlies by 20 days.

Chapter 5

This chapter sought the transient component of ISO and found:

• The eastward propagating mode dominates the intra-seasonal oscillations over tropical Africa in both convection and atmospheric circulation by 44% and 95% respectively. The standing mode is also significant in the OLR but not in the upper divergent circulation.

• Intra-seasonal oscillations occur over the Atlantic Ocean and Congo basin in addition to the Indian Ocean.

• Over east Africa, eastward propagation is suppressed by the meridional monsoon flow.

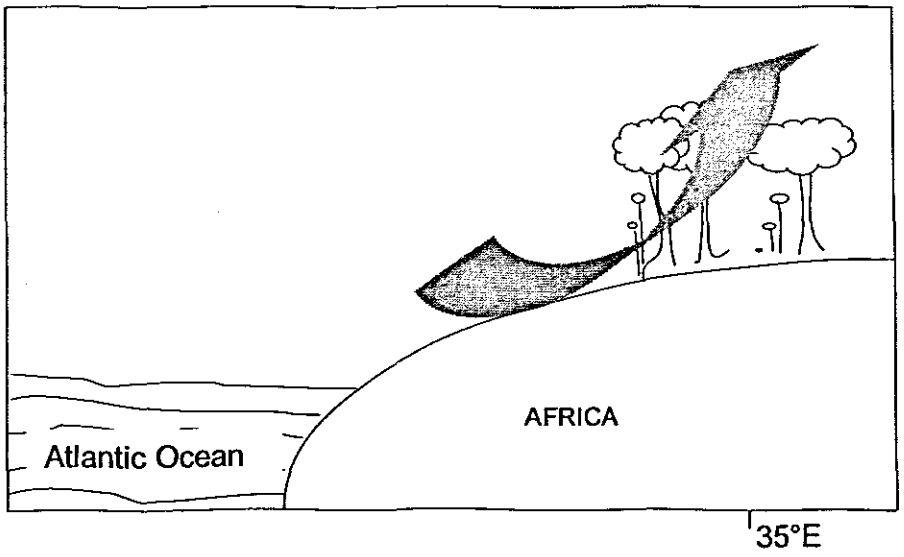

Schematic diagram showing the anchoring of intra-seasonal oscillations over the Congo via surface westerlies and increased transpiration. ISO propagation further east is weakened (refer to section 5.3.1).

Chapter six

This chapter employed high resolution satellite rainfall data and found:

- The optimum temperature threshold for the dry months is -50°C while for the wet months it is -30°C.
- Satellites underestimate rainfall over Uganda by 19%. This is explained by the existence of warm rain giving clouds. However the two rainy seasons are well captured by the satellite.
- Satellites reveal an optimal spatial distribution for rainfall than the gauge network. Since gauges give point measurements, they give a biased spatial distribution of rainfall.

8.3 Conclusion

One of the most important findings of this study is that intra-seasonal oscillations of 30-50 days are phase locked to the seasonal cycle. Surface westerlies modulate intra-seasonal rainfall at different lags over the region. The intra-seasonal oscillations are dominated by eastward propagation. A certain degree of predictability is implied in these results.

8.4 Recommendations

- Land-atmosphere interactions over the northern Congo should be studied to reveal the dynamics of circulation in the vertical plane over this region.
- Aircraft profiling systems should be put in place for provision of data for the study of vertical structure of the atmosphere.
- The rain gauge network should be supplemented in the Angola-Congo-Sudan axis to improve surface data availability.
- Radar installations in the region could assist in the provision of contemporaneous data for satellite algorithm calibration in the hope of improving satellite rainfall estimates.

This study has revealed the phase lockness of the ISO to the seasonal cycle. In order to improve the prediction of the seasonal cycle, a detailed study is required to find the causes of annual variations of ISO amplitudes over tropical Africa. A through understanding of the phenomenon has potential impact on prediction of long-range variations of the tropical atmospheric circulation.

References.

Anderson, J.R. and D.E. Stevens, 1994: The response of the tropical atmosphere to low frequency thermal forcing. J. Atmo. Sci., 44: 676-686.

Andler, R.F. and Negri, A.J., 1988: A satellite infrared technique to estimate tropical convective and stratiform rainfall. J. Climate and Appl. Meteorol., 27: 30-51.

Andler,R.F., 1990: Tropical rain estimates using a combination of low-orbit microwave and geo synchronous data. Preprints Vol.1, International workshop on the processing and utilisation of rainfall data from space, Tokyo.

Arkin. P.A. and Meisner, B.N., 1987: The relationship between large-scale convective rainfall and cold cloud over the western Hemisphere during 1982. Mon. Wea. Rev., 115: 51-74.

Arkin. P.A. and Ardanuy, E., 1989: Estimating Climatic-scale precipitation from space. A Review. J. Climate, 2: 1229-1238.

Asnani, G.C.1993: Tropical Meteorology; Noble Printers, Pune-India, 278-279 pp.

Atlas. D.D., Rosenfeld, D.B. and Wolff. F., 1990: Climatologically turned reflectivity-rain rate relations and links to area-time integrals. J. Appl. Meteorol., 29: 1120-1135.

Bjornsson.H and S.A Venegas, 1997: A manual for EOF and SVD Analysis of climatic Data, 1997: CCGCR Report No. 97-1, 50-52 pp.

Barret, E.C., 1970: The estimation of monthly rainfall from satellite data. Remote Sensing Rev., 11: 322-327.

Barret, E.C and M.J. Beaumont, 1994: Satellite rainfall monitoring: An over in Remote Sensing Reviews, 11: 303-373.

Bellerby, T.J. and Barret, E.C., 1993: Progressive refinement: a strategy for the calibration by collateral data of short period satellite rainfall estimates. J. Appl. Meteorol., 32: 1365-1378.

Chen, T. and Tzeng, R., 1990: Global scale intra-seasonal and annual variation of divergent-water vapor flux. Meteorol., and Atm. Phy., 44: 133-151.

Chen, T. and M. Murakami, 1988: The 30-50 day variation of convective activity over the western Pacific Ocean with the emphasis on the northwestern region. Mon. Wea. Rev., 116: 892-906.

Cook, S. K. and Wang, B., 2001: Equatorial waves and Air sea interaction in the Boreal Summer Intra-seasonal Oscillation (BSISO). J. climate, 14: 2923-2942.

Dugdale G., 1994: Satellite derived rainfall estimates over Africa. Their validation and use in monitoring climate change in global precipitations and climate change. Ed. M. Desbois & F.Desalmand. NATO ASI series1: Global Environmental Change, 26: 2695-2711.

Donaldson,P.J. and A.O.Tsui. 1990: The International family planning movement. Population Bulletin, 45(3): 1-45.

Dyer, T.G.J., 1981: On the interannual variation in rainfall over the subcontinent of Southern Africa. Int. J. Climatol, 2: 47-64.

Findlater, J., 1971: Mean monthly airflow at low levels over the western Indian Ocean. Geophys. Mem., 115, H.M.S.O., London, 53 pp.

Gill, A.E., 1980: Some simple solutions for heat-induced tropical circulation. Quart. J. Roy. Meteorol. Soc., 106: 447-462.

Grimes, D.I.F., E. Pardo-Igu'zquiza, and R. Bonifacio, 1999: Optimal areal rainfall estimation using rain gauges and satellite data. J. Hydrol, 222: 93-108.

Grimes, D.I.F., Milford, J.R. and Dugdale G., 1993: The use of satellite rainfall estimates in hydrological modelling. Presented at the 1st International Conference of East African Meteorol. Soc. Nairobi, Kenya.

Guillot, B., 1995: Satellite et precipitations. Contraintes techniques et physiques, analyse de quelques methodes, problemes de recherche et de validation. Veille Climatique Satellitaire, 55: 27-58.

Goddard L. and Graham N.E., 1999: Importance of the Indian Ocean for similating rainfall anomalies over eastern and Southern Africa. J. Geophy. Res., 104: 19099-19116.

Gollmer, S., Harshvardhan, R.F. Cahalan, and J.B. Snider, 1995: Windowed and Wavelet analysis of marine stratocumulus cloud inhomogeneity. J Atmos. Sci., 52: 3013-3030.

Griffiths, C.G., 1978: Rain estimation from geosynchronous satellite imagery-visible and infrared studies. Mon Wea. Rev., 106: 1153-1171.

Herman, A., V.B. Kumar, P.A. Arkin and J.V. Kousky, 1997: Objectively determined 10-day African rainfall estimates created for famine early warning systems. Int. J. Remote Sensing, 18: 2147-2159.

Hendon, H.H. and Liebmann, L., 1990: The Intra-seasonal (30-50) oscillations of the Australian Summer Monsoon. J.Atmos. Sci., 47: 2904-2923.

Hendon, H.H. and M.L. Salbay, 1994: The life cycle of the Madden Julian oscillation. J.Atmos. Sci., 51: 2225-2237.

Hastenrath, S., Greischar, L. and van Heerden, J. 1995: Prediction of the summer rainfall over South Africa. J. Climate, 8: 1511-1518.

Hastenrath, S. and Lamb, P.J., 1978, Heat budget atlas of the tropical Atlantic and eastern Pacific Oceans. Univ Wisconsin Press, 103 pp.

Huang, J. and Cho, H, 1998: Seasonal modulated intra-seasonal oscillations in a GCM simulation. Int. J. Climatol., 18: 1521-1532.

Hu, Q. and D.A. Randall, 1994: Low frequency oscillations in radiative-convective systems. J. Atmos.Sci., 51: 1089-1099.

Indeje, M., Semazzi, H.M. and Ogallo, L.J., 2000: ENSO signals in east African rainfall season. Int. J. of Climatol., 20: 19-46.

Journel, A.G. and Huijbregts, C.J., 1978. Mining Geostatistics, Academic Press, New York, 600 pp.

Jury, M.R., 1997: Inter-annual climate modes over southern Africa from satellite cloud OLR 1975-1994. Theor. Appl. Climatol. 57: 155-163.

Jury, M.R., Parker, B.A., Raholijao, N. and Nassor, A., 1995: Variability of summer rainfall over Madagascar: climatic determinants at interannual scales. Int. J. Climatol., 15: 1323-1332.

Jury, M. R., Pathack. B., Campbel, G., Wang, B. and Landman, W., 1991: Transient Convective Waves in the Tropical SW Indian Ocean. Meteorol. Atmos. Phys. 47: 27-36.

Jury, M.R. and Pathack, B.M.R., 1993: Composite climatic patterns associated with extreme modes of summer rainfall over southern Africa: 1975-1984. Theor. and Appl. Climatol., 47: 137-145.

Kabanda .T A., 1995: Seasonal and Intra-seasonal dynamics and Precursors of rainfall over northern Tanzania. MSc. Thesis, University of Cape Town, South Africa.

Kalnay et al., 1996: The NCEP/NCAR 40-year re-analysis project. Bull. Amer. Meteorol. Soc.,77: 437-471.

Lebel, T, Taupin, J. D. and D'Amato, N., 1997: Rainfall monitoring during HAPEX-Sahel: general rainfall conditions and climatology, J. Hydrol, 188: 74-96.

Lamb, P.J. and R.A. Peppler, 1991: West Africa in Teleconnections Linking Worldwide Climate Anomalies: Scientific Basis and Societal Impact (M.H. Glantz, R.W. Katz, and N. Nicholls, Eds.), Cambridge University Press, 121-189.

Lau, K.M. and H.Y. Weng, 1995: Climate signal detection using wavelet transform. How to make a time series sing. Bull. Amer. Meteorol. Soc., 76: 2391-2402.

Lyons, S.W., 1990: Origins of convective variability over equatorial southern Africa during austrial summer. Bull. Amer. Meteorol. Soc., 4: 23-39.

Majodina, M. and Jury, M. R., 1996: Composite winter cyclones south of Africa: evolution during eastward transit over the Agulhas warm pool, S Afr J. Marine Sci, 17: 241-252.

Mason, S.J. and Tyson, P.D., 1992: The modulation of sea surface temperature and rainfall associations over southern Africa with solar activity and the Quasi-biennial Oscillation. J. Geophy. Res., 97: 5847-5856.

Matitu, R. M., 2002: The response of tropical African rainfall to zonal circulations over adjacent Oceans. MSc. Thesis, Department of Geography and environmental studies. University of Zululand.

Matari , E. E. , 2003: Impacts of Congo convection on tropical Africa's circulation, Rainfall and resources. MSc. Thesis, Department of Geography and environmental studies. University of Zululand.

Meehl, G.A., 1988: Tropical mid-latitude interactions in the Indian and Pacific sectors of the southern Hemisphere. Mon. Wea. Rev., 116: 472-484.

Mulenga, H.M., 1998: Southern African Climatic anomalies, summer rainfall and the Angola low. Ph. D. Thesis, Oceanogr. Dept. Univ. Cape Town.

McGregor G.R. and S. Niewolt, 1998: Tropical climatology. An introduction to the climates of low latitudes. Published by John Wiley and Sons, Inc., New York.

Meyers, S.D., Kelley, B.G. and J.J. O'Brien, 1993: An introduction to wavelet analysis in oceanography and meteorology: With application to the dispersion of Yania waves. Mon. Wea. Rev., 121: 2858-2866.

Morgan, W.T.W., 1982: Geography of East Africa. Walchoring, New York. 192-199.

Morland, J., D.I.F. Grimes, G. Dugdale and T. Hewison, 1997: The effect of the land surface on microwave rainfall estimates. Preceedings 23rd Annual Conference Remote Sensing Society, Reading, 493-498.

Murakami, T., 1985: Intra-seasonal atmospheric teleconnection patterns during Northern Hemisphere summer. Monthly Wea Rev., 115: 2133-2154.

Madden, R.A., 1986: Seasonal Variation of the 40-50 day oscillation in the tropics. J. Atmos Sci, 43: 3138-3158.

Madden. R. A., and P.R. Julian, 1971: Detection of a 40-50 day oscillation in the zonal wind in the tropical Pacific. J. Atmos. Sci., 28: 702-708.

Madden, R. A. and P.R.Julian, 1972: Description of global-scale circulation cell in the tropics with a 40-50 day period. J. Atmos. Sci., 29: 1109-1123.

Milford and Dugdale, G.,1990: Estimation of rainfall using geostationary satellite data. In application of remote sensing in agriculture, (M.D.Steven and J.A.Clark eds), Butterworths, London, 97-110.

Michele .B., 1999: Favoured regions for the development and decay of the Tropical Madden-Julian Oscillation. Mon Wea Rev,.25: 1096-1112.

Mpeta, J.E., and M.R. Jury 2001: Intra-seasonal convective structure and evolution over tropical East Africa. Climate Research., 17: 83-92.

Mpeta, J.E, 1997: Intra-seasonal convection dynamics over Southwest and northeast Tanzania: An observational study. MSc. Thesis, University of Cape Town, South Africa.

Mutai, C. C., M. N. Ward, and A. W. Colman, 1998: Towards the prediction of the east Africa short rains based on sea-surface temperature-atmosphere coupling. Int. J. Climatol., 18: 975-997.

Mutai, C.C. and M. N. Ward, 2000: East African Rainfall and Tropical circulation/Convection on Intra-seasonal to Inter-annual time scales. J. Climate, 13: 3915-3939.

Nyenzi, B. S., and Nicholson, S. E., 1990, Temporal and spatial variability of SSTs in the tropical Atlantic and Indian Oceans. Meteorol. Atmos. Phys., 42: 1-17.

Nesbitt, S. W. and Zipser, E. J., 2000: A census of precipitation features in the tropics using TRIMM: Radar, Ice scattering and lightening observations. J. Climate, 13: 4087-4106.

Ogallo, L. J., Janiowiak, J. E., and Halpert, M. S., 1988: Teleconnections between seasonal rainfall over east Africa and global sea surface temperature anomalies. J. Meteorol. Soc., Japan, 6: 807-821.

Okoola, R.E., 1999: A diagnostic study of the East African monsoon circulation during the northern Hemisphere spring season. Int. J. Climate, 19: 143-168.

Porc'u F., Borga, M. and Prodi, F., 1999: Rainfall estimation by combining radar and infrared satellite data for nowcasting purposes. Meteorological Applications, 6: 289-300.

Prasad, K.D., S.D. Bansod and S.S.Sabade, 2000: Forecasting Indian summer Monsoon rainfall by outgoing longwave radiation over the Indian Ocean. Int. J. Climatol., 20: 105-114.

Reynolds, R.W., 1988: A real global sea surface temperature analysis. J. Climate, 1: 75-86.

Rouault, M., Jobard, I., S.A. White and J. R. E. Lutjeharms, 2001: Studying rainfall events over South Africa and adjacent oceans using the TRMM satellite. South African J. Science, 97: 455-460.

Rui, H. and Wang. B., 1990: Development characteristics and Dynamic Structure of Tropical Intra-seasonal Convective Anomalies. J. Atmos. Sci., 47: 357-379.

Salby, M.L., and H.H. Hendon, 1994: Intra-seasonal behavior of clouds, temperature and motion in the tropics. J. Atmos. Sci., 51: 2207-2224.

Semazzi, H. F. M., Lin, N. H., Lin, Y. L., and Giorgi, F., 1993: A GCM nested model study of the influence of sea surface temperature anomalies on Sahelian Climate. Geophys Res. Lett., 20: 2897-2900.

Spencer, R.W., Goodman, H.M. and Hood, R.E., 1997: Precipitation retrieval over land and ocean with SSMI: Identification and characteristics of the scattering signal. J. Atms. and Oceanic Tech., 6: 254-273.

Tait, A. B., Barret, E. C., Beaunmont, M. J., Brown, P. A., Terrner, M. J. and M. C. Todd, 1999: Interpretation of an Atlas of passive Microwave- derived rainfall over the eastern northern Atlantic Ocean and northern sea. Int. J. Climatol: 19: 231-252.

Tennant, W.J. and Hewitson, B. C., 2002: Intra-seasonal rainfall characteristics and their importance to the seasonal prediction problem. Int. J. Climatol. 22: 1033-1048.

Trenberth, K.E., T.R. Karl and T. W. Spence, 2002: The need for a systems approach to climate observations. Bull. Amer. Meteorol. Soc., 83: 1593-1602.

Tucker, C.J., Vanpraet, C. and Gaston, A., 1983: Satellite remote sensing of total dry matter production in the Senegalese Sahel. Remote Sensing Environment, 13: 461-474.

Tucker, C.J., Townshend, J.R.G. and Goff, T.E., 1985a: African land cover classification using satellite data. Science, 227: 369-375.

Todd, M.C. and Washington, R., 1999: A simple method to retrieve 3-hourly estimates of global tropical and subtropical precipitation from International satellite cloud climatology program (ISCCP) data. J. Atmos. Oceanogr. Tech., 19: 146-155.

Todd, M.C., Barrett, E.C., Beaumont, M.J., and Green, J., 1995: satellite identification of rain days over the upper Nile river basin using an optimum infrared rain/no rain threshold temperature model. J. Appl. Meteorol., 34: 2600-2611.

Thomas, A.R. and Patterson, V.L., 1983: A reliable method for Estimating precipitation amounts. Proceedings of Meteorological observations and instrumentation. Toronto, Amer. Meteorolo. Soc., 554-561.

Uganda National Environment Management Authority, 2000: Executive summary of state of environment report, pp 1.

Vicent, D.G., T. Sperling and A. Fink, 1991: Intraseasonal Oscillations of convective activity in the tropical Southern Hemisphere. J. Climatology, 4: 40-53.

Weng, H.Y. and K. M. Lau, 1994: Wavelet period doubling and time frequency localization with application to satellite data analysis. J. Atmos. Sci., 51: 2523-2541.

Wang, B. and Rui, H., 1990: Synoptic Climatology of Transient tropical intra-seasonal Convection anomalies. Meteorol. and Atmos. Phys., 44: 43-61.

Waliser, D.E., C. Jones, J.E. Schemm and N. Graham, 1999: A statistical extended range tropical model based on the slow evolution of the Madden-Julian Oscillation. J. climate, 12: 1918-1939.

Xie, P. and P.A. Arkin, 1997: Global precipitation: A 17 year monthly analysis based on gauge observations, satellite estimates, and numerical model outputs. Bull. Amer. Meteorol. Soc., 78: 2539-255.

Xie, P. and Arkin, P.A., 1995: An intercomparison of gauge observations and Satellite estimates of monthly precipitation. J. Appl. Meteorol., 34: 1143-1160.

Yeshanew, A.B., 2003: Mechanisms and prediction of climate variability in tropical north Africa. PhD. Thesis, Department of Geography and Environmental Studies. University of Zululand.

Zhang, C. and Hendon, H.H., 1996: Propagating and Standing Components of the Intra-seasonal Oscillation in Tropical Convection. J. Atmos. Sci., 54: 741-752.